

Aus dem Institut für Immunologie im Biomedizinischen Centrum

der Ludwig-Maximilians-Universität München

Leitung: Prof. Dr. Thomas Brocker

Functional Analysis of the mRNA Decay Factor Lsm1 in the Immune System

Dissertation

zum Erwerb des Doktorgrades

der Naturwissenschaften (Dr. rer. nat.)



an der Medizinischen Fakultät der
Ludwig-Maximilians-Universität zu München

vorgelegt von

Aicha Jeridi

aus Medenine/Tunesien

2018

Für meine Eltern

**Gedruckt mit Genehmigung der Medizinischen Fakultät der
Ludwig-Maximilians-Universität München**

Betreuer: Prof. Dr. Vigo Heissmeyer
Zweitgutachter: Priv. Doz. Dr. Klaus Dornmair
Dekan: Prof. Dr. med. dent. Reinhard Hickel
Tag der mündlichen Prüfung: 07.12.2018

Eidesstattliche Versicherung

Jeridi, Aicha

Name, Vorname

Ich erkläre hiermit an Eides statt, dass ich die vorliegende Dissertation mit dem Thema

“Functional Analysis of the mRNA Decay Factor Lsm1 in the Immune System”

selbständig verfasst, mich außer der angegebenen keiner weiteren Hilfsmittel bedient und alle Erkenntnisse, die aus dem Schrifttum ganz oder annähernd übernommen sind, als solche kenntlich gemacht und nach ihrer Herkunft unter Bezeichnung der Fundstelle einzeln nachgewiesen habe.

Ich erkläre des Weiteren, dass die hier vorgelegte Dissertation nicht in gleicher oder in ähnlicher Form bei einer anderen Stelle zur Erlangung eines akademischen Grades eingereicht wurde.

München, 07.12.2018

Ort, Datum

Aicha Jeridi

Unterschrift

Summary

Lsm1 is part of the cytoplasmic Lsm1-7 complex that plays a crucial role in induced mRNA decay. Binding of the doughnut-shaped complex to target mRNAs results in mRNA decapping and subsequent degradation. The Lsm1-7 complex targets oligouridylated histone mRNAs, the only class of eukaryotic mRNAs that are not polyadenylated and oligo-adenylated mRNA, the products of cellular deadenylating enzymes. An intrinsic binding preference for oligo-A or oligo-U stretches makes the Lsm1-7 ring a general activator of cellular mRNA degradation after induced deadenylation and/or oligouridylation. Lsm1 is a unique subunit of the Lsm1-7 ring with its long C-terminal extension. Knowledge about the function of Lsm1 was mostly obtained in yeast cells and until now only few experiments were performed in mammalian cell lines such as HeLa cells. The present work now addresses the role of Lsm1 in the mouse. The consequences of genetic disruption of Lsm1 encoding alleles were investigated in fibroblast or T cells, and Lsm1-deficient animals were analyzed with a focus on the development of the hematopoietic and immune systems.

On the molecular and cellular levels, Lsm1 deletion abolished the interaction of the residual components of the Lsm1-7 ring with its main interaction partner Pat1b. This finding was of particular importance, since binding to Pat1b is a requirement of Lsm1-7 binding to target mRNAs. Nevertheless, systemic deletion of Lsm1 in the mouse did not cause a profound deregulation of mRNAs as shown for induced degradation of histone mRNAs or by global mRNA sequencing of naïve and activated T cells. The absence of Lsm1 changed the expression of other factors involved in mRNA decay, suggesting ongoing compensatory changes. Moreover, induced acute conditional deletion of Lsm1 was able to reduce cellular P-body numbers, whereas permanent deletion did not. Finally, proximity-labeling of proteins close to Lsm1 within cells identified CNOT4 and 4E-T as potential interactors pointing at a possible role of Lsm1 in the repression of translation. These potential new functions as well as the molecular processes of compensation require additional future investigations.

Nevertheless, one striking consequence of the lack of Lsm1 function was revealed in the mouse immune system. Lsm1-deficient mice developed an autoimmune phenotype characterized by spontaneous T cell activation, accumulation of follicular helper T cells and germinal center B cells as well as production of autoantibodies. In summary,

this investigation of *Lsm1* deficiency in the mouse strongly expanded the current knowledge on the complexity of mRNA decay pathways in the mammalian system and revealed a new crucial role of *Lsm1* in regulating the immune response and preventing autoimmunity.

Zusammenfassung

Das Lsm1-Protein ist eine Untereinheit des Lsm1-7 Rings, eines Multiproteinkomplexes, der eine entscheidende Rolle im induzierten RNS-Abbau spielt. Durch die Bindung an spezifische Modifikationen der 3' Enden von Ziel-mRNS, ermöglicht der Lsm1-7 Komplex das Entfernen der Cap-Struktur am 5' Ende und leitet damit die Degradation der RNS ein. Der Lsm1-7 Komplex erkennt zum Einen oligouridylierte Histon-mRNS, welche keine Polyadenylierungssequenzen tragen, jedoch gegen Ende der S-Phase im Zellzyklus oligouridyliert werden. Zum Anderen erkennt der Lsm1-7 Komplex oligo-adenylierte mRNS, die poly-adenyliert waren, aber über Interaktion mit zellulären Enzymen der Deadenylierung eine Verkürzung des poly-A-Schwanzes erfuhren. Die intrinsische Bindungspräferenz für oligo-A bzw. oligo-U 3' Enden, die aus Deadenylierung bzw. Oligouridylierung resultieren, macht den Lsm1-7 Komplex zu einem generellen Aktivator des mRNS-Abbaus. Unter den sieben Untereinheiten des Rings, verfügt Lsm1 über eine besondere strukturelle Eigenschaft, eine C-terminale Verlängerung, die die Interaktion mit mehr als nur den benachbarten Untereinheiten ermöglicht.

Erkenntnisse über die Funktion von Lsm1 wurden größtenteils aus Experimenten in Hefe-Zellen abgeleitet und nur wenig Information konnte bislang in Säugerzellen gewonnen werden. In der vorliegenden Arbeit wurde zum ersten Mal die Funktion von Lsm1 in der Maus untersucht. Das kodierende Gen wurde hierzu in Fibroblasten oder systemisch in der Maus bzw. konditionell in T-Zellen inaktiviert. Die Konsequenzen des Fehlens von Lsm1 Protein wurden im Weiteren mit einem besonderen Fokus auf die Entwicklung des Blutbilds bzw. des Immunsystems analysiert.

Auf molekularer Ebene verursachte die Abwesenheit von Lsm1 eine Störung in der Bindung des Lsm-Rings an seinen Interaktionspartner Pat1b. Dieses Ergebnis war von großer Bedeutung, da bekannt ist, dass die Bindung von Ziel-RNS-Transkripten die Interaktion vom Lsm1-7-Komplex mit Pat1b voraussetzt. Dennoch resultierte das Fehlen von Lsm1 nicht in einer veränderten mRNS-Expression, wie die Untersuchung des induzierten Abbaus von Histon-mRNS und globale RNS-Sequenzierungsanalysen in T-Zellen zeigten. Die genetische Inaktivierung von Lsm1 bewirkte jedoch eine Veränderung in der Expression von anderen molekularen Effektoren des mRNS-

Abbaus und die induzierte nicht jedoch die permanente Deletion von Lsm1 konnte eine Verringerung der Anzahl zellulärer "P-Bodies", das heißt von zellulären Strukturen des mRNA-Abbaus bewirken, Diese Befunde deuten auf eine mögliche Kompensation der Lsm1-Funktion hin. Interessanterweise wurden in Versuchen der "Proximity-Markierung" CNOT4 und 4E-T als neue potentielle Interaktionspartner von Lsm1 identifiziert, welche auf eine mögliche neue Funktion von Lsm1 in der translationalen Repression von Ziel mRNA hinweisen könnten. Die Aufklärung dieser Funktion bzw. die molekulare Kompensation von Lsm1 bedürfen noch weiterer zukünftiger Untersuchungen.

Als beeindruckendes Ergebnis dieser Arbeit wurde die Entstehung von Autoimmunität in Lsm1-defizienten Mäusen beobachtet. Eine spontane Aktivierung von T-Zellen, die überproportionale Entstehung von Th1-Helfer Zellen *in vitro* und T_{FH}-Zellen *in vivo* bzw. von Keimzentrums B-Zellen sowie die Produktion von anti-nuklearen Autoantikörpern konnte in den untersuchten Tieren festgestellt werden.

Zusammenfassend wurden im Zuge dieser Arbeit neue Erkenntnisse zur Komplexität der zellulären mRNA-Abbauwege im System der Säugetiere gewonnen und eine neue Funktion von Lsm1 in der Vermeidung der Entstehung von Autoimmunität aufgedeckt

Directory

| | |
|---|-----------|
| Eidesstattliche Versicherung | 7 |
| Summary | 9 |
| Zusammenfassung | 12 |
| List of figures..... | 18 |
| List of tables | 20 |
| Abbreviations | 21 |
| 1 Introduction | 25 |
| 1.1 Post-transcriptional gene regulation | 25 |
| 1.1.1 mRNA degradation pathways..... | 26 |
| 1.1.2 Proteins involved in the different mRNA decay processes | 31 |
| 1.1.2.1 The Lsm1-7 complex..... | 31 |
| 1.1.2.2 The Trans-acting factors TTP, Roquin-1 and Regnase-1..... | 36 |
| 1.1.2.2.1 Tristetraprolin (TTP) | 37 |
| 1.1.2.2.2 Roquin and Regnase-1..... | 37 |
| 1.2 mRNA metabolism in innate and adaptive immunity | 39 |
| 1.2.1 The innate and adaptive immune system | 39 |
| 1.2.2 mRNA metabolism and autoimmunity | 41 |
| 1.2.3 mRNA metabolism in the innate immune system..... | 41 |
| 1.2.4 mRNA metabolism in the adaptive immune system | 42 |
| 2 Aim of the project | 45 |
| 3 Material and methods | 47 |
| 3.1 Material..... | 47 |
| 3.1.1 Mice | 47 |
| 3.1.2 Cell lines and cell culture | 48 |
| 3.1.3 Plasmids | 48 |
| 3.1.4 DNA oligonucleotides..... | 49 |
| 3.1.5 Antibodies and fluorescent dyes | 50 |
| 3.1.6 Chemicals, enzymes and kits..... | 52 |
| 3.1.7 Buffers..... | 54 |
| 3.1.8 Instruments | 56 |
| 3.1.9 Software | 57 |
| 3.2 Methods..... | 58 |
| 3.2.1 Work with nucleic acids | 58 |
| Polymerase chain reaction (PCR)..... | 58 |
| Agarose gelelectrophoresis and DNA extraction | 58 |

| | |
|---|-----------|
| Molecular cloning..... | 59 |
| RNA extraction | 60 |
| Reverse Transcriptase-polymerase chain reaction (RT-PCR) | 60 |
| Site-directed mutagenesis with Quikchange..... | 60 |
| Southern blot analysis..... | 61 |
| Poly(A) tail length determination assay | 62 |
| 3.2.2 Work with retroviruses..... | 62 |
| Virus production..... | 62 |
| Transduction | 63 |
| 3.2.3 Work with protein..... | 63 |
| Western blot analysis | 63 |
| Co-immunoprecipitation..... | 64 |
| Fractionation..... | 65 |
| 3.2.4 Work with cells..... | 65 |
| 3.2.4.1 Generation of MEF-cells..... | 65 |
| 3.2.4.2 Storage of cells | 66 |
| 3.2.4.3 Cell culture..... | 66 |
| 3.2.4.4 Treatment of MEF-cells with hydroxyurea | 66 |
| 3.2.4.5 Isolation of naïve CD4 ⁺ T-cells..... | 67 |
| 3.2.4.6 T-cell stimulation..... | 67 |
| 3.2.4.7 Flow cytometry..... | 68 |
| 3.2.4.8 BioID Experiment | 69 |
| 3.2.4.9 Detection of T cell proliferation | 69 |
| 3.2.4.10 Seahorse measurements | 70 |
| 3.2.4.11 Confocal microscopy | 71 |
| 3.2.4.12 Fluorescence microscopy..... | 71 |
| 3.2.5 Statistical analyses | 72 |
| 4 Results | 73 |
| 4.1 Evaluation of the <i>Lsm1</i> knockout mouse..... | 73 |
| 4.2 Molecular consequences of the <i>Lsm1</i> knockout..... | 74 |
| 4.2.1 Histone mRNA degradation occurs delayed in the absence of <i>Lsm1</i> | 74 |
| 4.2.2 P-body form in the absence of <i>Lsm1</i> | 77 |
| 4.2.3 The interaction of components of the <i>Lsm1-7</i> complex with <i>Pat1b</i> is impaired in <i>Lsm1</i> -deficient cells..... | 80 |
| 4.3 Consequences of the <i>Lsm1</i> knockout in the mouse..... | 82 |
| 4.3.1 Global <i>Lsm1</i> deletion in the <i>Lsm1^{neo/neo}</i> mouse..... | 82 |
| 4.3.2 Role of <i>Lsm1</i> in CD4 ⁺ T cells..... | 89 |
| 4.3.2.1 Stable expression of <i>Lsm1</i> protein in activated CD4 ⁺ T cells | 89 |
| 4.3.2.2 <i>Lsm1</i> -deficient CD4 ⁺ T cells proliferate normally | 90 |
| 4.3.2.3 T cell metabolism is unchanged in the absence of <i>Lsm1</i> | 91 |

| | | |
|----------|---|------------|
| 4.3.2.4 | Lsm1-deficient CD4 ⁺ T cells differentiate preferentially towards Th1 | 93 |
| 4.3.2.5 | RNA-Sequencing to identify direct Lsm1 targets in CD4 ⁺ T cells..... | 94 |
| 4.3.2.6 | Reduction of P-body numbers after acute deletion of Lsm1 in CD4 ⁺ T cells | 99 |
| 4.3.3 | Autoimmune phenotype of Lsm1-deficient mice | 100 |
| 4.3.3.1 | Comparing autoimmune phenotypes of <i>Lsm1^{neo/neo}</i> and <i>sanroque</i> mice | 102 |
| 4.3.4 | Conditional deletion of Lsm1 in T cells | 104 |
| 4.4 | Testing candidate interactors of Lsm1..... | 107 |
| 4.4.1 | Lsm1 interacts with 4E-T but not Roquin proteins | 107 |
| 4.4.2 | Cnot4 and 4E-T are newly identified interaction partners of Lsm1 | 108 |
| 5 | Discussion | 111 |
| | References..... | 122 |
| | Acknowledgements..... | 140 |

List of figures

| | |
|---|-----------|
| <i>Figure 1: Scheme of mRNA degradation pathways after deadenylation.....</i> | <i>29</i> |
| <i>Figure 2: The two Lsm complexes in the eukaryotic cell.....</i> | <i>33</i> |
| <i>Figure 3: Crystal structure of the Lsm1-7 ring in S. cerevisiae.....</i> | <i>34</i> |
| <i>Figure 4: Schematic structures of human TTP, Roquin and the MCPIP protein families</i> | <i>36</i> |
| <i>Figure 5: Targeting strategy of the Lsm1 allele.</i> | <i>47</i> |
| <i>Figure 6: Evaluation of Lsm1 gene deletion in MEF and T cells.....</i> | <i>73</i> |
| <i>Figure 7: Degradation of selected histone mRNAs in the presence and absence of Lsm1.....</i> | <i>75</i> |
| <i>Figure 8: HU-induced histone mRNA degradation in the absence of Lsm1 and presence of mutated Lsm1.....</i> | <i>76</i> |
| <i>Figure 9: Delayed histone mRNA degradation in the absence of Lsm1.....</i> | <i>77</i> |
| <i>Figure 10: P-bodies form in the absence of Lsm1.</i> | <i>78</i> |
| <i>Figure 11: Unchanged expression and localization of Lsm4 in the absence of Lsm1.....</i> | <i>79</i> |
| <i>Figure 12: P-body formation in Lsm1^{+/+} and Lsm1^{neo/neo} T cells.</i> | <i>80</i> |
| <i>Figure 13: Lsm2 and Lsm4 do not interact with Pat1b in the absence of Lsm1.</i> | <i>81</i> |
| <i>Figure 14: Effectors of mRNA decay differ in expression in the absence of Lsm1.</i> | <i>81</i> |
| <i>Figure 15: Efficient deletion of Lsm1 in Lsm1^{neo/neo} mice.....</i> | <i>83</i> |
| <i>Figure 16: Genotypes of offspring from Lsm1 breedings deviate from mendelian distribution.....</i> | <i>83</i> |
| <i>Figure 17: Body weights of Lsm1^{neo/neo} mice are significantly reduced.....</i> | <i>84</i> |
| <i>Figure 18: Lsm1 expression is high in testis, spleen and thymus.</i> | <i>84</i> |
| <i>Figure 19: Thymus weight and thymocytes number of Lsm1^{neo/neo} mice are unchanged.....</i> | <i>85</i> |
| <i>Figure 20: Deletion of Lsm1 does not affect T cell development in the thymus.</i> | <i>85</i> |
| <i>Figure 21: Frequencies of regulatory T cells in thymi of Lsm1^{neo/neo} mice are normal.</i> | <i>86</i> |
| <i>Figure 22: The frequencies of different hematopoietic lineages are not changed in splenocytes of Lsm1-deficient mice.</i> | <i>87</i> |
| <i>Figure 23: Spleen weights and splenocyte numbers are increased in Lsm1-deficient mice.</i> | <i>88</i> |
| <i>Figure 24: Lsm1-deficient CD4⁺ and CD8⁺ T cells show a phenotype of spontaneous activation. ...</i> | <i>89</i> |
| <i>Figure 25: Lsm1 protein expression during activation is unchanged.....</i> | <i>90</i> |
| <i>Figure 26: Proliferation of CD4⁺ T cells is unchanged after deletion of Lsm1.</i> | <i>91</i> |
| <i>Figure 27: The metabolic program of CD4⁺ T cells is not altered in the absence of Lsm1.</i> | <i>92</i> |
| <i>Figure 28: Lsm1-deficient CD4⁺ T cells differentiate preferentially towards Th1.....</i> | <i>93</i> |
| <i>Figure 29: No changes in differentiation program of Lsm1-deficient CD4⁺ T cells under Th2 or Th17 conditions.....</i> | <i>94</i> |
| <i>Figure 30: Overexpression of Ifng mRNA in Lsm1-deficient CD4⁺ T cells.</i> | <i>94</i> |
| <i>Figure 31: RNA sequencing to analyze gene expression in Lsm1-deficient Th1 cells.....</i> | <i>95</i> |
| <i>Figure 32: Usp18 is overexpressed in the absence of Lsm1.....</i> | <i>98</i> |

| | |
|---|------------|
| <i>Figure 33: Reduced P-body numbers upon acute deletion of Lsm1.....</i> | <i>99</i> |
| <i>Figure 34: Increased frequencies and numbers of T_{FH} and GC B cells in spleens from Lsm1-deficient mice.....</i> | <i>100</i> |
| <i>Figure 35: Lsm1-deficient mice have anti-nuclear autoantibodies in their sera.....</i> | <i>101</i> |
| <i>Figure 36: Age-dependent development of autoantibodies in sera from Lsm1-deficient mice.....</i> | <i>102</i> |
| <i>Figure 37: Lsm1-deficiency causes less severe phenotypes than observed in the sanroque mouse.....</i> | <i>103</i> |
| <i>Figure 38: Confirming absence of Lsm1 protein in CD4⁺ T cells from Lsm1^{fl/fl}; CD4Cre mice.....</i> | <i>104</i> |
| <i>Figure 39: Normal numbers of thymocytes and splenocytes in Lsm1^{fl/fl}; CD4Cre mice.....</i> | <i>105</i> |
| <i>Figure 40: Absence of Lsm1 in T cells does not affect frequencies of T cells or B cells.....</i> | <i>105</i> |
| <i>Figure 41: Elevated frequencies of activated CD4⁺ T cells and T_{FH} cells in Lsm1^{fl/fl}; CD4Cre animals.....</i> | <i>106</i> |
| <i>Figure 42: Lsm1^{fl/fl}; CD4Cre mice confirm cell-intrinsic activation of CD4⁺ T cells and T_{FH} accumulation upon deletion of Lsm1.....</i> | <i>106</i> |
| <i>Figure 43: Lsm1 and Roquin interact with 4E-T, but not with each other.....</i> | <i>107</i> |
| <i>Figure 44: Biotinylation and capture of biotin-conjugated proteins.....</i> | <i>109</i> |
| <i>Figure 45: Proteins identified using proximity-dependent biotinylation (BioID).....</i> | <i>109</i> |
| <i>Figure 46: Suggested model of possible binding features of Lsm1.....</i> | <i>119</i> |

List of tables

| | |
|---|----|
| <i>Table 1: Abbreviations</i> | 21 |
| <i>Table 2: Cell culture components</i> | 48 |
| <i>Table 3: Retroviral Gateway® destination vectors</i> | 49 |
| <i>Table 4: Primers for cDNA cloning; mutagenesis and Southern blot analysis</i> | 49 |
| <i>Table 5: Antibodies for flow cytometric analyses</i> | 50 |
| <i>Table 6: Dyes for cell proliferation experiments</i> | 50 |
| <i>Table 7: Antibodies for confocal microscopy</i> | 50 |
| <i>Table 8: Antibodies for Western blot analyses</i> | 51 |
| <i>Table 9: Antibodies for Immunoprecipitation</i> | 51 |
| <i>Table 10: Antibodies & cytokines for stimulation and differentiation of T cells</i> | 51 |
| <i>Table 11: Chemicals</i> | 52 |
| <i>Table 12: Enzymes</i> | 53 |
| <i>Table 13: Kits</i> | 53 |
| <i>Table 14: Buffers</i> | 54 |
| <i>Table 15: Consumables</i> | 55 |
| <i>Table 16: Instruments</i> | 56 |
| <i>Table 17: Software</i> | 57 |
| <i>Table 18: PCR composition and cycling conditions</i> | 58 |
| <i>Table 19: Composition of the DNA mix for calcium-phosphate transfection</i> | 62 |
| <i>Table 20: Composition of SDS PAGE gels</i> | 64 |
| <i>Table 21: Composition of Tricine gels</i> | 64 |
| <i>Table 22: Composition of antibody/cytokine mixes for T cell differentiation</i> | 68 |
| <i>Table 23: Composition of fluorescent antibody mix for differentiated T cells</i> | 69 |
| <i>Table 24: List of potential Lsm1 targets in Th1 differentiated CD4⁺ T cells</i> | 96 |

Abbreviations

Table 1: Abbreviations

| Abbreviation | Full name |
|-----------------------|---|
| 4E-T | Eukaryotic translation initiation factor 4E transporter |
| aa | Amino acid |
| AF488 | Alexa Fluor 488 |
| ANAs | Anti-nuclear antibodies |
| APC | Antigen-presenting cell |
| APS | Ammonium persulfate |
| ARE | AU-rich element |
| ATP | Adenosine triphosphate |
| BFA | Brefeldin A |
| BSA | Bovine serum albumin |
| C-terminus | Carboxy-terminus |
| CCR | C-C chemokine receptor type |
| CD | Cluster of differentiation |
| CDE | Constitutive decay element |
| cDNA | Complementary DNA |
| CDS | Coding sequence |
| CFSE | Carboxyfluorescein succinimidyl ester |
| Cnot/CNOT | Mouse/human CCR4-NOT complex subunit |
| CXCR | Chemokine (C-X-C Motif) receptor |
| Cy5 | Cyanine 5 |
| DNA | Deoxyribonucleic acid |
| Dcp/DCP | Mouse/Human decapping protein |
| Dcp5 | Scavenger decapping protein |
| DDX6 | DEAD box helicase 6 (RCK) |
| DEPC | Diethylpyrocarbonate |
| DMEM | Dulbecco's Modified Eagle's Medium |
| DN | Double negative |
| dNTP | Deoxynucleotide |
| DP | Double positive |
| dpc | Days post coitum |
| dsDNA | Double-stranded DNA |
| dsRNA | Double-stranded RNA |
| DTT | Dithiothreitol |
| ECAR | Extracellular acidification rate |
| <i>E. coli</i> | Escherichia coli |
| ECL | Enhanced chemiluminescence |
| Edc/Edc | Mouse/Human enhancer of mRNA decapping |
| EDTA | Ethylenediaminetetraacetic acid |

| | |
|--------------------------|--|
| eIF | Eukaryotic translation initiation factor |
| Env | Envelope gene |
| ER | Endoplasmatic reticulum |
| EtBr | Ethidium bromide |
| EtOH | Ethanol |
| FACS | Fluorescence-activated cell sorting |
| FBS | Fetal bovine serum |
| FITC | Fluorescein isothiocyanate |
| fl/fl | Floxed alleles |
| 4-OH-TAM | 4-OH-tamoxifen |
| Foxp3/Foxp3 | Mouse/human forkhead-box-protein P3 |
| FSC | Forward scatter |
| GAPDH | Glyceraldehyde-3-phosphate dehydrogenase |
| GC | Germinal center |
| GFP | Green fluorescent protein |
| H₂O | Water |
| HBS | Hepes buffered saline |
| HCl | Hydrochloric acid |
| HEK293T | Human embryonic kidney cells |
| HELA | Human cervical cancer cells |
| HEPES | N-2-hydroxyethylpiperazine-N-2-ethane sulfonic acid |
| Hprt/HPRT | Mouse/human hypoxanthine phosphoribosyltransferase |
| Icos/ICOS | Mouse/human inducible T cell costimulator |
| Ifng | Interferon γ |
| Ig | Immunoglobulin |
| IL | Interleukin |
| Iono | Ionomycin |
| IP | Immunoprecipitation |
| Kb | Kilobases |
| KD | Knockdown |
| Kda | Kilodalton |
| KO | Knockout |
| LB medium | lysogeny broth |
| Lsm/LSM | Mouse/human Like Sm protein |
| M199R | Methionine to arginine mutation at amino acid position 199 |
| m7G cap | 7-methylguanosine cap |
| MgCl₂ | Magnesium chloride |
| MEF | Mouse embryonic fibroblast |
| MCPIP | Monocyte chemotactic protein-induced protein |
| MHC | Major histocompatibility complex |
| μl | Microliter |
| min | Minute |
| miRNA or miR | MicroRNA |

| | |
|-------------------|--|
| ml | Milliliter |
| mRNA | Messenger RNA |
| mRNP | Messenger ribonucleoprotein |
| NEAA | Non-essential amino acids |
| N-terminus | Amino-terminus |
| NaCl | Sodium chloride |
| Neo | Neomycin |
| NFκB | Nuclear factor 'kappa-light-chain-enhancer' of activated B cells |
| ng | Nanogram |
| NGC | No-go-decay |
| NGS | Next-generation sequencing |
| NK cell | Natural killer cell |
| NKT cell | Natural killer T cell |
| NLS | Nuclear localization signal |
| nM | Nanomolar |
| NMD | Nonsense-mediated mRNA decay |
| nts | Nucleotides |
| OCR | Oxidation consumption rate |
| Ox40 | Mouse tumor necrosis factor receptor superfamily, member 4 |
| PAGE | Polyacrylamide gel electrophoresis |
| P-body | Processing body |
| PABP | Poly(A)-binding protein |
| PAN | Poly-A-nuclease complex |
| PBS | Phosphate buffered saline |
| PCR | Polymerase chain reaction |
| PD-1 | Programmed cell death 1 |
| % | Percent |
| pH | <i>Potentia hydrogenii</i> |
| PMA | Phorbol-12-myristate-13-acetate |
| pMol | Picomolar |
| pol | Polymerase |
| polyA | Multiple adenosine monophosphates |
| PRR | Pattern recognition receptor |
| PVDF | Polyvinylidene fluoride |
| qPCR | Real-time quantitative PCR |
| RBD | RNA-binding domain |
| RBP | RNA-binding protein |
| Rck/Ddx6 | DEAD (Asp-Glu-Ala-Asp) box helicase 6 |
| Rc3h1 | Ring finger and CCCH-type zinc finger domains 1 (Roquin-1) |
| Rc3h2 | Ring finger and CCCH-type zinc finger domains 2 (Roquin-2) |
| RING | Really interesting new gene |
| RIP kinase | Receptor-interacting serine-threonine kinase |
| RLR | RIG-I-like receptor |

| | |
|-------------------------------|---|
| RNA | Ribonucleic acid |
| RNP | Ribonucleoprotein |
| RNS | Ribonukleinsäure |
| RPMI | Roswell Park Memorial Institute medium |
| RT | Room temperature |
| San | <i>Sanroque</i> mutation (Roquin M199R) |
| SD | Standard deviation |
| SDS PAGE | Sodium dodecyl sulfate polyacrylamide gel electrophoresis |
| Sec | Seconds |
| SG | Stress granule |
| SLE | Systemic lupus erythemoatosis |
| SOC | Super optimal broth |
| SSC | Side scatter |
| TAC | Tetradecyldimethylbenzylammonium chloride |
| Taq | <i>Thermus aquaticus</i> polymerase |
| TBE | Tris-borate-EDTA |
| TBS | Tris buffered saline |
| TCR | T cell receptor |
| TE | Tris-EDTA |
| TEMED | Tetramethylethylenediamine |
| Temp | Temperature |
| T_{FH} cell | T follicular helper cell |
| TGF-β | Transforming growildtypeh factor beta |
| Th | T helper cell |
| TLR | Toll-like receptor |
| TNF | Tumor necrosis factor |
| Treg | Regulatory T cell |
| TS | Target site |
| TTP | Tristetraprolin |
| TUTase | Terminal uridylyltransferase |
| U | Uracil |
| Upf/UPF | Mouse/human regulator of nonsense transcripts homolog (Yeast) |
| Usp/USP | Mouse/human ubiquitin specific peptidase |
| UTR | Untranslated region |
| V | Volt |
| v/v | Volume per volume |
| Vs. | Versus |
| wildtype | Wildtype |
| Xrn/XRN | Mouse/human exoribonuclease |

1 Introduction

1.1 Post-transcriptional gene regulation

mRNAs transport the genetic information from the nucleus to the cytoplasm of the cell and serve as templates to generate protein products (Hentze, 1991; Zubay, 1963). Their stability is therefore a critical control point in regulating dynamic gene expression (Caponigro & Parker, 1996; Hentze, 1991; Tharun & Parker, 2001). Because of this crucial role intact mRNA molecules are protected during their journey from the nucleus to the cytoplasm primarily by two features (Proudfoot, Furger, & Dye, 2002): First, the 7-methyl guanosine cap structure at their 5' termini that, bound by the cap binding protein complex, prevents degradation from the 5' end. Second, a poly(A) tail at the 3' termini present in all cellular mRNAs except for replication-dependent histone (Marzluff, 2005). The poly(A) tail is bound by poly(A)-binding proteins (PABPs) to ensure protection from the 3' end (Cougot, van Dijk, Babajko, & Seraphin, 2004; Mangus, Evans, & Jacobson, 2003). In addition, both the cap structure and the poly(A) tail function in the enhancement of translation (Gallie, 1991; Tarun & Sachs, 1995). During translation initiation, the 5' cap is recognized by the cap-binding protein eIF4E. With the aid of a second factor, the eukaryotic initiation factor eIF4G, the 40S ribosomes can be recruited to the targeted mRNA (Hershey et al., 1996). Importantly, the 3' poly(A) tail together with the PABP are required for the 60S ribosomal subunit-dependent translation initiation (Sachs & Davis, 1989). Interestingly, eIF4G is able to bridge both ends by interacting with eIF4E and PABP leading to the circularization of the mRNA (Kahvejian, Roy, & Sonenberg, 2001). The circular shape facilitates recycling of ribosomes on the same mRNA and enhances mRNA stability (Kahvejian et al., 2001; Miras et al., 2017). The ribosome flow along a circularized mRNA was shown to be determinant for protein production rates and is described in the so-called ribosome flow model on a ring (RFMR), a model that demonstrates the importance of mRNA circularization in the translational process (Raveh, Zarai, Margaliot, & Tuller, 2015). The associations of mRNAs with ribosomes are called polysomes and are found either free in the cytoplasm or bound to the cytoskeletal or membrane of the cell (Moss, Pryme, & Vedeler, 1994).

Interestingly, mRNAs form ribonucleoproteins (RNP) with RNA binding proteins not only during translation but also under stress conditions or in the course of degradation. Cells that get stressed form stress granules containing protein-bound mRNAs that should neither be translated nor degraded and that can reenter the translational process (Kedersha & Anderson, 2009). Importantly, translational repression is a process that is not only induced under stress conditions but represent a way of regulating gene expression in eukaryotic cells. It involves many proteins of the decay process such as 4E-T, RCK and Pat1b but also CNOT4, one subunit of the CCR-NOT complex (J. Collier & Parker, 2005; Ozgur et al., 2015).

mRNAs targeted for degradation are also found associated with several RNA-binding proteins in distinct foci, so called processing bodies (P-bodies). P-bodies represent the assembly of many proteins involved in the degradation process and are in general very dynamic structures. They assemble or disassemble depending on different cellular processes. Changes of P-body dynamics was observed in T cells and mouse splenocytes, where P-bodies disappeared and reappeared again depending on the availability of nutrition (Aizer et al., 2008). Polysomes, stress granules and P-bodies are the so far known states of mRNAs in eukaryotic cells and represent different ways of regulating gene expression (Balagopal & Parker, 2009). Since the present work deals with mRNA degradation, the most abundantly used decay pathways by eukaryotic cells are described in the following in more detail.

1.1.1 mRNA degradation pathways

mRNA turnover contributes to gene suppression and is therefore highly regulated (Das, Sarkar, & Das, 2017; Fritz, Bergman, Kilpatrick, Wilusz, & Wilusz, 2004; Houseley & Tollervey, 2009). Generally, two types of mRNA degradation exist: deadenylation-independent and deadenylation-dependent mRNA decay. The latter is the most abundant degradation pathway in mammalian cells. For the degradation of bulk mRNAs, two major deadenylation-dependent pathways are known, the 5'-3' and 3'-5' decay pathways. Other specialized pathways target aberrant mRNAs. The nonsense mediated decay (NMD) targets mRNA harboring a stop codon in the middle of the mRNA transcript, so called premature termination codons. mRNAs lacking the termination codon are recognized by the non-stop decay (NSD) pathway (Maquat,

2002; Tourriere, Chebli, & Tazi, 2002; Wilusz, Wang, & Peltz, 2001). The No-go decay (NGD) pathway recognizes and eliminates defective mRNAs, stalled during translation elongation (Harigaya & Parker, 2010). All these processes have the common feature in that they involve nucleases that complete the last step of each decay process. Two major classes of RNases are known to carry out this task: endonucleases that cut internally and exonucleases that, as the name indicates, hydrolyze the RNA from either the 5' end or 3' end (Arraiano et al., 2010). In the following, emphasis will be put on the two major pathways involving exonucleases that involve the deadenylation-step of their target mRNAs as starting point for the decay process.

Deadenylation by which the 3' poly(A) tail gets gradually shortened is the key event that reduces translatability of mRNAs and initiates the degradation process (J. M. Coller, Gray, & Wickens, 1998; J. M. Coller, Tucker, Sheth, Valencia-Sanchez, & Parker, 2001; Decker & Parker, 1993; Tucker et al., 2001; Yamashita et al., 2005). mRNA transcripts exit the nucleus carrying on average a poly(A) tail of ~70 nucleotide length in yeast and of ~200-250 nucleotides (nt) in higher eukaryotes (Sheets & Wickens, 1989; Zhao, Kessler, Helmling, O'Connor, & Moore, 1999). Two highly conserved complexes remove the poly(A) tail gradually in two consecutive phases (Daugeron, Mauxion, & Seraphin, 2001; Tucker et al., 2001). Studies focusing on poly(A) tail lengths revealed that the first phase termed 'initial deadenylation' is relatively slow and results in similar shortening of the poly(A) tail of all observed mRNAs to ~100 nt. This step was shown to be catalyzed by the poly(A) nuclease 2 and 3 (PAN2-PAN3) complex (Decker & Parker, 1993). In the second phase the poly(A) nuclease CCR4-CAF1 complex together with the large scaffolding subunit CNOT1 further hydrolyzes the poly(A) tail to oligo(A) tails of different lengths ranging from 16 nt to 7 nt (Decker & Parker, 1993). Interestingly, impairment of the first phase by inhibiting PAN2 resulted only in a slower deadenylation but did not affect the decay process. The activity of CCR4 and CAF1 however, was shown to be absolutely necessary for complete mRNA degradation, since inactivation of one of the two proteins resulted in the accumulation of partially deadenylated mRNAs (Boeck et al., 1996). After the second deadenylation step PABP can no longer bind to the short (A) tail. The actual mRNA decay process is activated once mRNAs lost the interaction to poly(A) binding proteins (PABPs) and exhibited a weaker interaction with the cap-binding eukaryotic initiation factor 4E (eIF4E). These two key events lead to the decircularization of the targeted mRNA and the reduction of translation efficiency (Schwartz & Parker, 1999, 2000; Tharun & Parker, 2001). Elimination of the mRNA occurs then predominantly

through two alternative pathways: 5'-3' degradation, in which deadenylation is followed by decapping and hydrolysis of the mRNA from 5' end and 3'-5' degradation, which also requires deadenylation to proceed with hydrolysis of the mRNA from 3' end and involves decapping as a last step (Figure 1). In the 5'-3' decay pathway oligoadenylated mRNAs are recognized and bound at their 3' ends by the heteroheptameric Lsm1-7 ring together with its interaction partner Pat1b. These interactions concurrently lead to the recruitment of decapping enzymes and prevent the binding of the exosome to the same mRNA (He & Parker, 2001). In addition to Lsm1 and Pat1b, other factors were identified as activators of the decapping process *in vivo*, such as the helicase RCK and Edc proteins (Beelman et al., 1996; Boeck, Lapeyre, Brown, & Sachs, 1998; Bouveret, Rigaut, Shevchenko, Wilm, & Seraphin, 2000; Dunckley & Parker, 2001; Fischer & Weis, 2002; Wyers, Minet, Dufour, Vo, & Lacroute, 2000). Decapping is in general a strongly controlled step that can be influenced by several factors and is antagonistic to the translation process (Caponigro & Parker, 1995; J. Coller & Parker, 2004; J. M. Coller et al., 1998; Gao, Wilusz, Peltz, & Wilusz, 2001; Khanna & Kiledjian, 2004; Schwartz & Parker, 1999). The cap structure at the 5' end, which was protected during the translation process by the initiation factors eIF-4E and eIF-4G is then removed by DCP2 (Fillman & Lykke-Andersen, 2005; Jacobson, 2004; Long & McNally, 2003; Piccirillo, Khanna, & Kiledjian, 2003). Interestingly, DCP2 activity was shown to be dependent on the stimulation by DCP1 (She et al., 2004). The cap-less mRNA becomes easily accessible for the exonuclease XRN1 that eventually performs the degradation step (Stevens, 2001; Tharun & Parker, 1999; Tourriere et al., 2002). Importantly, decapping factors and the exonuclease XRN1 are in close proximity during this process. This is achieved by the newly described eIF4E-transporter protein (4E-T), a factor that binds eIF4E to bridge the 5' and 3' termini of the mRNA and thereby mediate circularization. 4E-T contains nuclear localization and export-signals and was originally described to function in shuttling eIF4E to the nucleus and eIF4E to P-bodies, therefore 'transporter protein' (Dostie, Ferraiuolo, Pause, Adam, & Sonenberg, 2000; Ferraiuolo et al., 2005). Interestingly, 4E-T interacts with proteins of the translation as well as degradation machineries and was shown to reduce the availability of eIF4E levels and thereby inhibiting the general protein synthesis (Nishimura et al., 2015).

In the absence of the Lsm1-7 complex mRNAs can be targeted by the exosome, a macromolecular machine of ring-shaped structure that consists of many different proteins. Once bound by the exosome, mRNAs are degraded from their 3' ends

(Anderson & Parker, 1998; Mitchell, Petfalski, Shevchenko, Mann, & Tollervey, 1997; Tharun, 2009b). The cap at the 5' end gets then cleaved by the decapper DCP Scavenger (DcpS) (Allmang et al., 1999; N. Chen, Walsh, Liu, Parker, & Song, 2005). Interestingly, in vitro studies of the exosome in mammalian cells showed also its role in mediating the efficient degradation of mRNAs bearing AU-rich elements (C. Y. Chen et al., 2001; Mukherjee et al., 2002).

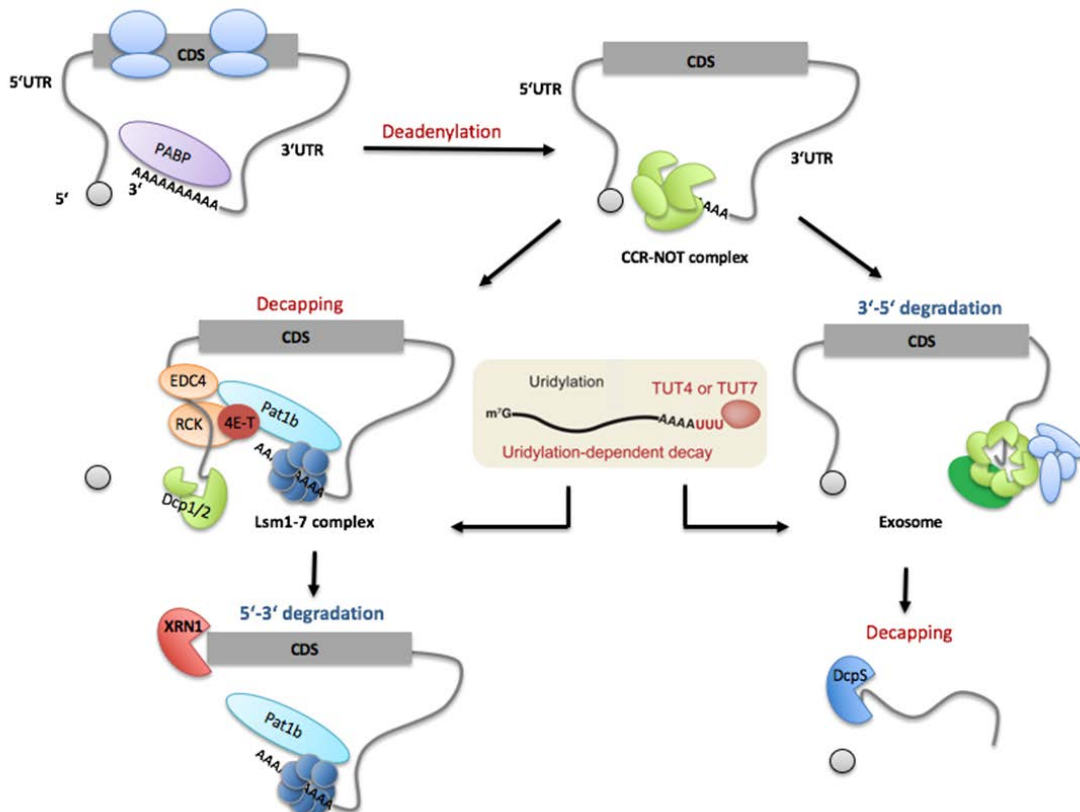


Figure 1: Scheme of mRNA degradation pathways after deadenylation.

Deadenylation represents the starting point of the degradation process. The shortening of the poly(A) tail to an oligo(A) tail results in the removal of the Poly(A)-binding protein (PABP) and the decircularization of the targeted mRNA. Degradation occurs through two optional pathways, the 5'-3' or the 3'-5' decay pathway. The exonucleases XRN1 or the exosome perform the degradation step, respectively.

Recent studies extended the described pathways by a newly discovered modification, the so-called oligouridylation of mRNAs that additionally marks deadenylated mRNAs for degradation (Lim et al., 2014; Norbury, 2010). This type of mRNA modification was noticed first on miRNAs and histone mRNAs and was only recently suggested as a major process that most probably targets almost all mRNAs present in the cell (Mullen

& Marzluff, 2008; Shen & Goodman, 2004; Su et al., 2013). In contrast to polyadenylation, oligouridylation decreases the stability of the targeted mRNA resulting in its rapid decay. This is catalyzed by enzymes called Tutases and happens after deadenylation of the mRNA. The two 3' terminal uridylyl transferases TUT4 and TUT7 were shown to catalyze mRNA oligouridylation in mammalian cells (Lim et al., 2014). This mark was suggested to target mRNAs for rapid turnover by attracting the decay machinery and distinguishing uridylated mRNAs from a pool of oligoadenylated mRNAs in the cytoplasm. Interestingly, knockout of TUT4 and TUT7 in somatic cells did not result in drastic phenotypes, indicating that oligouridylation is an alternative instrument for mRNA decay, pointing to the compensatory function of oligouridylation, being an alternative way of mRNA decay process. Similar to oligoadenylated mRNAs oligouridylated mRNAs were shown to be recognized by both the Lsm1-7 complex triggering 5'-3' decay but also degraded by the exosome-dependent in a 3'-5' direction (Norbury, 2010). Very recently 3' uridylation was also described in the activation process of CD4⁺ T cells influencing the stability and function of miRNAs (Gutierrez-Vazquez et al., 2017). Although very similar in function, protein complexes and enzymes involved in the two pathways are found in different locations in the cell. While catalyzer of the 5'-3' pathway assemble in P-bodies, proteins of the 3'-5' pathway are not enriched in distinct foci (Ingelfinger, Arndt-Jovin, Luhrmann, & Achsel, 2002; Sheth & Parker, 2003; Teixeira & Parker, 2007; Teixeira, Sheth, Valencia-Sanchez, Brengues, & Parker, 2005). The fact that not only enzymes of the 5' to 3' decay pathway exist in P-bodies but also the components of the two poly(A) nuclease complexes, PAN2, PAN3, CCR4 and CAF1, combines all factors of the decay pathway except for the exosome in one active center within the cytoplasm. This might be the reason, that cells favor the degradation of mRNAs via the 5' to 3' pathway over the 3'-5' pathway (J. Coller & Parker, 2004; Sheth & Parker, 2003). This idea is further supported by the presence of eIF4E in P-bodies (Andrei et al., 2005). Generally, the order of recognition of the target mRNA by different proteins of the P-body is still strongly discussed and is subject of many studies. Some suggest the assembly of two preexisting complexes: The Dcp1/Dcp2/RCK/Edc3 complex and the Pat1/XRN1/Lsm1-7 complex (Bouveret et al., 2000; Fenger-Gron, Fillman, Norrild, & Lykke-Andersen, 2005; Gavin et al., 2006; Teixeira & Parker, 2007; Tharun & Parker, 2001). These two complexes than bind target mRNAs and assemble to large RNA-protein complexes (Nissan, Rajyaguru, She, Song, & Parker, 2010; Pilkington & Parker, 2008). In other studies, the link between translation and degradation has been

interpreted such that oligoadenylated mRNAs are already bound or in contact with a decay-factor while still being associated with polysomes. This model further suggests an influence of the polysome-associated decay factor on the P-body formation or size, since it guides the targeted mRNA to P-bodies. Pat1b was suggested for this task, since it was found associated with the translational machinery and present in P-bodies. Pat1b-binding proteins include RCK, Edc3 and Edc4 as well as CCR4-NOT, Dcp1/2 and XRN1 (Ayache et al., 2015; Braun et al., 2010; Haas et al., 2010; Ozgur, Chekulaeva, & Stoecklin, 2010). Importantly, deletion of Pat1b decreases the size of P-bodies supporting this theory (Sheth & Parker, 2003). In a very recent study, Vindry and colleagues demonstrated an additional new role of Pat1b in human cells in the splicing process. They showed the localization of Pat1b also in the nucleus of the cell as interaction partner of Lsm2-8 (Vindry et al., 2017). Whether Pat1b stays associated to the same mRNA until its transport to the cytoplasm is not clear yet. The list of proteins that associate with mRNAs during induced mRNA decay, besides Pat1b, is growing but only those proved to be critical are described in the following passage.

1.1.2 Proteins involved in the different mRNA decay processes

mRNA decay is complex and involves different proteins that are crucial in the maintenance of appropriate mRNA levels in the cell. Some crystal structures of proteins that are known to catalyze different steps in the degradation process have been presented already, such as the exosome or the DcpS scavenger decapping complex (N. Chen et al., 2005; Makino, Baumgartner, & Conti, 2013). Others like the Lsm1-7-Pat1 or Dcp1-Dcp2 were only very recently solved (Mugridge, Ziemniak, Jemielity, & Gross, 2016; Sharif & Conti, 2013). Their roles in ensuring the elimination of specific mRNAs were intensively studied during the last few years. Here, the structure, composition and mode of function of some of these proteins that are of interest for this project are described in more detail.

1.1.2.1 The Lsm1-7 complex

The Lsm1-7 complex is evolutionarily conserved and functions in the decay process of mRNAs by connecting mRNA deadenylation to decapping. Lsm (Sm-like) proteins are a family of small RNA-binding proteins with sizes between 8 and 28 kDa, present in all

cell types (Bouveret et al., 2000; Salgado-Garrido, Bragado-Nilsson, Kandels-Lewis, & Seraphin, 1999). As their names indicate, Lsm proteins are “like Sm” proteins because of their similarities in domain structure (Seraphin, 1995). Sm proteins were first identified as antigens targeted by anti-Sm specific antibodies in a nuclear extract of a patient suffering from the autoimmune disease systemic lupus erythematosus (SLE) named Stephanie Smith, therefore the designation Sm proteins (Lerner & Steitz, 1979; Tan, 1989). The Sm protein family consists of eight small proteins that are all involved in the maturation process of small nuclear RNAs (snRNAs) being thereby important for the splicing of nuclear pre-mRNAs (Kambach et al., 1999). By using X-ray crystallography, the structure of the Sm polypeptides within the Sm domain could be identified (Kambach et al., 1999). The common domain of Sm and Lsm proteins is characterized by an identical folding pattern, with an N-terminal alpha-helix and five stranded antiparallel beta-sheets (Anantharaman & Aravind, 2004; Hermann et al., 1995; Seraphin, 1995; Zhou et al., 2014). This conserved region is also responsible for the interactions of the Sm proteins among each other (Hermann et al., 1995; Kambach et al., 1999). Although very similar in composition, the assembly of Sm- and Lsm proteins to complexes occur differently. Sm proteins require snRNAs to form a heptameric ring around it and bind the central part of the snRNAs. Lsm proteins, in contrast can assemble spontaneously in the absence of target RNAs and bind to the 3' end of the target mRNA. They form two different heteroheptameric Lsm complexes i.e. the Lsm1-7 and Lsm2-8 complexes. Similar to Sm proteins, the Lsm2-8 complex is present in the cell nucleus and functions in the pre-mRNA splicing as part of the U6 snRNP (Achsel et al., 1999; Mayes, Verdone, Legrain, & Beggs, 1999; Vidal, Verdone, Mayes, & Beggs, 1999). The Lsm2-8 ring shows very strong similarity in shape and size to complexes of the canonical Sm proteins, as was observed using electron microscopy (Achsel et al., 1999; Zhou et al., 2014). However, unlike Sm proteins that are located only in the nucleus of the cell, Lsm complexes are also present in the cytoplasm, where the Lsm1-7 complex is enriched in P-bodies (Ingelfinger et al., 2002; Lykke-Andersen, 2001; Sheth & Parker, 2003) (Figure 2).

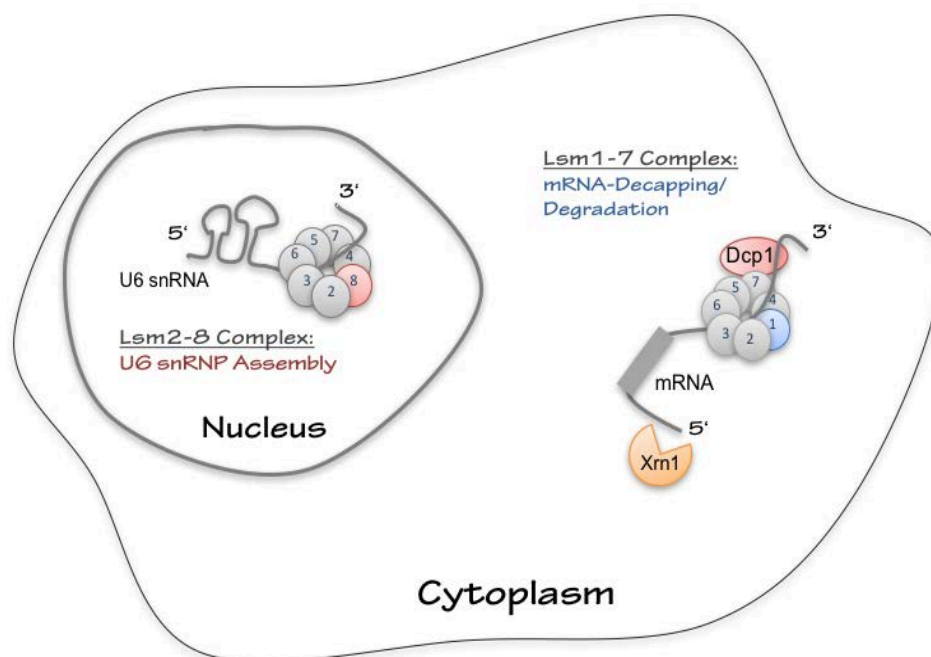


Figure 2: The two Lsm complexes in the eukaryotic cell.

Two Lsm complexes are located differently in the eukaryotic cell. The Lsm1-7 complex is a cytoplasmic heptameric ring that binds oligoadenylated and oligouridylated mRNAs leading to their decapping and subsequent degradation. The Lsm2-8 complex is located in the nucleus of the cell where it is associated with the U6-snRNA and involved in the splicing process.

Since this study is dealing with the decay of mRNAs in the cytoplasm of the cell, specifically with the Lsm1 subunit of the cytoplasmic Lsm1-7 ring, the focus in the following is set on the Lsm1-7 complex. Studies of the Hfq protein, the homolog of the Lsm1-7 complex and the only Sm family member in bacteria helped to understand structure and function of the Lsm1-7 ring (Hajnsdorf & Regnier, 2000; Mikulecky et al., 2004; Schumacher, Pearson, Moller, Valentin-Hansen, & Brennan, 2002; Zhang, Wassarman, Ortega, Steven, & Storz, 2002). Although the two complexes are similar in that they both can form ring structures, Hfq was shown to only form homomeric hexamers while Lsm complexes contain 7 heteromeric subunits. Lsm proteins are organized with Lsm 1-2-3-6-5-7-4 topology (Sharif & Conti, 2013). Within the ring, especially the Lsm1 subunit shows a unique structural feature. The structure of the Lsm1-7 ring in *S. cerevisiae* revealed that among all Lsm proteins, Lsm1 was the only subunit containing an extension, which partially blocks the central hole of the ring structure, thereby preventing mRNA from exiting the complex (Figure 3). This 57-amino acid long C-terminal overhang is required in addition to the Sm domain for the functioning of the ring in RNA-binding and oligomerization. Mutations or deletions in this part of Lsm1 led to impaired mRNA decay *in vivo* underlining its importance in

this pathway (Chowdhury, Kalurupalle, & Tharun, 2016). Interestingly, Lsm1 is the only subunit that interacts not only with the two neighboring Lsm proteins Lsm2 and Lsm4 but contacts also Lsm3 and Lsm6 (Zhou et al., 2014). Functionally, Hfq and Lsm1-7 complexes are connected to RNA processing. Both interact with 3' ends of RNAs with preference for oligo(A) and oligo(U) tails. Interestingly, the binding induces also to degradation by recruiting proteins that first initiate decapping, which is followed by hydrolysis (He & Parker, 2001). In addition, both complexes inhibit the 3'-5' decay pathway by preventing exonucleases from binding at the 3' end. Hfq is known to block the Polynucleotide Phosphorylase (PNPase) and Lsm1-7 inhibits the exosome (Link, Valentin-Hansen, & Brennan, 2009; Tharun, 2009a). Interestingly, Hfq targets RNAs with longer poly(A) tails whereas Lsm1-7 favors oligo-adenylated mRNAs over poly-adenylated transcripts (Chowdhury, Mukhopadhyay, & Tharun, 2007; Sauer, 2013; Schumacher et al., 2002). Contrary to the Lsm1-7 ring, Hfq is also able to recognize A-rich sequences located internally (Zhang et al., 2002). To recognize target mRNAs, both Hfq and Lsm1-7 need to interact with other proteins, Hfq with PAPI and PNPase as well as the Rnase E and Lsm1-7 in the first place with Pat1b (Chowdhury, Kalurupalle, & Tharun, 2014; Folichon et al., 2003; Hajnsdorf & Regnier, 2000). Lsm2 and Lsm3 components mediate complex formation of the Lsm ring with Pat1b (Wu et al., 2014). To effectively bind the target mRNA residues from both Pat1b and Lsm1-7 cooperate (Chowdhury et al., 2014). Importantly, Pat1b is not only a direct interaction partner of the Lsm1-7 ring, but it additionally interacts with the CCR4-NOT deadenylase complex linking thereby deadenylation to decapping (Braun et al., 2010; Haas et al., 2010).

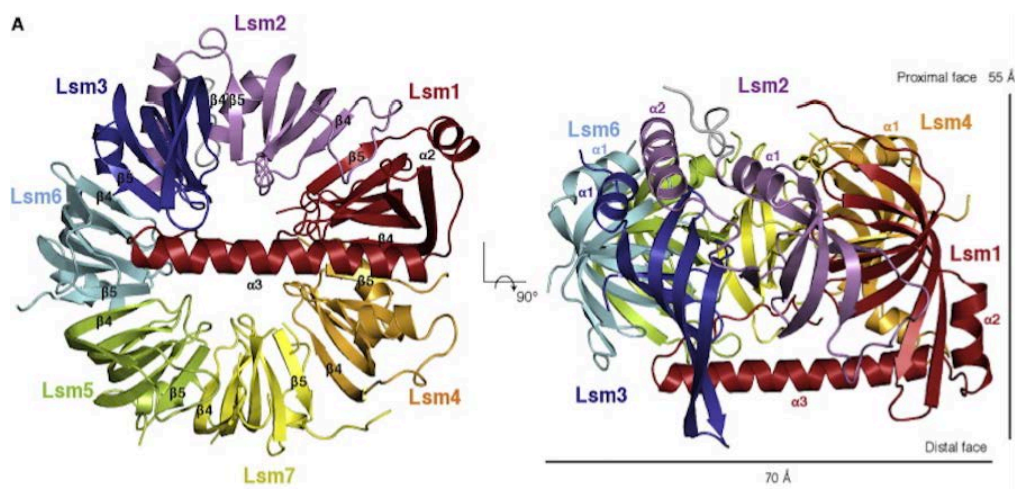


Figure 3: Crystal structure of the Lsm1-7 ring in *S. cerevisiae* (Sharif & Conti, 2013).

Another interaction partner of Lsm1-7 is the exonuclease Eri1. In studies of the decay process of histone mRNAs, the subunit Lsm1 was found to be associated with Eri1, being present in a complex together with the stem-loop-binding protein (SLBP) (Herrero & Moreno, 2011; Hoefig et al., 2013; Mullen & Marzluff, 2008). Involvement of the Lsm1-7 complex in the degradation of this special class of mRNAs in addition to oligouridylated and oligoadenylated mRNAs reaffirms the importance of this complex in the general mRNA decay process in the cell. Cell cycle-regulated histone mRNAs are special and unique in that they do not contain poly(A) tails at their 3' end. Instead, they possess a highly-conserved stem-loop structure that is bound by SLBP. At the end of the S phase these mRNAs are oligouridylated and rapidly degraded. Interestingly, Lsm1-7 was shown to also be important in the ARE-mediated decay (AMD) pathway, the process by which mRNAs carrying AU-rich elements are degraded. The group of Stoecklin found that the knock down of Lsm1 inhibited AMD and caused increased levels of the tested ARE-containing mRNAs underlining a special role of Lsm1 in the degradation of ARE-containing mRNAs (Stoecklin, Mayo, & Anderson, 2006).

Importantly, Lsm1-7 performs another task in addition to the degradation of mRNAs in the cell. Its role in controlling translation and replication of single-stranded RNA viruses in infected cells was shown in several studies (Diez, Ishikawa, Kaido, & Ahlquist, 2000; Mas, Alves-Rodrigues, Noueir, Ahlquist, & Diez, 2006; Noueir, Diez, Falk, Chen, & Ahlquist, 2003). Lsm1 contributes to the replication process by binding to regulatory elements on the viral positive-strand RNA. Studies of the Brome mosaic virus (BMV) replication in yeast revealed that the Lsm1-7-Pat1 complex binds to the RNA and thereby influences viral RNA translation (Galao et al., 2010; Jungfleisch, Chowdhury, Alves-Rodrigues, Tharun, & Diez, 2015). By using a system that allows the replication of the insect flock house virus (FHV) in yeast cells, it could be demonstrated that replication was regulated by Lsm1 (Gimenez-Barcons et al., 2013). Another positive-stranded RNA virus that needs interaction with Lsm1 for successful replication is the Dengue virus (Dong et al., 2015). Binding of Lsm1 to the 3' UTR of the virus RNA enhances the replication process and was demonstrated to take place in P-bodies. The replication of the hepatitis C virus (HCV) was likewise demonstrated to be Lsm1-dependent and, in addition, involved the miR-122 (Roberts, Doidge, Tarr, & Jopling, 2014; Scheller et al., 2009). The Lsm1-7 complex as regulator of viral mRNA is not very surprising, since other proteins present in P-bodies such as RCK were also implicated in the replication of many RNA viruses like the BMV, West Nile virus, poliovirus and HCV (Beckham & Parker, 2008; Chahar, Chen, & Manjunath, 2013).

1.1.2.2 The Trans-acting factors TTP, Roquin-1 and Regnase-1

One very special group of RNA binding proteins are the Cys-Cys-Cys-His (CCCH) zinc finger proteins (Maeda & Akira, 2017). The Zinc finger protein family consists of nearly 60 members that are characterized by one or more CCCH zinc finger domains (Liang, Song, Tromp, Kolattukudy, & Fu, 2008) (Figure 4). Member of this protein family contain a zinc finger domain that recognizes specific secondary structures in the 3' UTR of target mRNAs. The functions of many of them have not been determined, yet. By contrast, some of them were studied intensively and were shown to be crucial regulator of immune responses such as tristetraprolin (TTP), Roquin-1 and MCPIP1 or also called Regnase-1 (Figure 4).

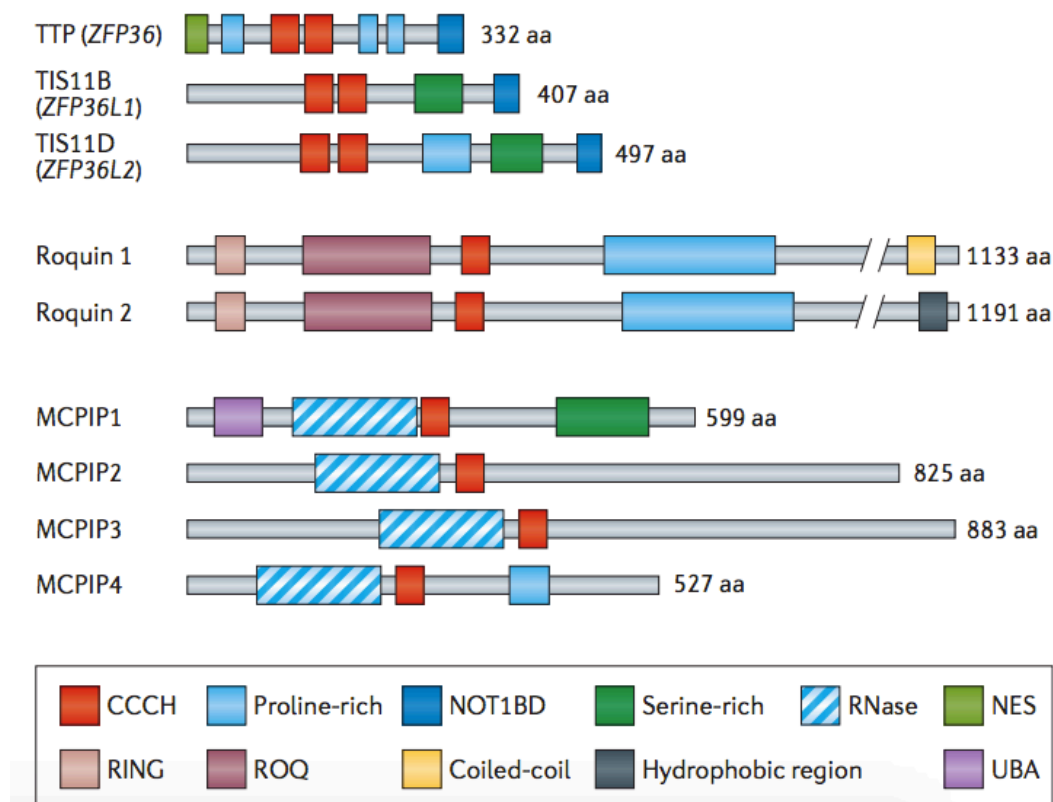


Figure 4: Schematic structures of human TTP, Roquin and the MCPIP protein families (taken from Fu M; Blakeshear PJ, 2017).

One common feature of TTP, Roquin-1 and Regnase-1 is the recognition of characteristic sequences and secondary structures in the 3' UTR of target mRNAs. In contrast to TTP and Roquin-1, Regnase-1 is itself an endonuclease that can internally

cleave mRNAs after binding to specific *cis*-elements in their 3' UTR (Matsushita et al., 2009). Emerging evidence suggests that these three proteins control immune homeostasis by regulating their target mRNAs and modulating multiple signaling pathways in immune cells. Thus, mice carrying mutation in those genes or a genetic null allele suffer from severe autoimmune diseases. The known target mRNAs of these individual trans-acting factors, their recognized elements, the mode of induced mRNA decay as well as the consequences of their loss-of-function will be discussed in the following passages.

1.1.2.2.1 *Tristetraprolin (TTP)*

Tristetraprolin (TTP) is the best-characterized ARE-binding protein. It was first identified by Lai and colleagues as an insulin-stimulated gene and was some years later described as part of a negative feedback loop that post-transcriptionally regulates TNF production (Carballo, Lai, & Blackshear, 1998; Lai, Stumpo, & Blackshear, 1990). TTP contains tandem CCCH zinc finger domains, three proline-rich domains and a carboxy-terminal sequence that was shown to bind NOT1 (Fabian et al., 2013)(Figure 4). TTP shuttles from the nucleus to the cytoplasm, involving a nuclear export sequence (NES) present at its amino terminus (Phillips, Ramos, & Blackshear, 2002) (Figure 4). The CCCH tandem motif of TTP was shown to recognize specific ARE elements in the 3' UTR of mRNAs and thereby inducing deadenylation and subsequent degradation of target mRNAs (Lai, Carballo, Thorn, Kennington, & Blackshear, 2000). *Tnf* alpha mRNA is the best-described target mRNA of the TTP protein. Interestingly, TTP also interacts with the exonuclease XRN1 and the heterodimeric decapping complex Dcp1 and Dcp2. Once phosphorylated it also interacts with the exosome (C. Y. Chen et al., 2001).

1.1.2.2.2 *Roquin and Regnase-1*

Another well-characterized RNA-binding protein of the family of (CCCH) zinc finger proteins is the E3 ubiquitin ligase Roquin-1 (*Rc3h1*). Roquin-1 was identified in 2005 in an ENU (N-ethyl-N-nitrosourea) mutagenesis screen in the group of Chris Goodnow testing for the spontaneous development of anti-nuclear antibodies (Vinuesa et al., 2005). Roquin-1 contains a single CCCH zinc finger domain, a RING (Really Interesting New Gene) finger domain, a ROQ domain and proline-rich region (Yu et al., 2007)

(Figure 4). By regulating ICOS expression, Roquin-1 was described as a crucial regulator of T_{FH} cell differentiation and repressor of autoimmunity (Linterman et al., 2009). The ROQ domain recognizes the stem-loop-forming constitutive decay element (CDE) in the 3' UTR of target mRNAs, while additional interactions of Roquin-1 with the CCR4/NOT1 complex as well as with Edc4 and the helicase RCK induces the degradation of the mRNA (Leppek et al., 2013; Murakawa et al., 2015; Sgromo et al., 2017; Stoecklin, Lu, Rattenbacher, & Moroni, 2003; Vogel et al., 2013). By using SELEX (systematic evolution of ligands by exponential enrichment) assays, a novel U-rich hexaloop motif was identified as an alternative decay element (ADE) recognized by Roquin (Janowski et al., 2016). The interaction of Roquin-1 with the CCR4-CAF1-NOT complex was shown to first induce deadenylation leading to decapping and subsequent degradation of target mRNAs from their 5' end. More and more mRNA targets of Roquin-1 were identified; most importantly in addition to *ICOS* are *OX40* and *TNFA* (Leppek et al., 2013; Mino et al., 2015). During T cell activation Roquin is cleaved by a paracaspase called MALT1 resulting in the upregulation of all so far known Roquin targets (Jeltsch et al., 2014). Loss of Roquin-1 in mice causes very early death due to impaired lung development and a caudal spine defect (Bertossi et al., 2011). When the gene was deleted in the whole hematopoietic system the mice exhibited elevated ICOS levels on $CD4^+$ and $CD8^+$ T cells, expansion of macrophages, eosinophils and most significantly effector-like $CD8^+$ T cells. In subsequent experiments, the paralog of Roquin-1 named Roquin-2 was suggested to carry out the task when Roquin-1 was absent and thereby preventing the generation of the autoimmune disease (Pratama et al., 2013). Deletion of alleles encoding Roquin-2 encoding resulted in no immune phenotypes compared to Roquin-1 deficient mice, nevertheless it caused postnatal lethality (Vogel et al., 2013). In contrast, combined deletion of Roquin-1 and Roquin-2 encoding alleles in T cells caused massive T cell activation and very high levels of ICOS as well as excessive T_{FH} cell production. However, ANAs could not be detected in this case potentially because of the observed destroyed spleen architecture (Pratama et al., 2013; Vogel et al., 2013). Regnase-1 or MCP1P1 is another important CCCH zinc finger domain containing protein that, similarly to Roquin proteins, is also cleaved by MALT1 during T cell activation. Interestingly, both Roquin and Regnase-1 share common target mRNAs and were shown to cooperatively repress them (Jeltsch et al., 2014). In total 4 MCP1P proteins exist in the cell (Figure 4). Liang and colleagues for the first time identified MCP1P1 in 2008 as a negative regulator of inflammatory activation in macrophages (Liang et al., 2008). It contains a PIN domain-

like RNase domain, an ubiquitin-associated domain and a serine-rich region (Figure 4). In Monocytes, Regnase-1 promotes the decay of the cytokine mRNAs IL-6 and IL-12B and it targets c-Rel, Ox40 and IL-2 transcripts in T cells (Jeltsch et al., 2014; Mino et al., 2015).

All these examples illustrate the importance of intact post-transcriptional gene regulation systems especially in the context of the rapid adaptation to changes in cellular environment and the critical roles of these proteins. The link between RBPs, their targets and the development of autoimmunity will be discussed in the following section.

1.2 mRNA metabolism in innate and adaptive immunity

1.2.1 The innate and adaptive immune system

The immune system is a complex network consisting of many different immune cells from the bone marrow, thymus and the lymphatic system that communicate either by direct physical contact or indirectly by releasing their specific cytokines. According to the specificity of the defense mechanism, the immune system is divided into two categories: the non-specific innate immunity and the antigen-specific adaptive immunity. The immune system includes also the so-called complement system consisting of about 25 proteins circulating in the blood that functions in the inflammatory response by activating a cascade of proteolytic reactions only on the microbial surface leading to pathogen opsonization and the attraction of phagocytic cells (Nesargikar, Spiller, & Chavez, 2012). The innate immune system is activated immediately after the recognition of a foreign antigen in the body (Ausubel, 2005). Protection is mainly ensured here by three inflammatory cell types: the phagocytic macrophages, dendritic cells and neutrophils. These tissue-resident immune cells carry different pattern recognition receptors (PRRs) that identify surface structures of invading pathogens (Janeway & Medzhitov, 2002). One special group of PRRs that recognizes different microbial components are the Toll-like-Receptors (TLRs). Binding of TLRs to respective ligands, for example double stranded RNA to TLR3 or LPS to TLR4, activates different intrasignaling pathways (Kawai & Akira, 2010). Pathogens that survived the first line of defense need to face the second line of defense, the adaptive immune system. The main differences between the innate and the adaptive

immune response are the specificity and the memorization of the adaptive immune response compared to the innate immune response. The specificity of the adaptive system is produced by a process called somatic V(D)J recombination. In contrast to PRRs, receptors of B and T cells, the two main types of lymphocytes of the adaptive immune system are encoded by different gene segments. The variable (V), diversity (D) and joining (J) gene segments get rearranged during cell-maturation by RAG1 and RAG2 proteins (recombination activating genes) resulting in an enormous repertoire of antigen receptors (Grawunder, Zimmer, Fugmann, Schwarz, & Lieber, 1998). Naïve B cells that detect and bind a specific antigen with the membrane-bound antibody divide quickly and differentiate to become either memory B cell or an effector B cell (plasma cell), which produces and release antibodies against the bound antigen (Estep et al., 2013). Importantly, helper T cells that express CD4 and cytotoxic T cells that express CD8, two mature forms of T cells carry T cell receptors (TCR) that need MHC (Major Histocompatibility Complex) molecules to recognize antigens. During their maturation, T cells are exposed to several self-molecules and undergo two selection processes to ensure the effective binding and detection of the corresponding antigen and the elimination of self-reactive cells (Shortman, Egerton, Spangrude, & Scollay, 1990). The first selection process ensures the functioning of the recognition capacity of matured cells. The second selection process prevents the immune system from attacking own healthy tissues and is known as immune tolerance. Besides this type of tolerance, also referred to as central tolerance it exists a peripheral tolerance, called clonal anergy, where lymphocytes that circulate in the body are kept silenced and can only respond and become active in the presence of chemical signals (Bullock, 1976). In addition, there is a special subgroup of T cells, regulatory T cells (Tregs) that contributes to the maintenance of the immune tolerance by preventing the activation of other T cells. Consequences of absence of Tregs were visible in *scurfy* mice that carried mutations in the transcription factor Foxp3 (Brunkow et al., 2001). Yet, not only Tregs play a crucial role in an appropriate immune response. Failure in the activation of other CD4⁺ T cells resulted also in inappropriate immune reactions against own tissues. CD4⁺ T cells are divided into different subsets, characterized according their cytokines: Th1 (IFN- γ) that is involved in the immune response against intracellular parasites, Th2 (IL-4) that mainly developed during infections with helminths are counter regulated. A relatively newly discovered subset is Th17 (IL-17). Especially, Th1 and Th17 cells are important modulator of the immune response and play crucial roles in autoimmunity (Zhu & Paul, 2008).

1.2.2 mRNA metabolism and autoimmunity

The link between the development of autoimmune diseases and ribonucleoproteins (RNPs) was first described in association with the 'Sm' autoantigens. By using antibodies from the patient Stephanie Smith who suffered from systemic lupus erythematosus (SLE), it was clear that this patient produced autoantibodies against self-antigens (Tan, Schur, Carr, & Kunkel, 1966). Two kinds of autoimmune diseases exist: organ-specific and systemic autoimmune diseases (Ikehara et al., 1990). In contrast to the organ-specific autoimmune disease, where antibodies are produced against one specific organ in the host, in systemic autoimmunity, autoimmune responses are directed against self-antigens present in several organs and tissues in the patient body. Therefore, patients suffering from systemic autoimmune diseases produce many different autoantibodies. However, the most common autoantibody found in the sera of SLE patients is directed against double stranded DNA (dsDNA). The disorder behind the production of antibodies against own tissues and the responsible failure in the defense mechanisms is complex and is the subject of many studies. Some of the interesting studies investigating causes of the development of autoimmune diseases in the innate and adaptive immune responses are described in more detail in the following passage.

1.2.3 mRNA metabolism in the innate immune system

One very exciting defense mechanism is the detection of viral RNA or DNA within a virus-infected cell, which involves a central exonuclease of the degradation pathway, the exosome (Sanchez et al., 2016). Innate immune sensors need to distinguish foreign nucleic acid from the cellular RNA and DNA. This task is challenging and mistakes in the self/non-self-discrimination process have serious consequences for the host. For the two different classes of nucleic acids in the cell DNA and RNA, two sensor mechanisms exist that rely on unique structural features in the viral nucleic acids to take the right decision (Goubau, Deddouche, & Reis e Sousa, 2013). One important family of pattern recognition receptors is the RIG-I-like receptors or short RLRs. The RLR family consists of three different receptors, retinoic acid-inducible gene I (RIG-I); melanoma differentiation-associated gene 5 (MDA5) and laboratory of genetics and physiology 2 (LGP2) that are expressed in immune cells but also non-immune cell

types (Kowalinski et al., 2011). The so-called interferon stimulatory DNA (ISD) pathway is activated when foreign double-stranded DNA is detected. Little is known about the mechanism by which the detection occurs but recent published data suggest a sequence-independent recognition of DNA (Barber, 2014). The detection of foreign nucleic acid that leads to the activation of the immune system needs to be regulated to prevent aberrant responses. For both sensors, mechanisms were identified that negatively regulate the sensing pathway (Eckard et al., 2014). Trex1 is an ISD binding protein that negatively regulates the ISD pathway thereby preventing the initiation of autoimmunity (Achleitner et al., 2017). More recently also the exonuclease that limits the activation of RLRs could be identified. The exosome subunit Skiv2L RNA helicase catabolizes endogenous RNA resulting in a negative regulation of RLRs (Eckard et al., 2014). Interestingly; patients suffering from the rare disease tricohepatoenteric syndrome carried loss-of-function mutations in *SKIV2L* and showed a strong type I IFN signature (Fabre et al., 2012). The IFN signature caused by *SKIV2L* deficiency in peripheral blood cells of THES patients underlie the relevance of the degradation element *SKIV2L* of the exosome to human disease. Although THES patients do not develop autoimmunity despite the strong IFN signature, this very important link between an element of the degradation system and the development of a human disease illustrates the relevance of those proteins in influencing immune responses.

1.2.4 mRNA metabolism in the adaptive immune system

Another example of an RNA binding protein that regulates the stability of its target RNAs and which was shown to be crucial for the course of the adaptive immune response is the protein Roquin-1. One single mutation in the gene *Rc3h1* that encodes for Roquin-1 resulted in the amino acid exchange M199R. Mice carrying this mutation are called *sanroque* mice and show severe autoimmunity. They develop hypergammaglobulinemia, anemia and autoimmune thrombocytopenia, as well as autoimmune arthritis (Pratama et al., 2013; Yu et al., 2007). T cell activation, excessively high levels of ICOS on T cells, T_{FH} cell expansion, spontaneous germinal center formation and production of anti-nuclear antibodies (ANAs) in mice are linked to the observed phenotypes (Vinuesa et al., 2005). The generation of ANAs was proposed to result from increased activity of T_{FH} cells, stimulating B cells reactive against self-antigens in the germinal center reaction (Linterman et al., 2009; Vinuesa

et al., 2005). In addition, T cell-transfer experiments revealed that the observed phenotype is T cell-intrinsic (Linterman et al., 2009).

Similar observations were made in mice lacking Regnase-1. Except for glomerulonephritis, Regnase-1 deficient mice resemble to the *sanroque* phenotype. Since Regnase-1 also regulates mRNA transcripts that encode cytokines and chemokines such as IL-6, depletion of it in the mouse led to increased levels of those inflammatory cytokines accompanied by hyperactivated T cells, infiltration of lymphocytes into lung and other organs, disruption of the splenic architecture, production of ANAs and eventually the development of a spontaneous autoimmune disease (Matsushita et al., 2009).

Another well described example of autoimmunity caused by the absence of an RNA-binding protein and the accumulation of its target mRNA in immune cells is the TTP-KO mouse. TTP binds the 3' UTR of the Tnf mRNA leading to its instability and subsequent degradation. Because of the missing TTP that normally binds and regulates Tnf alpha mRNA decay, mRNA levels were abnormally increased. This finding was first observed in TTP-KO macrophages that were stimulated with LPS and treated with actinomycin D to stop transcription. In those cells, Tnf mRNA was found to be degraded more slowly than in wildtype (Mijatovic et al., 2000). Many other mRNA transcripts encoding for cytokines have been reported to be also targets of TTP such as IL-2, IL-6, IL-10, IFN- γ as well as mRNAs encoding chemokines such as Cxcl 10 or Gdf 15 (Datta et al., 2008; Ogilvie et al., 2005; Stoecklin et al., 2008; Tiedje et al., 2016). TTP deficient mice exhibited arthritis, inflammation and autoimmunity. This example again emphasized the importance of proper functioning of post-transcriptional gene regulation for the cell and for the whole organism.

These examples of proteins involved in the degradation process of RNAs and in the prevention of autoimmune diseases underscore their importance and raise the question whether other members of the decay machinery play similar roles.

2 Aim of the project

The Lsm1-7 ring functions in the decay of mRNAs in yeast, human and plant cells and as very recently shown also in algae. By binding to the 3' UTR of mRNAs the Lsm1-7 complex induces decapping and degradation of its targets. The ability to recognize and bind oligo-A and oligo-U stretches makes the Lsm1-7 complex a general inducer of the mRNA decay. Although previous studies point to the conserved role of the Lsm1-7 complex, there are still no data available about its function in the mouse system.

We aimed to analyze the function of Lsm1 in the mouse and by that offer new data about the two crucial processes decapping and degradation of mRNA transcripts in mammals. By analyzing already described functions of Lsm1 in yeast cells such as degrading histone mRNA transcripts and its contribution to P-body formation we examined the presumption of a conserved function of Lsm1. Proximity-labeling of proteins close to Lsm1 should furthermore determine potential interactors and by that provide a clearer picture of the mode of Lsm1 function in mouse cells.

Moreover, we speculated about additional roles of Lsm1 in the immune system of the mouse, since it was found overexpressed in spleen and thymus. Our hypothesis was also derived from studies on upstream regulators of RNA decay such as the RNA-binding proteins Roquin or TTP that revealed the functions of preventing excessive immune responses and autoimmunity in mice. Thus, the second aim in this study was to investigate the impact of Lsm1-deficiency *in vivo* with a focus on the development and homeostasis of the hematopoietic and immune systems in mice.

3 Material and methods

3.1 Material

3.1.1 Mice

Mice with $Lsm1^{tm1b(EUCOMM)Hmgu}$ alleles were obtained from the International Knockout Mouse Consortium. Transgenic mice that are homozygous for this allele do not express $Lsm1$. Standard targeting procedures were used to generate $Lsm1^{neo/neo}$ mice (Figure 5).

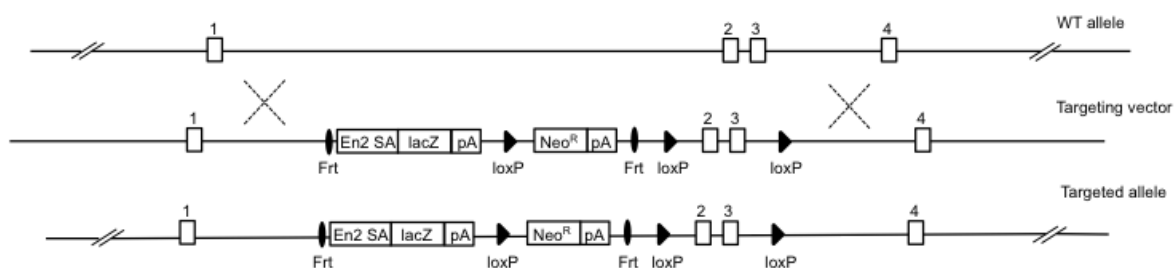


Figure 5: Targeting strategy of the $Lsm1$ allele.

Schematic representation of genetically modified alleles used in this study.

In a second approach, crossing resulted in the removal of the Frt-flanked Neo^R cassette to generate $Lsm1^{fl/fl}$ mice that carry loxP-flanked exons 2 and 3. T-cell specific deletion of $Lsm1$ was then achieved by using $CD4Cre$ mice (Lee et al. 2001). Mice were used not only for T-cell specific loxP site recombination of the $Lsm1^{fl/fl}$ alleles but also as control in combination with $Lsm1^{+/+}$ alleles.

San/san mice derived from an ENU-mutagenesis screen (Vinuesa et al., 2005).

All animals were bred on a C57BL/6 genetic background and housed in a special pathogen-free barrier facility in accordance with the Helmholtz Zentrum Muenchen or LMU university munich institutional, state and federal guidelines.

3.1.2 Cell lines and cell culture

Human embryonic kidney cells (HEK293T) were purchased from ATCC.

Primary immune cells used in this study were obtained from wildtype, *Lsm1^{neo/neo}*, *Lsm1^{fl/fl}*; *CD4Cre* mice and *san/san* mice unless stated otherwise.

Mouse embryonic fibroblasts (MEFs) were generated from embryos with different genotypes. The *Lsm1^{neo/neo}* MEFs were produced by Dr. Kai Höfig and showed complete lack of the *Lsm1* protein. *Rc3h1/2^{-/-}* MEF cells *Rc3h1/2^{fl/fl}* were produced as previously described (Vogel et al., 2013).

Media used for cell culture are described below (Table 2).

Table 2: Cell culture components

| Component | Supplier |
|---|-------------------------|
| Dulbecco's Modified Eagle Medium (DMEM) | ThermoFisher Scientific |
| Fetal bovine serum (FBS) | PAN BIOTECH |
| HEPES pH 7.4 (1M) | ThermoFisher Scientific |
| L-Glutamine 200mM | ThermoFisher Scientific |
| MEM non-essential amino acids (NEAA) 100x | ThermoFisher Scientific |
| MEM vitamin solution (100x) | ThermoFisher Scientific |
| Penicillin-streptomycin (10,000 U/ml) | ThermoFisher Scientific |
| RPMI 1640, no glutamine | Lonza |
| Sodium pyruvate (100mM) | Lonza |
| β -mercaptoethanol | Sigma-Aldrich |

3.1.3 Plasmids

The wildtype *Lsm1* gene was amplified from the entry vector pEntr11-GFP-*Lsm1*. The two mutated genes *Lsm1^{*R33A-D36A}* and *Lsm1^{*R67A-G68W-E69A}* were generated by using site-directed mutagenesis. All three genes were subsequently cloned into Gateway® entry vectors by TOPO® cloning. From GW8 vectors, genes were recombined into the retroviral expression destination vector pMSCV by performing Gateway® LR reactions. pMSCV plasmids with desired genes were then used for viral transduction (Table 3).

Table 3: Retroviral Gateway® destination vectors

| Destination vector | Insert |
|--------------------|----------------------|
| pMSCV-GFP | Lsm1 |
| pMSCV-GFP | Lsm1*R33A-D36A |
| pMSCV-GFP | Lsm1* R67A-G68W-E69A |
| pMSCV-empty | - |
| pMSCV-GFP | GFP |

3.1.4 DNA oligonucleotides

DNA oligonucleotides were purchased from Metabion (Planegg, Germany).

Table 4: Primers for cDNA cloning; mutagenesis and Southern blot analysis

| Name | Sequence (5'-3') |
|-------------------------------|--|
| Lsm1*R33A-D36A sense | TCGAGATGGAAGAACAACCTTATAGGTTTTTTAGCAAGCATTGCTCAATTTGCTAACTTAGTGC |
| Lsm1*R33A-D36A antisense | GCACTAAGTTAGCAAATTGAGCAATGCTTGCTAAAAACCTATAAGTGTTCTTCCATCTCGA |
| Lsm1*R67A-G68W-E69A sense | ATATTCCTCGAGGGATTTTCGTGGTCGCATGGGCGAATGTGGTCCTACTAGGAGAAATAG |
| Lsm1*R67A-G68W-E69A antisense | CTATTTCTCCTAGTAGGACCACATTCGCCCATGCGACCACGAAAATCCCTCGAGGAATAT |
| Lsm1-3'EcoRV-probe sense | TGTCAAATGCATATAACCACCCC |
| Lsm1-3'EcoRV-probe antisense | CCAATCCTCCTGCCCATTA |
| Lsm1-5' Swa1-probe sense | CAGATGCCCATTTATTCATTTCCA |
| Lsm1-5' Swa1-probe antisense | CAGAAGTTACGTGGAAGAAGG |
| Usp18 sense | AGATGCAGTGCTTAGGTGA |
| Usp18 antisense | CCCTGGCATGTTGTATCCCC |
| BirA*-Lsm1 sense | AGAGGTCGACACCGTGAGCAAGGGCG |
| BirA*-Lsm1 antisense | AGAGGCGGCCGCTTACTTGTACAGCTCGTCCATG |

3.1.5 Antibodies and fluorescent dyes

Antibodies employed for different experiments are listed in the following tables.

Table 5: Antibodies for flow cytometric analyses

| Name | Supplier |
|-----------------------------|-------------------------------|
| Anti-B220 (RA3-6B2) | eBioscience |
| Anti-CD4 (GK1.5) | eBioscience |
| Anti-CD8a (53-6.7) | eBioscience |
| Anti-CD11c (N418) | eBioscience |
| Anti-CD21/35 (7G6) | eBioscience |
| Anti-CD23 (B3B4) | eBioscience |
| Anti-CD44 (IM7) | eBioscience |
| Anti-CD62L (MEL-14) | eBioscience |
| Anti-CD279 (PD-1) | eBioscience |
| Anti-CXCR5 (2G8) | In-house production |
| Anti-F4/80 (BM8) | BMA Biomedicals AG |
| Anti-Foxp3 (FjK-16s) | eBioscience |
| Anti-GL-7 (GL7) | eBioscience |
| Anti-Gr-1 (RB6-8C5) | eBioscience |
| Anti-IFN γ (XMG1.2) | eBioscience |
| Anti-KLRG1 (2F1) | eBioscience |
| Anti-MHCII | eBioscience |
| Anti-NK1.1 (PK136) | eBioscience |
| Anti-rat IgG (biotinylated) | Jackson Immuno Research |
| Anti-Siglec-F (E50-2440) | eBioscience |
| Anti-TCR β (H5-597) | eBioscience |
| PBS57-loaded CD1d Tetramer | National Institutes of Health |
| Streptavidin | eBioscience |

Table 6: Dyes for cell proliferation experiments

| Name | Supplier |
|--|------------------|
| Cell proliferation Dye eFluor [®] 450 | eBioscience |
| CFSE (Carbonyfluorescein diacetate succinimidyl ester) | Molecular probes |

Table 7: Antibodies for confocal microscopy

| Name | Supplier |
|--|-------------------------------|
| DAPI | Sigma-Aldrich |
| 4',6-Diamidino-2-phenylindole | |
| Alexa Fluor [®] 680 goat anti-rat IgG | Molecular probes [®] |
| Anti-rabbit Cy5 | Jackson laboratories |

| | |
|----------------|----------------------|
| Anti-mouse Cy3 | Jackson laboratories |
|----------------|----------------------|

Table 8: Antibodies for Western blot analyses

| Name | Supplier |
|-----------------------------------|-----------------------------|
| Anti-Edc4 (RCD8) | Bethyl |
| Anti-GAPDH (6C5) | Calbiochem |
| Anti-I κ B α (44D4) | Cell signaling |
| Anti-Lsm1 (5F3-11) | In-house production |
| Anti-Lsm4 (GW22314F) | Sigma-Aldrich |
| Anti-Lsm8 (F-8) | Santa Cruz |
| Anti-Pat1b | Bethyl |
| Anti-RNA-Polymerase II | Abcam |
| Anti-Mouse IgG | Cell Signaling Technologies |
| Anti-Rabbit IgG | Cell Signaling Technologies |
| Anti-Rat IgG | Cell Signaling Technologies |
| Anti-Roquin-1/2 (3F12) | In-house production |
| Anti-Tubulin (sc-23948) | Santa Cruz Technologies |
| P70 S6 kinase α (H-9) | Santa cruz |
| Anti-Rck (A300-561A) | Bethyl |

Table 9: Antibodies for Immunoprecipitation

| Name | Supplier |
|--------------------|---------------------|
| Anti-Lsm1 (5F3) | In-house production |
| Anti-Roquin (Q4.2) | In-house production |
| Anti-Pat1b | Bethyl |

Table 10: Antibodies & cytokines for stimulation and differentiation of T cells

| Name | Supplier |
|--------------------------------------|---------------------|
| Anti-CD3 (145-2C11) | In-house production |
| Anti-CD28 (37N) | In-house production |
| Anti-hamster IgG (goat) | MP biochemical |
| Anti-IFN γ (XMG1.2) | In-house production |
| Anti-IL2 | Novartis |
| Anti-IL4 (IIB11) | In-house production |
| Anti-IL-12 (C17.8) | In-house production |
| IL-4 supernatant | In-house production |
| Recombinant human IL-2 (Proleukin S) | Novartis |
| Recombinant human TGF-b1 | R&D Systems |
| Recombinant human IL-6 | PeptoTech |
| Recombinant mouse IL-12 | BD Biosciences |

3.1.6 Chemicals, enzymes and kits

Table 11: Chemicals

| Compound | Supplier |
|--|--|
| 2-Propanol | Merck |
| 2log DNA ladder | New England Biolabs |
| Acrylamide 4K solution | AppliChem |
| Amersham™ ECL™ Prime | GE Healthcare |
| Ammonium persulfate (APS) | Serva |
| Ampicillin | Roche |
| APS | 10% APS w/v in ddH2O |
| Bio-rad protein assay (Bradford assay) | Bio-rad |
| Biozym LE agarose | Biozym |
| Boric acid | Calbiochem |
| Bovine serum albumin (BSA) | Carl Roth |
| Brefeldin A | eBioscience |
| Calcium chloride | Sigma-Aldrich |
| Chloroform | Sigma-Aldrich |
| Chloroquine diphosphate salt | Sigma-Aldrich |
| DEPC | Carl Roth |
| DETAChA [®] BEAD [®] Mouse CD4 (L3T34) | Invitrogen |
| Dimethyl sulfoxide | Sigma-Aldrich |
| Dithiothreitol (DTT) | AppliChem |
| DNA dye (6x) | 0.25% bromophenol blue 0.25% xyleneanol 30% glycerol |
| dNTP set | ThermoFisher Scientific |
| Dynabeads [®] M-280 Streptavidin | Invitrogen |
| Dynabeads [®] Mouse CD4 | Invitrogen |
| Dynabeads [®] MyOne™ Tosylactivated | ThermoFisher Scientific |
| Dynabeads [®] Protein G for immunoprecipitation | ThermoFisher Scientific |
| EDTA, pH 8.0, 0.5M | Roth |
| Ethanol | Merck Millipore |
| Ethidium bromide (0.07%) | AppliChem |
| Formaldehyde solution 36.5-38 % | Sigma-Aldrich |
| GlycoBlue™ coprecipitant | Ambion |
| Hygromycin B | ThermoFisher Scientific |
| Ionomycin, free acid, <i>Streptomyces globatus</i> | Merck Millipore |
| Kanamycin | Carl Roth |
| Methanol | Merck Millipore |
| Nonfat dry milk powder | AppliChem |
| Nonident P40 | Sigma-Aldrich |
| Phorbol-12-myristate-13-acetate (Jeltsch et al.) | Merck Millipore |

| Compound | Supplier |
|--|-------------------------|
| Polybrene | Sigma-Aldrich |
| Protease inhibitor tablets, cOmplete™ Mini EDTA-free | Roche diagnostics |
| Protein Marker VI (10 - 245) prestained | AppliChem |
| Saponin GPR RECTAPUR® | VWR |
| Sodium dodecylsulfate, pellets | Serva Electrophoresis |
| Spectinomycin | AppliChem |
| TEMED | AppliChem |
| TRI reagent® solution | Ambion |
| Trypsin-EDTA | ThermoFisher Scientific |
| Tween 20 | AppliChem |

Table 12: Enzymes

| Enzyme | Supplier |
|------------------------------------|-------------------------|
| Gateway® LR Clonase® II enzyme mix | ThermoFisher Scientific |
| Herculase II Fusion DNA polymerase | Agilent Technologies |
| <i>NotI</i> -HF® | New England Biolabs |
| Proteinase K | Roche |
| <i>SalI</i> -HF® | New England Biolabs |
| <i>SwaI</i> | New England Biolabs |
| T4 DNA ligase | New England Biolabs |
| T4 polynucleotide kinase | New England Biolabs |
| <i>Taq</i> DNA polymerase | ThermoFisher Scientific |
| Vent® polymerase | New England Biolabs |

Table 13: Kits

| Kits | Supplier |
|---|--|
| EasySep™ Mouse CD4 ⁺ T Cell Isolation Kit | Stemcell Technologies |
| Gateway® LR Clonase® II enzyme mix | ThermoFisher Scientific |
| Indirect immunofluorescence Kit | Euroimmun Medizinische Labordiagnostika AG |
| LightCycler® 480 Probes Master Universal probe library | Roche |
| NucleoBond® Xtra Maxi | MACHEREY-NAGEL |
| OneStep RT-PCR Kit | QIAGEN |
| pCR™8/GW/TOPO® TA Cloning® Kit | ThermoFisher Scientific |
| PureYield™ Plasmid Miniprep System | Promega |
| QIAquick® Gel Extraction Kit | QIAGEN |
| QIAquick® PCR Purification Kit | QIAGEN |
| QuantiTect® Reverse Transcription Kit | QIAGEN |
| USB® Poly(A) Tail Length-Assay Kit | Affymetrix |

| Kits | Supplier |
|---|----------------------|
| QuikChange® II XL Site-Directed Mutagenesis Kit | Agilent Technologies |
| RNeasy® Mini Kit | QIAGEN |
| Seahorse XF Cell Mito Stress Kit | Agilent Technologies |

3.1.7 Buffers

Table 14: Buffers

| Buffer name | Composition |
|--|--|
| Acrylamide-bisacrylamide (AB)-3 stock solution | 40g acrylamide 1.5g bisacrylamide in 100ml ddH ₂ O |
| Anode buffer (10X) | 1M Tris 225mM HCL |
| Buffer A for nuclear fractionation | 10mM HEPES (pH 7.9) 10mM KCL 0.1 mM EDTA 1mM dithiothreitol protease inhibitor mix with EDTA (Roche) in ddH ₂ O |
| Blotting buffer | 25 mM Tris 192 mM glycine 20 % methanol |
| Cathode buffer (10X) | 1M Tris 1M Tricine 1% SDS (w/v) |
| Digestion buffer (Southern blot) | 10mM NaCl 10mM Tris-HCL, pH7.5 10mM EDTA 0.5% Sarcosyl=N-Lauroylsarcosine 0.4 mg/ml proteinase K |
| ECL solution 1 | 100 mM Tris-HCl pH 8.8 1.25 mM Luminol 200 nM p-Coumaric-acid |
| ECL solution 2 | 3 % H ₂ O ₂ |
| FACS staining buffer | PBS 2 % FCS 2 mM EDTA |
| Gel buffer (3x) for tricine-PAGE | 3M Tris 1M HCL 0.3% SDS (w/v) |
| HBS (2x) | 274 mM NaCl 10 mM KCl 1.4 mM Na ₂ HPO ₄ , pH 7.0 |
| Laemmli SDS sample buffer (4x) | 200 mM Tris-HCl, pH 6.8 |

| Buffer name | Composition |
|------------------|---|
| | 8 % SDS 40 % glycerol 0.1 % bromophenol blue 10 % β -mercaptoethanol |
| Lysis buffer | 20 mM Tris-HCl pH 7.5 150 mM NaCl 0.25 % NP-40 1.5 mM $MgCl_2$ |
| PBS | 137 mM NaCl 10 mM Na_2HPO_4 , pH 7.4 2.7 mM KCl |
| RIPA buffer | 20mM Tris-HCL, pH 7.5 150mM NaCl 1% TritonX-100 1% Sodium deoxycholate 0.1% SDS 5mM EDTA 1mM dithiothreitol |
| Saponin buffer | PBS 0.5 % saponin 1 % BSA |
| SDS PAGE buffer | 25 mM Tris 250 mM glycine 0.1 % SDS |
| TAC lysis buffer | 13 mM Tris 140 mM NaH_4Cl , pH 7.2 |
| TE | 10 mM Tris-HCl pH 7.5 1 mM EDTA pH 8 |
| TBE (1x) | 89 mM Tris-borate 2 mM EDTA, pH 8 |
| TBS | 10 mM Tris-HCl pH 8 150 mM NaCl |
| TBST | 10 mM Tris-HCl pH 8 150 mM NaCl 0.05 % Tween-20 |

Table 15: Consumables

| Name | Supplier |
|-------------------------------|-------------------|
| 1.5 ml, 2 ml centrifuge tubes | Eppendorf |
| 15 ml, 50 ml tubes | Falcon |
| 96-well reaction plate (qPCR) | 4titude |
| Cell culture plates | Thermo Scientific |
| Cell scraper | Sarstedt |

| | |
|------------------------------------|---------------------------|
| Clear seal foils for qPCR | 4titude |
| Cryotubes | Thermo Scientific |
| Cuvettes | Brand |
| Disposable pipetting reservoirs | VWR |
| Filter paper Whatman, 3 mm | VWR |
| Gloves | ShieldSkin™ orange Nitril |
| Immobilon® Nitrocellulose membrane | Merck |
| Pipette tips | Sorenson |
| Surgical disposable scalpels | Braun |
| X-ray films | Agfa health Care |

3.1.8 Instruments

Table 16: Instruments

| Instrument Name | Supplier |
|---------------------------------|--|
| Agarose gel chambers | Peqlab |
| Bacterial incubator | Brutschank BINDER BF 53 (Binder Labortechnik) Innova 4400 incubator shaker (New Brunswick Scientific GmbH) |
| Balances | KERN ABJ-220-4M (Kern und Söhne GmbH) KERN EW 220-3NM (Kern und Söhne GmbH) |
| BD LSRFortessa cell analyzer | BD Biosciences |
| Benchtop working rack 1.5 ml | Stratagene |
| Cell freezing container | CoolCell® (Biocision) |
| Blotting chamber | Bio-Rad |
| Centrifuges and rotors | Beckman Coulter Avanti-J-26XP (Beckman Coulter); JA-10 Rotor, Fixed Angle (Beckman Coulter) Allegra®X-12R Centrifuge (Beckman Coulter); Rotor SX 4750 (Beckman Coulter) Eppendorf Centrifuge 5810R (Eppendorf); Rotor A-4-62 and F-34-6-38 |
| Confocal microscope | Leica TCS SP5 |
| CO ₂ incubator | Forma Direct Heat CO ₂ Incubator HEPA Class 100 (Thermo Electron Corporation) |
| Gel documentation system | Quantum ST4 (Vilber) |
| High-throughout sampler | BD Biosciences |
| Ice machine | Scotsman AF 200 (Scotsman Icesystem) |
| Magnet stirrer | RCT basic safety control (IKA) |
| Microscope | Axiovert 40C (Zeiss) |
| Microwave | Bosch |
| Neubauer improved hemocytometer | Marienfeld |
| pH meter | pH-Meter inoLab® pH 720 (W TW) |

| Instrument Name | Supplier |
|----------------------------------|--|
| Pipettor | Pipetboy acu (Gibson & Jacobson) |
| Power supplies | Stromgeber EC105 (Thermo Electron Corporation) Power Pac200 (Bio-Rad) |
| Phospho-image reader | FLA 5100 Image analysis system (Fujifilm) |
| Sterile-working bench | BDK, Luft und Reinraumtechnik |
| Spectrophotometer | NanoDrop™ 1000 Spectrophotometer (ThermoFisher Scientific) |
| Table centrifuge | Centrifuge 5415D (Eppendorf) Centrifuge 5417R (Eppendorf) |
| Thermocycler | DNA Engine 48/48 Dual Alpha Unit (Bio-Rad) Light Cycler 480II (Roche) |
| Thermo mixer | Thermomixer comfort (Eppendorf) |
| UV crosslinker | Stratagene |
| Vacuum pump | Diaphragm Vacuum Pump MZ 2C (Vacuubrand) |
| Vertical electrophoresis chamber | Bio-Rad Eppendorf BioPhotometers (Eppendorf) |
| Vortex MS2 mini shaker | IKA |
| Waterbath | WB7 (Mettler) |

3.1.9 Software

Table 17: Software

| Name | Application |
|---|------------------------------|
| Adobe Illustrator CS5 | Image processing |
| Adobe Photoshop CS5 | Image processing |
| ApE | Analysis of DNA sequences |
| Endnote X8 | Literature organization |
| FlowJo 3 | Flow cytometry data analysis |
| GraphPad Prism | Graphs, statistics |
| Light Cycler 480 software release 1.5.1 | qPCR data analysis |
| Microsoft Office for Mac 2011 | Writing in Word |

3.2 Methods

3.2.1 Work with nucleic acids

Polymerase chain reaction (PCR)

PCR was used for several applications, such as DNA amplification for cloning approaches, mouse genotyping and site-directed mutagenesis as well as RT-PCR. To amplify specific nucleotide sequences, gene-specific primer (with an annealing temperature of 53-62°C) and the thermostable Taq polymerase were used and PCR was performed according to standard protocols. The amplification reaction consisted of 0,3µl Taq polymerase; 2,5µl 10X reaction buffer; 1µl MgCl₂ (50mM); 0,5µl dNTP (10mM each); 0,5µl forward primer (10pM); 0,5µl reverse primer (10pM) and 20ng template DNA. H₂O was added to reach a final reaction volume of 25µl. PCR reactions were carried out in a thermocycler with the cycling conditions shown in table 18.

Table 18: PCR composition and cycling conditions

| Step | Temp | Duration | |
|--------------|-----------------------|---------------|-------|
| Activation | 95°C | 2 min | |
| Denaturation | 95°C | 15 sec | } 32x |
| Annealing | ~T _m - 5°C | 30 sec | |
| Elongation | 72°C | 1 min/kb cDNA | |

Agarose gelelectrophoresis and DNA extraction

In order to separate DNA products according to their sizes, agarose gelelectrophoresis was performed. Samples were resuspended in a 10X DNA loading dye and loaded next to an DNA standard marker to determine their sizes. The negatively charged nucleic acid migrated through an agarose gel matrix coupled to an electric field of 100 – 130V in TBE buffer. To visualize the DNA fragments, 50µl Ethidium bromide/100ml agarose solution was used and detection was possible after excitation with 254nm UV light. To extract the desired DNA product from the agarose gel, the band detected under UV light was cut out and purified using the gel extraction and PCR purification KIT according to the manufacturer' protocol (QIAquick® Gel Extraction Kit).

Molecular cloning

Cloning was performed to generate retroviral expression vectors. Extracted DNA fragments (section 3.2.1.2) were purified using the DNA-purification Kit and were transferred into so called entry vectors by using the TOPO cloning technique following the manual of the kit (pCR™8/GW/TOPO® TA Cloning® Kit). Successfully cloned DNA could be then transferred into any desired so-called destination vector (in the present study only pMSCV vector was used) by performing Gateway cloning. This efficient and fast technique relies on specific recombination sites in the entry and destination vector, respectively (AttI1 and 2; AttR1 and 2) that allowed the direct transfer of DNA sequences between both vectors. For plasmid DNA amplification, plasmids were propagated into chemically competent *E. coli* DH5alpha bacteria (in-house production). Transformation was achieved by incubation of desired plasmid (ca. 100ng) with 50µl of bacterial suspension for 20min on ice. After a heat shock on 42°C for 30sec, cells were put on ice for additional 2min. 250µl of glucose-containing SOC medium was added and cells were gently shaken (600rpm) for 1h at 37°C in a thermomixer. Suspension was subsequently spread onto LB-agar plates with the respective antibiotics (Ampicillin for pMSCV). Plates were incubated in a bacterial incubator at 37°C o/n. Only these bacteria, that carried the destination vector with the correct recombination survived. This is ensured by the removal of the toxin-encoding *ccdB* gene and the antibiotic resistance present only on the destination vector. Single colonies were used to inoculate a 5ml bacterial culture o/n. For the isolation of amplified plasmids, PureYield™ Plasmid Miniprep Kit was used according the manufacturer's protocol. For large scale Plasmid amplification, 300ml cultures were inoculated with single colonies and the NucleoBond Xtra® Maxi Kit was used for DNA isolation. LB media and LB agar were prepared using the LB medium powder (Servaes, Jacobson, & White) and supplemented with ampicillin (100µg/ml), spectinomycin (50µg/ml), kanamycin (30µg/ml) or chloramphenicol (170µg/ml). Confirmation of right fragment sizes was achieved by digestion with respective restriction enzymes and subsequent gelelectrophoresis. Enzymatic digestion was performed by mixing 2µg of plasmid DNA with 3µl of 10X buffer and 0.2µl of needed restriction enzyme in a 30µl reaction volume. Incubation at the appropriate temperature for 1.5h ensured cutting of the plasmid at the right position. Digested plasmid fragments were visible as bands on an agarose gel after separation by electrophoresis. Procedure was performed for the cloning of *Lsm1^{+/+}*, *Lsm1^{*R33A}*; *D36A* and *Lsm1^{*R67A}*; *G68W*; *E69A*. Genes were

cloned into the GW8 vector and insertion was tested by restriction with EcorI. After the LR reaction, right insertion into the MSCV-vector was analyzed by sequencing.

RNA extraction

For the isolation of RNA, TRI reagent was used. MEF cells or splenocytes were centrifuged for 5 min at 300Xg and the pellet was resuspended in 1ml TRI reagent. For lysis, samples were incubated for 5 min at room temperature. 200µl chloroform was added and two phases (organic and aqueous) were separated through a centrifugation step (12,500g, 15min). The aqueous phase was subjected to isopropanol in a new tube. The precipitation step was performed at room temperature for 5min and RNA was centrifuged at 4°C for 15min. A washing step of the RNA pellet with 70% Ethanol followed. The isolated RNA was air-dried and subsequently resuspended in Rnase free water. RNA concentrations were determined using the Nano-drop.

Reverse Transcriptase-polymerase chain reaction (RT-PCR)

To obtain complementary DNA (cDNA) from RNA, reverse transcription reactions were performed. Total RNA, isolated from MEF or T cells was used as starting material. By following the provided protocol of the QuantiTect® Reverse Transcription Kit (Qiagen) cDNA sequences were synthesized. Newly generated cDNA was diluted in an end volume of 100µl and used for quantitative PCR assays. qPCR was performed using the Roche Universal Probe library. The Light cycler480 SW 1.5.1 software was used to determine relative expression levels. Normalization was achieved with housekeeping genes (Hprt and 18sRNA).

Site-directed mutagenesis with Quikchange

The QuikChange® II XL Site-Directed Mutagenesis Kit was employed to introduce mutations into plasmid DNA. Mutagenic primers were designed according to the guidelines and Quikchange reaction was performed as indicated in the manufacturer's instructions. Sequences of the primer used in this study are listed in Table 3. Mutagenesis was used to generate the two mutated *Lsm1*-genes: *Lsm1**R33A; D36A that was not able to bind any mRNAs and *Lsm1**R67A; G68W, which could not bind oligoadenylated mRNAs.

Southern blot analysis

Southern blot analysis was employed to investigate the targeting of the *Lsm1* gene in the *Lsm1^{neo/neo}* mouse and was performed together with Dr. Sven Brenner. For the DNA material mice tails were digested in a well of a 96 well plate. Each tail was digested in 50µl lysis buffer and plate was incubated in a water saturated chamber at 56°C o/n. The next day, plate was cooled down at RT for at least 1 h. 100µl of ethanol (100%) was added and plate was incubated for additional 8 hours at RT. Plate was then inverted in order to remove the liquid (DNA remained on the bottom of plate). Wells were washed three times with ethanol and then dried for 15min at RT. For DNA fragmentation, 40µl digestion mix was added to each well and plate was sealed with parafilm and incubated in the special chamber o/n in the appropriate temperature for the used enzymes. To run the digested DNA on the agarose gel, 8µl of 6x loading dye were added to each well and samples were loaded onto a 0.8% precooled gel. Gel electrophoresis was performed in the cold room for 4-5hours at 100V. Gel was prepared for blotting by swiveling in 0.25M HCL for 30 min at RT. Ongoing reaction can be followed by eye (color change from light blue to green as a result of acidic pH). Next, gel was washed in water (color change to blue again) and DNA denaturation was achieved by incubation in a solution containing 1.5M NaCl and 0.5 NaOH for 30min on a shaker. Before blotting, gel was washed in transferbuffer with 0.4 M NaOH and then blotted for 2 hours on a GeneScreen membrane. Subsequently, membrane was washed twice with SSC-buffer. To covalently bind DNA on the membrane, a UV-crosslinker was used (program: auto-crosslink) and membrane was then ready for hybridization. The hybridization probe for detection of the DNA fragment on the membrane was designed according to the *Lsm1* gene sequence and amplification was performed using the Expand high fidelity PCR system radioactive labeling was performed following the instructions of the Prime-It II Randomer primer labeling Kit and NucTrap® Probe purification columns. For the hybridization of the probe with the DNA, membrane was incubated in 20ml of MiracleHyb Hybridization solution in a tube for 20 min at 65°C in a special hybridization oven. The probe was mixed in 350µl Hybridization solution and denaturated at 95°C for 2 min and subsequently added to the hybridization tube. The hybridization reaction was performed o/n at 65°C. Membrane was washed and incubated with 2X SSC buffer containing 0.1% SDS at 65°C for 20min. A second washing step was performed with 0.2% SSC-buffer containing 0.1% SDS. Excessive

solution was removed and membrane was incubated for 18h on a phosphoimager film. For the final readout, a phosphoimager was used.

Poly(A) tail length determination assay

The Poly(A) tail-length assay was used to determine the length distribution of poly(A) tails of Usp18 mRNAs isolated from CD4⁺ T cells. In principle two PCR amplification products are generated: the PCR with gene specific primers that serves as a control for the gene-of-interest and the second PCR that is performed using the same forward primer but a different reverse primer provided by the company to generate a product with the poly(A) tail. By comparing the two products on an agarose gel, different polyadenylation products can be determined. The four steps of the assay procedure are performed according the standard protocol of the Poly(A) length determination Kit.

3.2.2 Work with retroviruses

Virus production

To produce retroviral supernatants, calcium-phosphate transfection of HEK293T cells was performed; 18h prior to transfection 8-14x10⁶ HEK293T cells were seeded per 14cm plate to achieve a 50-70% cell confluence on the day of transfection. Pretreatment of HEK293T cells consisted of the incubation with fresh DMEM medium containing chloroquine (25μM) for 1h at 37°C. In parallel, respective retroviral expression vector was mixed as described in Table 19 and was added dropwise to HBS and incubated at RT for 15min, allowing the formation of DNA/CaCl₂ precipitates. The mix was added dropwise to the chloroquine-pretreated HEK293T cells. Because of the toxicity of chloroquine, medium was replaced 6-8h later. Virus containing supernatant was harvested 48h post transfection, filtered (0,45μm), concentrated by centrifugation (6,000g; 4°C; o/n) and frozen the next day at -80°C in aliquots ready for direct use.

Table 19: Composition of the DNA mix for calcium-phosphate transfection.

| Amphotropic Retroviruses | transfer vector | Env | gag/pol | CaCl ₂ (2.5 M) | H ₂ O |
|---------------------------------|-----------------|-----|---------|---------------------------|------------------|
| | 50μg | 5μg | 5μg | 125μl | 1250μl |

Transduction

Generated retroviruses were used for the transduction of MEF cells. In practice, 18h prior transfection, 100.000 MEF cells were seeded onto a well of a six-well plate. After replacing the medium by the virus supernatant and addition of polybrene (8 μ g /ml), MEF cells were subjected to spin infection by centrifugation for 2h at 32°C, 300g. Cells were cultured for 8-10hours with the virus supernatant, which was then removed and replaced by fresh medium. Because all pMSCV-constructs used carried in addition to the gene of interest also GFP, transduction efficiency could be determined by measuring percentage of GFP positive MEF cells using the flow cytometer.

3.2.3 Work with protein

Western blot analysis

Western blot analyses were used to investigate presence and expression levels of proteins of interest. For the lysis, cells were harvested in a precooled tube, centrifuged and washed once with PBS. Three times of the volume of cell pellet was the amount of lysis buffer used for successful lysis. The incubation on ice for 10min (with vortexing after each 2min) was followed by a centrifugation step (15min, 10.000g, 4°C) to remove cell debris. Supernatant was transferred into a fresh precooled tube. Protein concentration was determined by using the Bio-rad protein assay according to the manufacturer's instructions. By using SDS page, proteins were separated according their sizes and could subsequently be visualized allowing information about expression level in the cell. In practice, desired amount of protein lysate (50-80 μ g) were complemented with Laemmli SDS sample buffer, boiled for 5min at 95°C and loaded onto an SDS polyacrylamide gel. The compensation of the used SDS gels is listed in Table 20. Since Lsm proteins, such as Lsm1, Lsm4 or Lsm8 are very small, samples were loaded here on Tricine-gels. The compensation of this special kind of gel is listed in Table 21. For protein size determination, a protein marker was loaded in parallel. Separation was achieved by electrophoresis at 120V for 45-90min depending on the size of the protein of interest. For immunoblotting procedure, proteins that were separated in the SDS Page were blotted on PVDF membranes at 40V o/n in blotting buffer at 4°C. Depending on the following primary antibodies, membrane was

blocked in either 5% milk or 5% BSA dissolved in TBS. After 2h blocking, membrane was washed three times with 1% nonfat dry milk in TBS-T (TBS containing 0.05% Tween) and then incubated with primary antibody for two hours at RT or o/n at 4°C on a mixing wheel. Three washing steps with 1% milk in TBST-T were followed by incubation with HRP-coupled secondary antibodies for 1h at RT. Subsequently, the membrane was washed three times, once with 1% milk in TBS-T, followed by washing with TBST and TBS, each for 10min on the shaker. For final detection, protein bands were visualized on an X-ray film by staining the membrane with ECL solution and developing in the dark.

Table 20: Composition of SDS PAGE gels

| Stacking gel | Separating gel (8% or 10%) |
|----------------------------------|-----------------------------------|
| 5% Polyacrylamide | 8 % or 10 % Polyacrylamide |
| 125mM Tris-HCl pH 6.8 | 375mM Tris-HCl pH 8.8 |
| 0.1 % SDS | 0.2 % SDS |
| 0.1 % APS | 0.2 % APS |
| 0.1 % TEMED | 0.06 % TEMED |
| up to 5 ml with H ₂ O | up to 10 ml with H ₂ O |

Table 21: Composition of Tricine gels

| Stacking gel (4%) | Separating gel (10%) |
|--------------------------|----------------------|
| 1.05ml AB3 buffer | 6.3ml |
| 1.5ml Gel buffer(3X) | 5ml |
| - glycerol | 1.5g |
| 45µl APS (10%) | 75µl |
| 5µl TEMED | 8µl |
| 3.45 ml H ₂ O | 2.5ml |

Co-immunoprecipitation

Immunoprecipitation is a simple technique to investigate interactions between proteins. This technique was used in this study to identify interaction partners of Lsm1, Roquin and the interaction of Pat1b with the Lsm1-7 ring. MEF cells were harvested, centrifuged (300g, 4°C) and cell pellets were shock frozen in liquid nitrogen, stored at -80°C and were thawed at the day of experiment. Lysis was performed using lysis buffer and protein was isolated (as described in section 3.2.3.1). 2-3mg of protein was used for each IP reaction. For Roquin and Lsm1 IPs, anti-Roquin1/2 antibody (Q4-2) or anti-Lsm1 antibody 5F3 were coupled to tosylactivated

dynabeads and 50µl of bead-suspension was used for each IP. For Pat1b IPs coupling was performed one-day prior day of experiment. For this 50µl of protein-G magnetic beads (Invitrogen) were incubated overnight with 5µg Pat1b antibody (Bethyl) in Meister lysis buffer at 4°C. Coupled beads were washed twice with Meister lysis buffer and protein and beads were incubated at 4°C for 4 hours. By using a magnetic separator, beads were removed out of the lysate solution. Beads were washed 3x with lysis buffer and were mixed with 20µl of SDS sample buffer. For elution beads were boiled at 95°C for 5min and supernatant was used for western blotting.

Fractionation

Fractionation of cells into cytoplasmic and nuclear fractions was used to investigate protein distribution upon *Lsm1* deletion in MEF cells. For this purpose, cells were harvested and washed once with PBS. Cell pellets were then resuspended in 5x of the volume of cell pellet in buffer A (table 19) and incubated 10min on ice. After centrifugation (300g, 5min and 4°C), supernatant was removed and 2 times of cell pellet volume Triton-X solution was added. A trypan-blue test was performed at this step to see free nuclei under microscope. After an additional centrifugation step, supernatant containing cytoplasmic fraction was transferred in a fresh tube and used for westernblotting. The pellet containing the nuclear fraction was washed with PBS and lysed with RIPA buffer (protease inhibitor mix without EDTA) and incubated on ice for 15 min. After a last centrifugation step, supernatant containing nuclear proteins can be used for further analysis.

3.2.4 Work with cells

3.2.4.1 Generation of MEF-cells

MEF cells that were used in this study were generated and tested by Dr. Kai Höfig. After crossing *Lsm1^{neo/+}* mice, pregnant mice were sacrificed and embryos were removed at 13.5 dpc (days *post coitum*). The head of the embryos were lysed and used for genotyping. The trunk of the embryos except for liver was sliced carefully into small pieces. After incubation with trypsin for 15min for further digestion, suspension was resuspended in DMEM medium and cultivated for several days by splitting them

each day to achieve clear cell suspensions. Cells were then immortalized with the SV40 large T ecotropic retrovirus and selected with hygromycin (100µg/ml) for two weeks. A small aliquot was used for westernblot analysis to confirm right genotype and rest was either taken directly in culture for experiments or stored to be used later.

3.2.4.2 Storage of cells

Stocks of cell lines were stored in multiple cell aliquots. To this end, 10^7 cells were centrifuged and taken up in 1.8 ml of 90%FCS and 10% DMSO and transferred into cryotubes. Cell aliquots were placed into a special freezing box that allows slow freezing avoiding ice crystal formation in cell samples. Stocks were kept at -80°C for short-time usage or transferred in liquid nitrogen tanks for long-term storage.

3.2.4.3 Cell culture

Mouse embryonic fibroblasts and HEK293T cells were cultured in DMEM containing 10% (v/v) FCS, HEPES (10nM) pH 7.4 and 1% penicillin-streptomycin at 37°C in a 10% CO_2 humidified cell incubator (table1). Primary mouse T cells were cultured in RPMI 1640 medium supplemented with 10% FCS, 1% penicillin-streptomycin, 1% HEPES, 1% non-essential amino acids (NEAA), 1% sodium pyruvate, 1% vitamin solution, 1% L-glutamine and 0.1% beta-mercaptoethanol at 37°C and 5% CO_2 (table 1). Cell confluency and morphology was analyzed microscopically and cells were splitted every 2-3 days. T cells were split using IL-2 containing T cell medium to maintain ability to proliferate. Cells were normally used for experiments within maximum 7 days after isolation.

3.2.4.4 Treatment of MEF-cells with hydroxyurea

For the analysis of the degradation process of histone mRNAs, cells were treated with the drug Hydroxyurea (HU) in order to mimic the end of S-phase in vitro. To do so, 1×10^6 cells were seeded in a 10cm dish one-day prior experiment. For the treatment, medium was removed and replaced by fresh medium containing Hydroxyurea (5mM as previously described by Mullen & Marzluff, 2008). As control for steady-state levels of mRNA one additional dish was left untreated. After incubation at 37°C for 15min,

30min or 45min, medium was removed, cells were washed twice with PBS and removed from the bottom of the plate by resuspending in 1ml trizol and frozen at -80°C. RNA extraction and qPCR were performed as described in section 3.2.16.

3.2.4.5 Isolation of naïve CD4⁺ T-cells

For primary T cell culture, spleen and LN of mice with desired genotype were mashed using a 150µm mesh and harvested cells were subjected to red blood cell lysis by resuspending cell pellets in 1.5 ml TAC lysis buffer/mouse spleen. After an incubation step of 5min at RT, cells were washed with cold PBS containing 2%FBS. Cell suspension was filtered and naïve CD4⁺ T cells were isolated using the EasySep™ Mouse naïve CD4⁺ T cell negative selection kit, according to the manufacturer's instructions. A small aliquot was stained with antibodies against CD62L, CD44 and CD4 and analyzed via flow cytometry to check for purity of cells. Cells were used for differentiation and stimulation analyses.

3.2.4.6 T-cell stimulation

CD4⁺ T cells stimulation was based on the activation through binding of CD3 of the TCR complex and to the costimulatory molecule CD28. For this purpose, cells were incubated in RPMI medium containing α-CD3 (0.25µg/ml) and α-CD28 (2.5µg/ml) for 20min on ice and were then seeded in precoated plates (goat anti-hamster IgG; MP biochemicals). Depending on the desired differentiation conditions, RPMI complete medium contained different stimulation antibody/cytokine mixes (table 22). After 48hours of activation, cells were either harvested for RNA-isolation and qPCR analysis or amplified by addition of IL-2 (20 U/ml) or restimulated with PMA/Iono for cytokine production analysis. For the last aim, after 48hours, cells were centrifuged in the plate and resuspended in 250µl/well of RPMI medium containing PMA (20nM) and Ionomycin (1µM). After 2.5 hours incubation at 37°C, 50µl with BrefeldinA (BFA) (10µg/ml) were added to each well and an incubation step of additional 2.5 hours followed. For cytometric analysis, cells were subsequently washed and stained with respective antibodies according the protocol described in the following section.

Table 22: Composition of antibody/cytokine mixes for T cell differentiation

| Condition | Antibody/cytokine | Concentration |
|-------------|----------------------------|---------------|
| Th0 | - | - |
| Th1 | anti-IL-4 | 10µg/ml |
| | IL-12 | 10ng/ml |
| Th2 | anti-IL-12 | 10µg/ml |
| | anti-IFN γ | 5µg/ml |
| | IL-4 hybridoma supernatant | 1:10 (v/v) |
| Th17 | anti-IL-12 | 10µg/ml |
| | anti-IFN γ | 5µg/ml |
| | anti-IL4 | 10µg/ml |
| | anti-mIL-2 | 2.5µg/ml |
| | IL-6 | 5ng/ml |
| | TGF- β | 1ng/ml |

3.2.4.7 Flow cytometry

By using flow cytometry, phenotyping of cell populations according size, granularity, cell surface as well as intra- and extracellular marker expression is possible in one single analysis. For extracellular staining, primary cell suspensions from Thymus or spleen were filtered, spun down (300g, 5min, 4°C) and resuspended in 50µl FACS buffer containing desired antibodies. Dilution of antibodies was (if not tested and noted differently) 1:200. MEF cells had to be trypsinized prior to that. Staining was performed for 20min at 4°C in the darkness. Cells were washed once. If biotinylated-antibodies were used, a second round of staining with streptavidin-allophycocyanin is needed. For staining of CXCR5, cells were incubated for 1h at 4°C with rat anti-mouse CXCR5 hybridoma supernatant in staining buffer, 20min with biotinylated mouse anti-rat IgG followed by an additional 20 min with Streptavidin-APC. After a final washing step cells were directly measured on a flow cytometer. For intracellular staining of Foxp3 in Tregs, Foxp3 fixation kit (eBioscience) was used. As described in the manufacturer's protocol, cells were fixed for 1h at 4°C in provided fixation buffer (diluted 1:3) followed by membrane permeabilization using provided permeabilization buffer (diluted 1:10 with water) for 30min at 4°C. Foxp3 antibody was diluted in permeabilization buffer and added in a last step to cells that were stained for 30min at 4°C. For intracellular cytokine staining of differentiated CD4⁺ T cells, cell suspensions were first stained with life/dead stain and were fixed with 4% paraformaldehyde for 15 min at RT. Permeabilization was achieved here by washing cells with PBS containing 0.5% saponin and 1% BSA. Antibody mix (Table 23) was

added to cell suspension and incubated for 30min at RT. After washing twice with saponin buffer and once with PBS, flow cytometer readouts were acquired.

Table 23: Composition of fluorescent antibody mix for differentiated T cells

| Condition | Antibody/cytokine |
|-----------|-------------------|
| Th0/1/2 | life/dead dye |
| | IFN γ -APC |
| | IL-4-PE |
| Th17 | life/dead dye |
| | IFN γ -APC |
| | IL-17A-PE |

3.2.4.8 BioID Experiment

In order to investigate interaction partners of Lsm1 in CD4⁺ T cells, we performed BioID Experiments. To do so, CD4⁺ T cells were isolated from *Lsm1^{fl/fl}; CD4Cre* mice and were stimulated with α -CD3/CD28 for 40h. Cells were then transduced with BirA*-Lsm1 Retroviruses that were generated according the protocol described in 3.2.2.1. As control another cell sample was transduced with BirA*-GFP. Transduction was achieved by a centrifugation step at 18°C, 850g for 1h and subsequent incubation with the virus for 6h. T cells were then transferred to IL2 containing T cell medium. 18h later, doxycycline was added and cells were incubated for additional 6h. Biotin was then added to the cells that were again cultured for additional 18h. Cells were then washed with PBS and cell pellets were either stored at -80°C or directly treated according to the protocol described in Roux et al. 2013.

3.2.4.9 Detection of T cell proliferation

To follow proliferation of cells, two different staining protocols were used. In this study, cells from wildtype mice and *Lsm1^{neo/neo}* mice were stained with two different labeling dyes and were then incubated together in one cell-culture-well to minimize variation coming from different wells. For analysis, cells could be distinguished according their labeling. The two proliferation dyes, CFSE and eFluor450 were used. For CFSE labeling, cells were centrifuged and cell pellet was resuspended in 1 ml of PBS containing 5% (v/v) FCS in a fresh tube. The tube was laid horizontally and 110 μ l

of PBS was added to the non-wetted portion of the plastic at the top of the tube, whereby it is important to ensure no mixing of both solutions. 1.1µl of CFSE (5mM) was added to the 110µl PBS. The tube was then capped and quickly inverted several times. After thorough mixing, cells were incubated for 7 min at RT in the dark. Three washing steps followed using ten volumes of PBS containing 5% (v/v) FCS. For eFluor450 labeling, cells were mixed with eFluor450 proliferation dye (20µM) in a 1:1 ratio and were incubated for 20 min at RT in the dark. Four washing steps followed using five time volumes of RPMI medium. For the starting peak, one small aliquot of labeled cells was measured with flow cytometer at the same day. Cells were then incubated together with CFSE-labeled cells in fresh RPMI medium under Th0 or Th1 conditions as described in table 18. To control for differentiation, unlabeled cells were cultured in parallel under same conditions. For proliferation analysis, cells were not restimulated unlike the unlabeled cells but kept in cell culture medium until analysis. Cells were analyzed after 72hours in flow cytometer. For the end-point Peak, unlabeled cells were measured in parallel.

3.2.4.10 Seahorse measurements

To follow the cellular metabolism of Lsm1-deficient CD4⁺ T cells, Seahorse experiments were carried out in the lab of Dr. Martin Jastroch (Helmholtz Zentrum Garching). For this purpose, CD4⁺ T cells were isolated as described in section 3.2.4.5 and 2X10⁵cells/well were incubated in a 96 well plate and were differentiated in Th0 conditions. After 48hours T cell media was exchanged by seahorse media. Cells were first washed 4x with seahorse medium and were then incubated with 180µl of the same medium for 1h at 37°C in a CO₂-free incubator (first equilibration step). Four Inhibitors (compounds) were used for this experiment: oligomycin (8µg/ml), FCCP (4mM), Antimycin/Rotenone (100mM) and 2-DG (10µM). In a second equilibration step, compounds were filled in the cartridge and were prepared in a seahorse XFe96 Analyzer. Compounds were injected into the cell plate in 20min intervals. The two parameters oxygen consumption rate (OCR) and the extracellular acidification rate (ECAR) could then be determined. Results were analyzed using the Agilent SeahorseXFe analyzer software.

3.2.4.11 Confocal microscopy

For investigation of protein localization in cells, immunofluorescence staining and confocal microscopy were performed. One day prior experiment 1×10^5 MEF cells were seeded in a well of a 6-well plate and incubated at 37°C. Medium was removed and cover slips were left in the well during the complete experiment. Before staining, cells were washed once with PBS and incubated with 2% Paraformaldehyde for 15min at RT for fixation. Three washing steps of 5min each with PBS/Triton (0,15% Triton X-100 in PBS) were performed, followed by additional two washing steps with PBS+ (PBS containing 1% BSA and 0,15% Glycine). For staining with primary antibodies such as Lsm1, RCK, Lsm4 and S6-kinase, cells were incubated in respective antibody concentration for 1h at RT. After four washing steps, cells were incubated with secondary antibodies for 45min at RT in the darkness. To remove antibody solution, cells were again washed with PBS. To stain the nuclei of cells DAPI solution (1:10 000 in PBS) was added to the cells and incubated for 90 sec. Last washing steps were performed and coverslips were applied upside down on object slides by using 8 μ l of 90% glycerine. Coverslips were fixed with nail polish on the object slides. Confocal microscopy was performed at the same day; pictures were captured with a Leica TCS SP5 microscope and analyzed using the confocal LAS AF software.

3.2.4.12 Fluorescence microscopy

For the detection of autoantibodies in sera of different mice, special slides with BIOCHIPS of fixed HEP-2 cells from EUROIMMUN were used. For all dilution and washing steps, PBS containing 0.2% Tween was used. All solutions (blocking solution, primary AB solution, secondary AB solution) that were in contact with the fixed cells on the BIOCHIP had a volume of 30 μ l. First, slides were blocked by using 5% v/v donkey serum (Killian, Tiwari, Jacobson, Jackson, & Lupski). To this end, solution was applied to each reaction field of the reagent tray and incubated for 45min at RT. Blocking solution was removed by washing for 5min at RT on a shaker. Subsequently, diluted sera (1:40) were applied to each field and slides were incubated for 45min at RT. After washing, secondary antibody (anti-mouse IgG A488 from Invitrogen) was diluted 1:400 and cells were stained for 20min at RT in the dark. Next, cells were rinsed and stained with DAPI (1:10 000) for 90sec at RT. After a last washing step,

mounting medium was dropped onto a cover glass and slides were dried and fixed with nail polish.

3.2.5 Statistical analyses

Where indicated, results were analyzed for statistical significance using the paired two-tailed Student's test. Statistical analysis was performed with Prism Graph Pad Software and differences between groups were considered as significant at p-values < 0.05.

4 Results

4.1 Evaluation of the *Lsm1* knockout mouse

We successfully generated a conditional knockout mouse from the gene targeting of the *Lsm1* gene in embryonic stem (ES) cells that was performed within the EUCOMM consortium (Figure 6A-D).

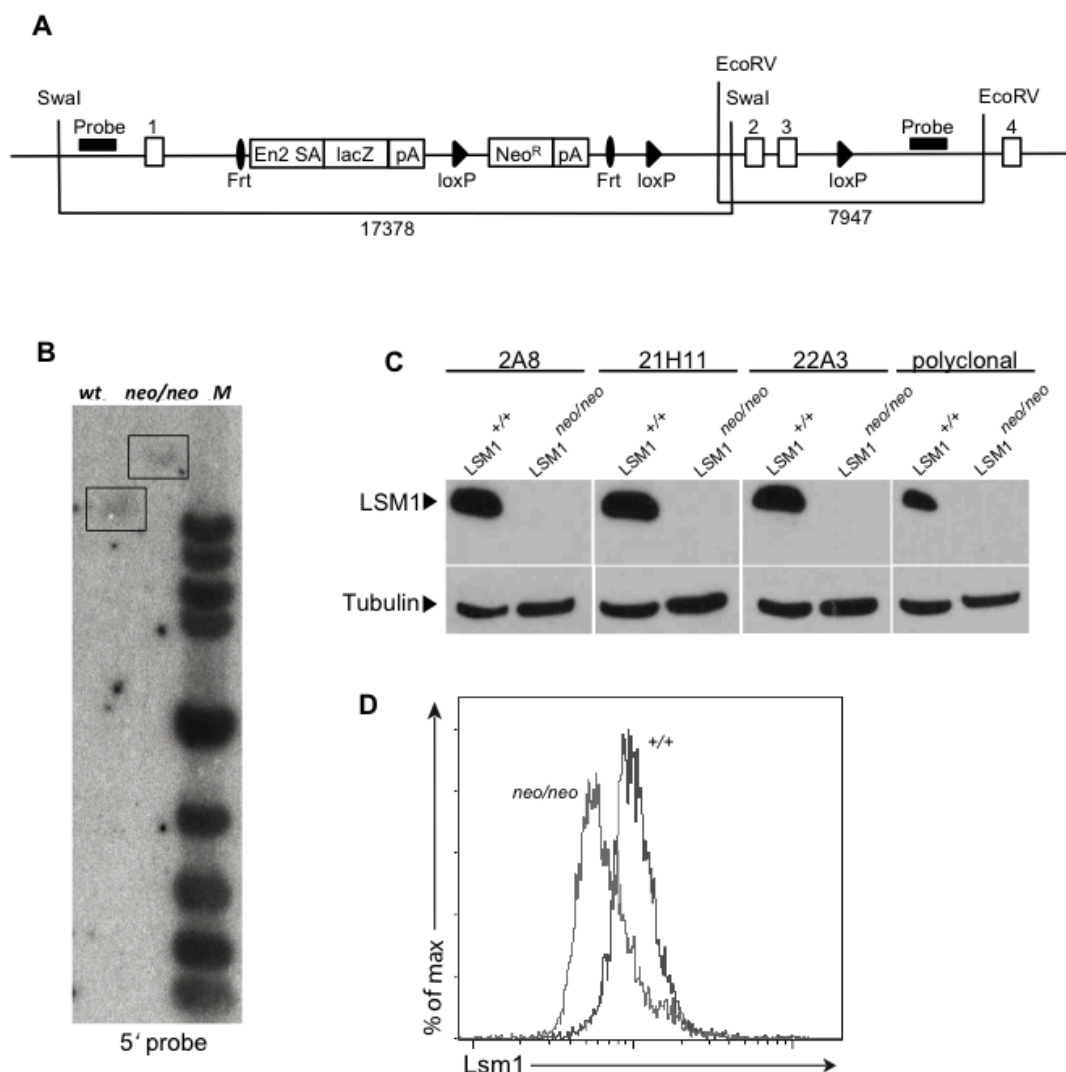


Figure 6: Evaluation of *Lsm1* gene deletion in MEF and T cells.

(A) Schematic representation of the gene targeting construct indicating positions of restriction sites and probes to validate the *Lsm1* gene targeting strategy. **(B)** Southern blot analysis of genomic DNA from wildtype and *neo/neo* digested tails of mice showing the detection of SwaI/EcoRV restriction digest fragments with a 5' probe to determine the size difference between *Lsm1*^{+/+} (10298 bp) and *Lsm1*^{neo/neo} (17378 bp) alleles. **(C)** Western blot analysis of *Lsm1* and tubulin proteins in extracts from *Lsm1*^{+/+} and *Lsm1*^{neo/neo} immortalized MEF cells detected with different monoclonal and polyclonal antibodies against *Lsm1*. **(D)** Intracellular flow cytometry staining of *Lsm1* protein in *Lsm1*^{+/+} and *Lsm1*^{neo/neo} T cells using the 5F3 monoclonal *Lsm1*-specific antibody.

Correct insertion of the targeting vector (Figure 6A) was verified by Southern blotting using genomic DNA of digested tails of *Lsm1^{+/+}* and *Lsm1^{neo/neo}* mice (Figure 6B). The insertion of the neomycin cassette into intron 1 produced the expected larger fragment after restriction digest of genomic DNA from *Lsm1^{neo/neo}* as compared to wildtype cells when the samples were analyzed by hybridizing the 5' probe to detect the *Lsm1* locus (Figure 6B). In protein extracts from *Lsm1^{neo/neo}* MEF cells the absence of the Lsm1 protein was confirmed by Western blotting. Different antibodies were used to detect possible truncated versions of Lsm1 that may arise from the open reading frame in exon 1 of the gene and the samples were separated on a tricine-buffered SDS gel to provide resolution of protein sizes even below 10kDa. In the *Lsm1^{neo/neo}* samples there were no signals detectable at the expected size of 15kDa and also below (Figure 6C). Absence of Lsm1 was also confirmed by intracellular staining and flow cytometry. In these experiments wildtype CD4⁺ T cells (right) were clearly positive for Lsm1, while *Lsm1^{neo/neo}* CD4⁺ T cells (left) showed a left-shifted Lsm1 signal indicating background reactivity of the antibodies (Figure 6D). This confirmation that disruption of the *Lsm1* allele leads to an absence of Lsm1 protein in different cell types represented the starting point of the following analyses.

4.2 Molecular consequences of the Lsm1 knockout

Having confirmed the absence of the Lsm1 protein in *Lsm1^{neo/neo}* MEF and T cells, the consequences of Lsm1 deficiency on the molecular level were analyzed by focusing on known functions of the Lsm1-7 complex, including histone mRNA degradation, P-body formation and interaction with Pat1b.

4.2.1 Histone mRNA degradation occurs delayed in the absence of Lsm1

During early S phase, the levels of replication-dependent histone mRNAs are strongly upregulated to provide histones proteins for the ongoing DNA replication (Whitfield M.L. et al., 2000). At the end of S phase, these mRNAs are rapidly degraded. This induced decay involves the exonuclease Eri1, which targets histone mRNAs after they are oligouridylated. In a stepwise manner Eri1 degrades through the histone stem-loop that normally stabilizes these mRNAs, which lack a poly(A) tail, thereby causing instability of the entire transcript (Hoefig et al., 2013). The additional involvement of the Lsm1-7 heteroheptamer in this process was already demonstrated in 2008 by

Mullen and Marzluff (Mullen & Marzluff, 2008). The complex was shown to recognize the added uridines at the 3' end of histone mRNA molecules and to enable the decay process (Mullen & Marzluff, 2008). Importantly, impaired function of Eri1 resulted in the accumulation of histone mRNAs in mouse cells and similarly histone mRNAs also accumulated due to absence of Lsm1 in yeast cells (Herrero & Moreno, 2011). We therefore asked whether deletion of Lsm1 in MEF cells causes a similar phenotype. To answer this question, we treated wildtype and *Lsm1^{neo/neo}* MEF cells with hydroxyurea (HU) (see 3.2.4.4) in order to mimic the cellular situation at the end of the S-phase and induce the degradation process. Total RNA was extracted and expression levels of selected replication-dependent histone mRNAs were analyzed by qPCR (Figure 7).

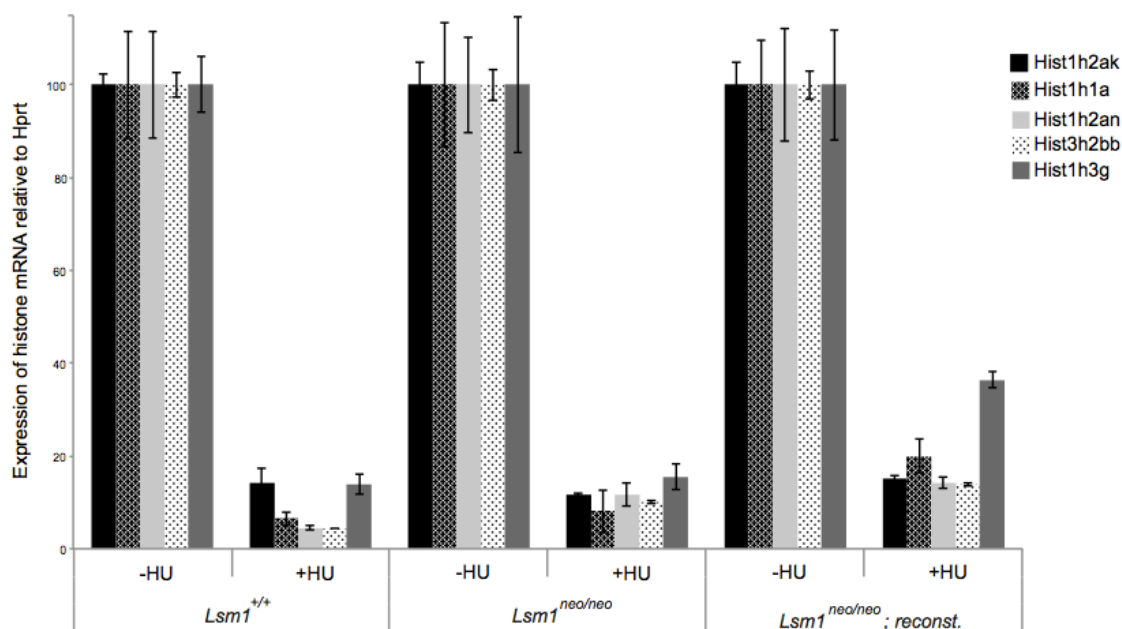


Figure 7: Degradation of selected histone mRNAs in the presence and absence of Lsm1.

qPCR data showing the expression of five different histone mRNAs in cells before and after 45min of HU-treatment analyzing the three different cell lines: *Lsm1^{+/+}* (left), *Lsm1^{neo/neo}* (middle) and *Lsm1^{neo/neo}* reconstituted (*reconst.*) (right) with wildtype *Lsm1* construct. The histone mRNA expression levels were calculated relative to *Hprt* expression and displayed in percentage of untreated cells. The experiment was repeated 5 times with 3 technical replicates.

Analyzing histone mRNA levels in wildtype (*Lsm1^{+/+}*) and Lsm1 KO (*Lsm1^{neo/neo}*) as well as in Lsm1-reconstituted KO MEF cells (*Lsm1^{neo/neo};reconst.*) revealed a similar decrease to approximately 20% of the initial amount for all five histone mRNAs after treatment with HU, regardless of Lsm1 presence or absence (Figure 7).

Because these results were not consistent with data obtained in yeast, we hypothesized that histone mRNAs in *Lsm1*-deficient mouse cells were degraded due to compensation. We therefore reconstituted knockout cells with functionally impaired *Lsm1* mutants, which could potentially interfere with the hypothesized compensatory adaptation of the histone mRNAs degradation process. To this end, we used two *Lsm1* mutations that were studied in yeast cells by the group of Parker in 2005. Combined mutation of R33A; D36A caused severe defects of the *Lsm1*-7 complex in binding to mRNA in general and another *Lsm1* mutant harboring combined R67A; G68W; E69A mutations affected the function of the *Lsm1*-7 complex partially, by preventing its binding to oligoadenylated mRNAs (Tharun, Muhrad, Chowdhury, & Parker, 2005). We compared retroviral transductions with different multiplicities of infections to select conditions under which mutant *Lsm1* protein expressions were close to the endogenous *Lsm1* expression levels in wildtype cells (Figure 8A), and used them for HU treatment (Figure 8B).

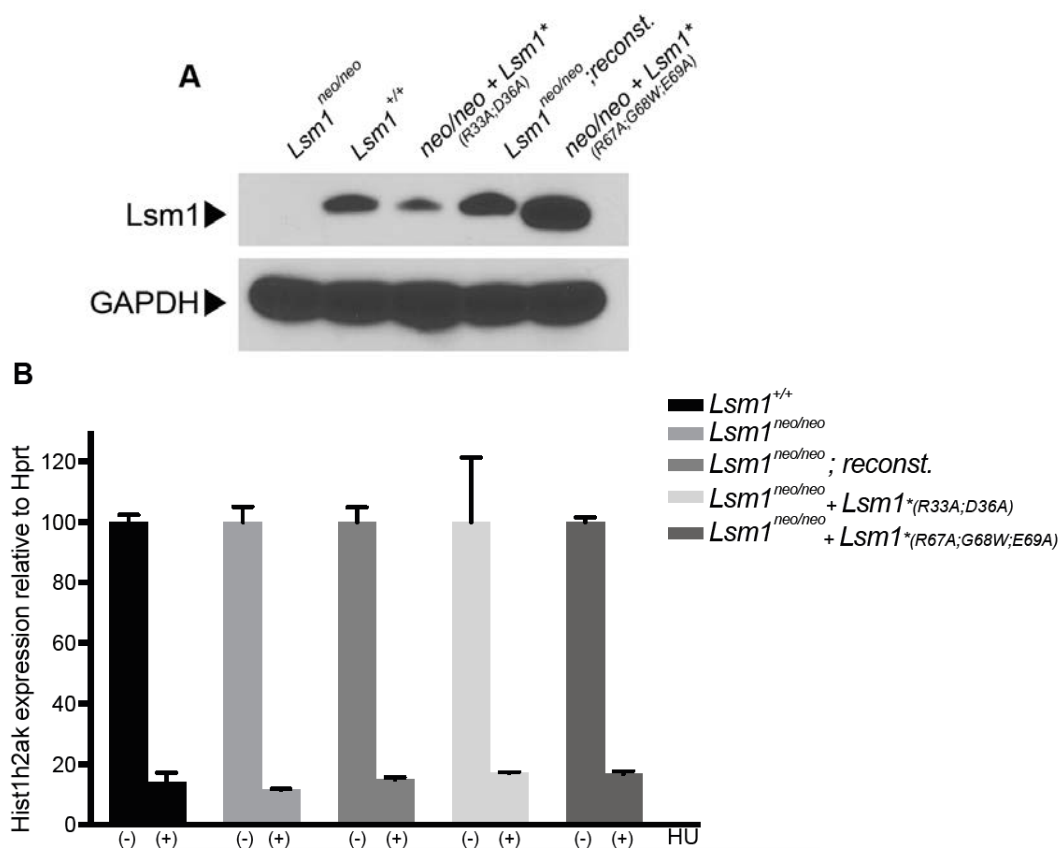


Figure 8: HU-induced histone mRNA degradation in the absence of *Lsm1* and presence of mutated *Lsm1*.

(A) Western blot analysis showing expression levels of endogenous or reconstituted wildtype and mutant *Lsm1* in the cells analyzed in (B). (B) qPCR data showing expression of the histone *Hist1h2ak* mRNA relative to *Hprt* before and after 45min of HU-treatment as percentage of untreated cells. The experiment was repeated 3 times with 3 technical replicates.

Surprisingly, also here HU treatment led to same strong decrease of Hist1h2ak transcripts in cells with presence of endogenous Lsm1, cells with complete absence of Lsm1 or in cells with Lsm1 being present in different mutated forms (Figure 8B). We also tried to find indication for compensatory mRNA decay in absence of Lsm1 at different time points (Figure 9). Importantly, after 15min and 30min of HU treatment, the levels of the three different investigated histone mRNAs were higher in *Lsm1^{neo/neo}* MEF compared to those in wildtype cells. These findings indicate that Lsm1 deletion causes a delay in the HU-induced histone mRNA decay. However, at 45min of HU treatment, all three analyzed histone mRNAs decreased to the same extent in both samples consistent with our previous results.

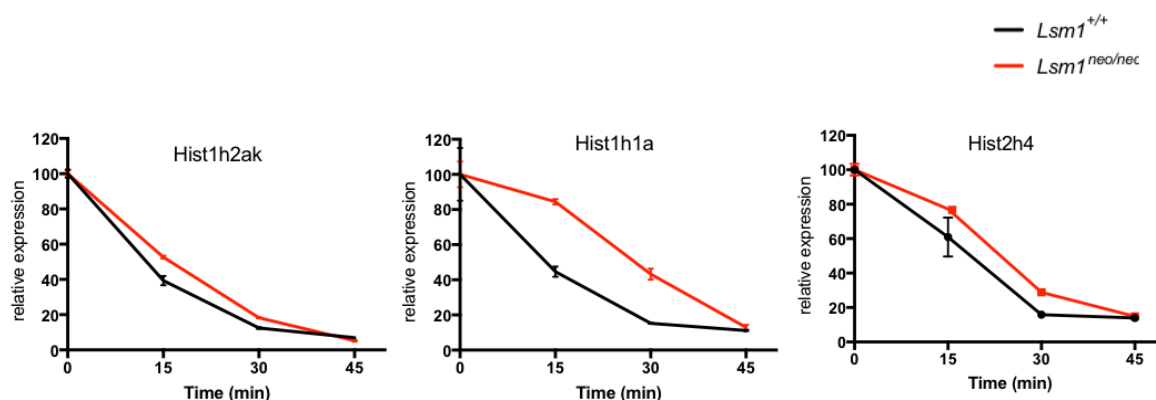


Figure 9: Delayed histone mRNA degradation in the absence of Lsm1.

Analysis of expression levels of the three histone mRNAs *Hist1h2ak*, *Hist1h1a* and *Hist2h4* at 15, 30 and 45 min of HU-treatment are shown for *Lsm1* wildtype (black) and *Lsm1^{neo/neo}* KO cells (red). The experiment was repeated 2 times with 3 technical replicates.

4.2.2 P-body form in the absence of Lsm1

P-bodies are distinct membrane-less foci in the cytoplasm of the eukaryotic cell that contain aggregates of mRNAs with proteins involved in mRNA degradation. Proteins like RCK or Edc4 are markers of P-bodies and their presence is required for the formation of P-bodies. Importantly, also Lsm1 is a P-body marker, and its knockdown was shown to also significantly reduce the proportion of cells with visible P-bodies in different cell types (Andrei et al., 2005; Chu & Rana, 2006; Kedersha et al., 2005; Stoecklin et al., 2006; Vindry et al., 2017). We therefore analyzed Lsm1-deficient MEF cells by confocal microscopy for P-body formation using RCK as marker as described in 3.2.4.11 (Figure 10).

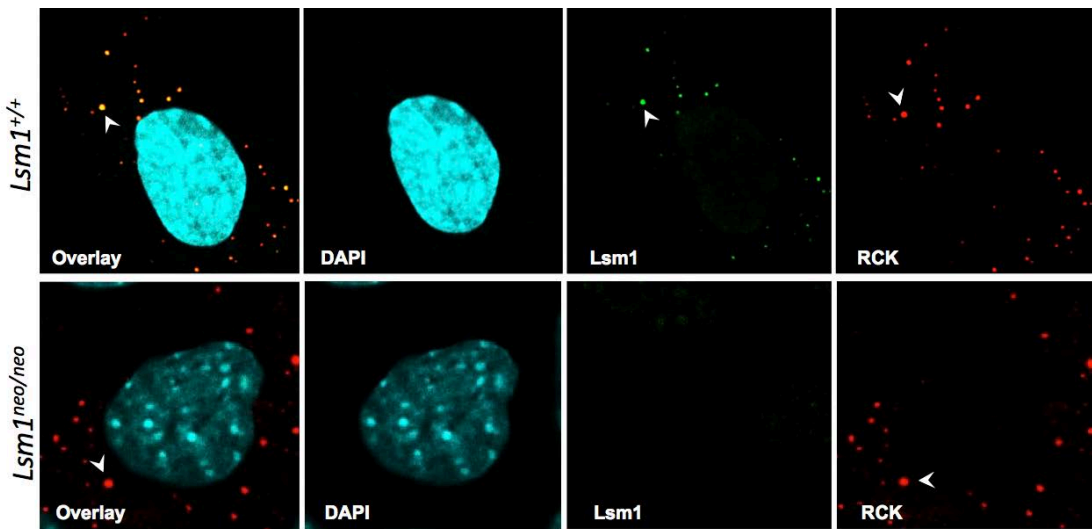


Figure 10: P-bodies form in the absence of Lsm1.

Confocal microscopy analyzing co-localization of Lsm1 with RCK (red) in P-bodies of *Lsm1^{+/+}* and *Lsm1^{neo/neo}* MEF cells, white arrowheads indicate RCK- and Lsm1- marked foci, respectively.

In wildtype MEF cells Lsm1 was found to co-localize with the P-body marker RCK (Figure 10 upper panel) and knockout cells did not show an Lsm1 signal (Figure 10 lower panel). Contrary to the expectations the knockout cells still showed a clearly focused RCK signal that was indistinguishable from wildtype cells. Since P-bodies were still detectable in the absence of Lsm1, the question arose, whether the Lsm2-7 proteins that are shared in the two cytoplasmic and nuclear Lsm1-7 and Lsm2-8 complexes, respectively, showed altered distribution when Lsm1 was deleted. To answer this question MEF cells were stained with an antibody against Lsm4, as a representative subunit of both complexes. The Lsm4 signal was not only detectable in the nucleus and cytoplasm of wildtype cells, but also localized similarly to cytoplasmic Edc4 containing foci in the absence of Lsm1 (Figure 11A). To further confirm these observations, nuclear and cytoplasmic fractionation was performed. Lsm4 was present in both the nuclear and cytoplasmic fractions, consistent with it being part of the cytoplasmic Lsm1-7 and nuclear Lsm2-8 complex. In contrast, Lsm8 was only present in the nuclear fraction, consistent with being a subunit of the Lsm2-8 complex. Successful fractionation was confirmed through detection of proteins with predominant localization to the nucleus (Polymerase II, shortly Pol II) and the cytoplasm (IkB α) in the respective fractions (Figure 11B).

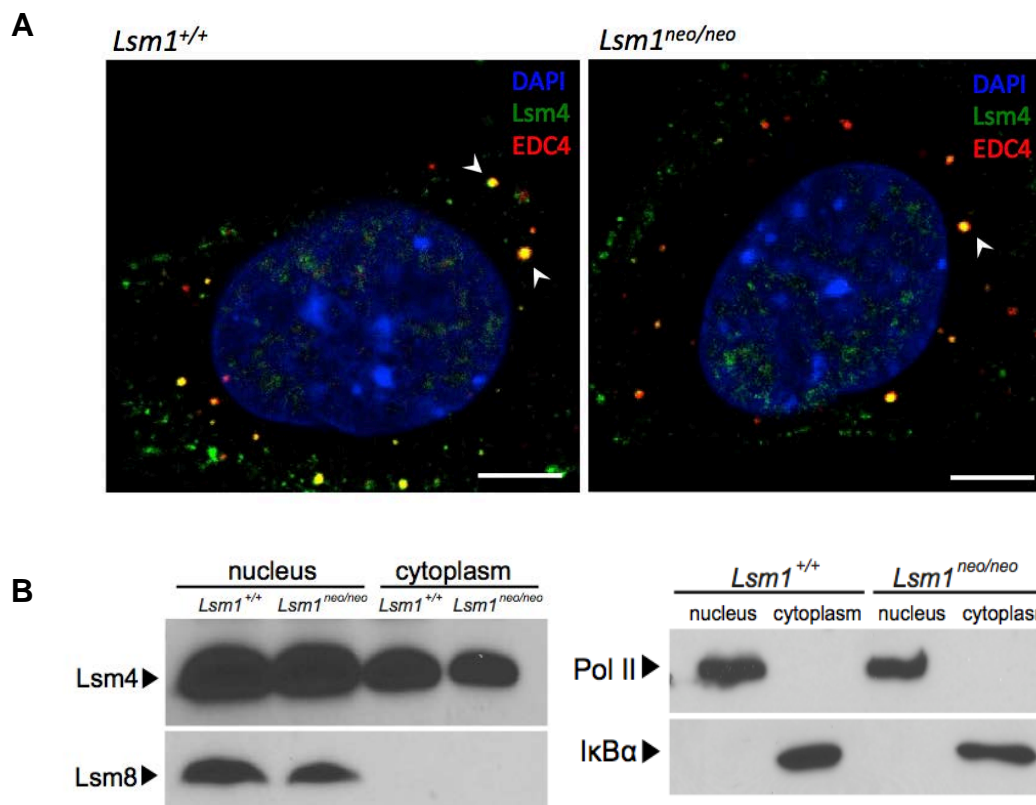


Figure 11: Unchanged expression and localization of Lsm4 in the absence of Lsm1.

(A) Staining of Lsm4 (green) and Edc4 (red) in *Lsm1*^{+/+} and *Lsm1*^{neo/neo} MEF cells. **(B)** Immunoblot analysis showing expression levels of Lsm4 and Lsm8 in the nucleus- and cytoplasm-fractions of *Lsm1*^{+/+} and *Lsm1*^{neo/neo} MEF cells (left). Appropriate separation of proteins in the two fractions was confirmed by the detection of the protein Pol II that is exclusively present in the nucleus and the cytoplasmic protein IκBα. Representative blots of 3 independent experiments.

These results confirmed our observations in confocal microscopy, demonstrating that Lsm1 deletion did not prevent the localization of Lsm4 to P-bodies or increase the abundance of Lsm4 in the nuclear Lsm2-8 complexes. To determine whether Lsm1 is not essential but regulates the formation of P-bodies, we quantified the number of P-bodies in T cells in imaging flow cytometry. P-bodies were identified by RCK staining in CD4⁺ T cell population of splenocytes. It was noticeable that T cells display a range of different P-body counts distributed from one single P-body to as many as ten (see Figure 12). The majority of stained T cells in our experiment, however, exhibited rather few P-bodies with half of the cells having less than 5 P-bodies per cell, and Lsm1-deficient cells showed a similar distribution (Figure 12). Together these data establish that the formation of P-bodies and their abundance per cell remained unchanged in Lsm1-deficient CD4⁺ T cells or fibroblasts.

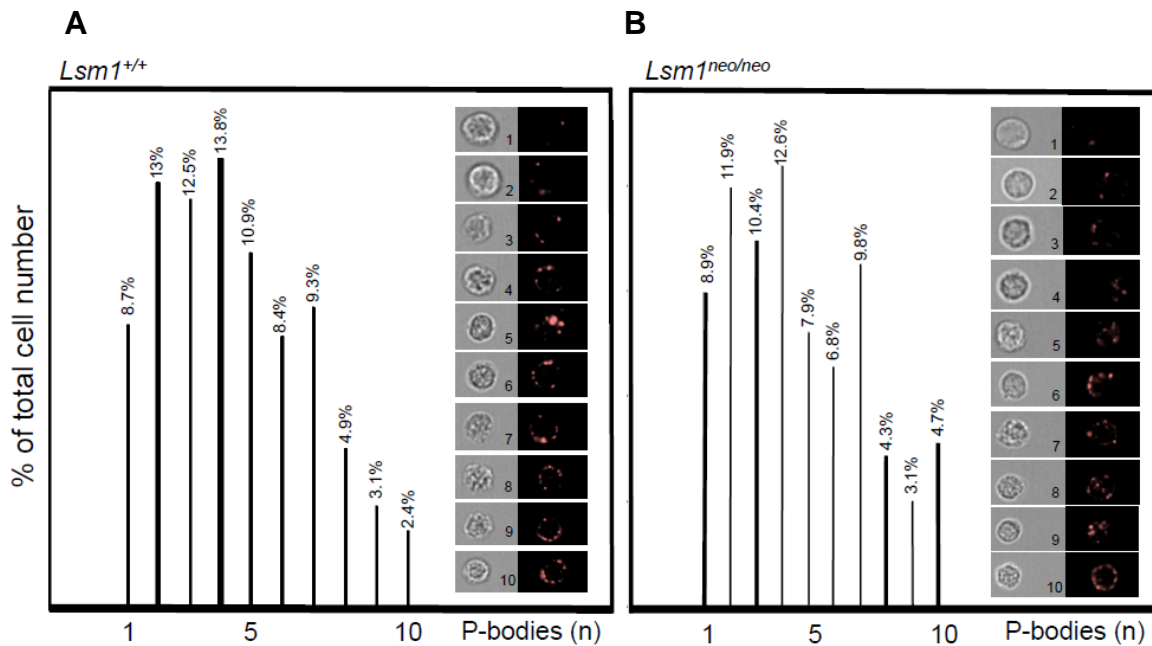


Figure 12: P-body formation in *Lsm1*^{+/+} and *Lsm1*^{neo/neo} T cells.

Imaging flow cytometry analysis performed on CD4⁺ T cells within splenocytes of *Lsm1*^{+/+} and *Lsm1*^{neo/neo} mice. P-bodies were detected by staining the RCK marker protein as shown in the representative images on the right. 448 CD4⁺ T cells from *Lsm1*^{+/+} and 507 CD4⁺ T cells from *Lsm1*^{neo/neo} mice were analyzed. Detected signals were counted for each analyzed CD4⁺ T cell and percentages of cells carrying P-body ranging from 1-10 are displayed for *Lsm1*^{+/+} (A) and *Lsm1*^{neo/neo} (B).

These results showed in MEF and T cells that depletion of Lsm1 did not influence formation of P-bodies.

4.2.3 The interaction of components of the Lsm1-7 complex with Pat1b is impaired in Lsm1-deficient cells

Since depletion of Lsm1 did not impair P-body formation or localization of Lsm4 to P-bodies, we asked whether ring formation and known interactions still take place even without the Lsm1 subunit. Interaction of Patb1 with the Lsm1-7 ring was shown to be absolutely necessary for the recognition and binding of mRNAs targeted for decay (Chowdhury et al., 2014). To address alternative complex formation and Pat1b interaction we performed immunoprecipitations in protein extracts from *Lsm1*^{+/+} and *Lsm1*^{neo/neo} MEF cells using an antibody against Pat1b. Although Pat1b was slightly lower expressed in Lsm1-deficient MEF cells, it was detectable in either cell lysate and was equally represented in both immunoprecipitations (Figure 13).

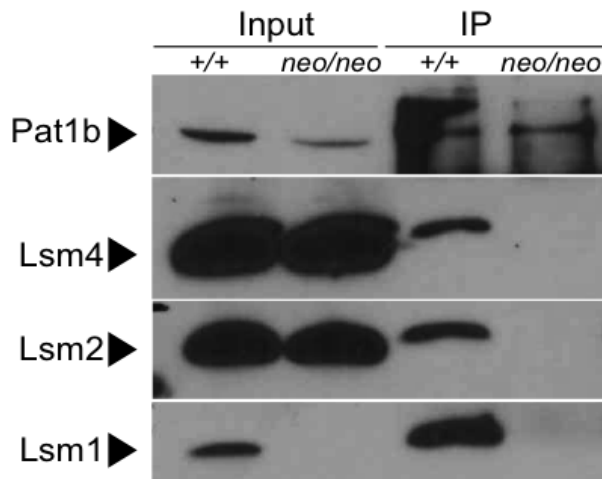


Figure 13: *Lsm2* and *Lsm4* do not interact with *Pat1b* in the absence of *Lsm1*.

Co-immunoprecipitation of *Lsm2* and *Lsm4* with *Pat1b* from extracts of MEF cells derived from wildtype (+/+) and *Lsm1^{neo/neo}* mice. The autoradiograph depicts one representative result from 5 independent experiments.

Neither *Lsm4* nor *Lsm2* levels changed in the input, however both proteins were absent in the immunoprecipitations of *Pat1b* from extracts of *Lsm1* knockout MEF cells (Figure 13). In the course of repeated experiments, we noticed that expression of *Pat1b* in the *Lsm1^{neo/neo}* samples was reduced when compared to wildtype samples. This observation suggested a direct or indirect regulation of *Pat1b* protein expression by *Lsm1*. Since *Lsm1* has several interaction partners, we asked whether this effect was also observed for other proteins in the 5'-3' or 3'-5' mRNA decay pathways. To answer this question, *Lsm1^{+/+}* and *Lsm1^{neo/neo}* MEF cells were lysed and expression of proteins of the decay machinery was analyzed by SDS-PAGE and subsequent immunoblotting.

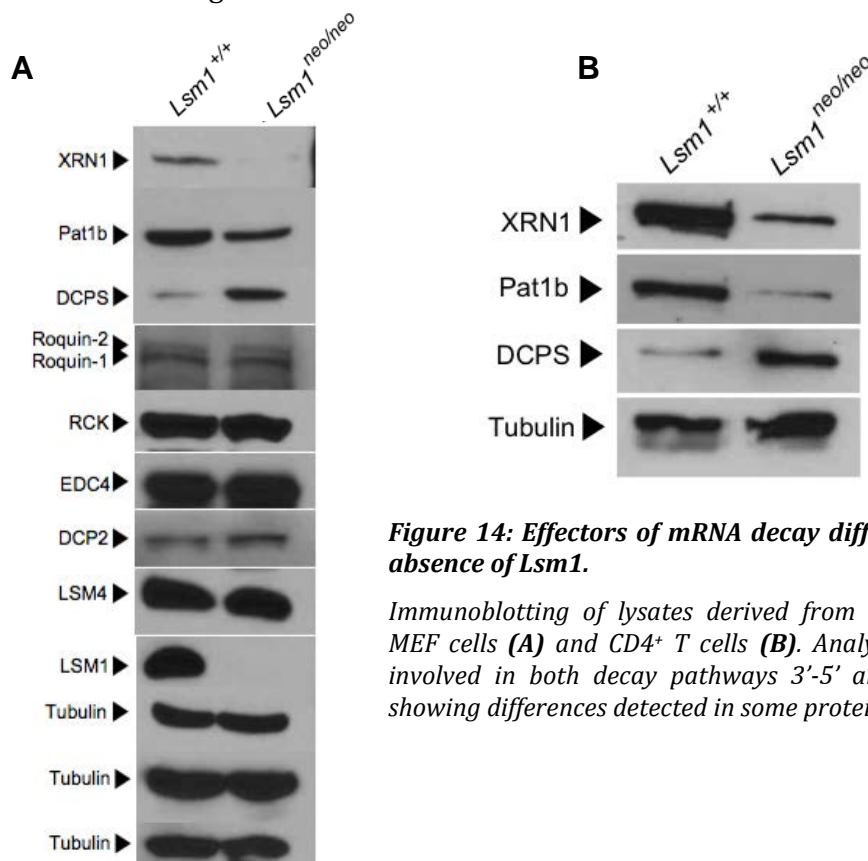


Figure 14: Effectors of mRNA decay differ in expression in the absence of *Lsm1*.

Immunoblotting of lysates derived from *Lsm1^{+/+}* and *Lsm1^{neo/neo}* MEF cells (A) and *CD4⁺* T cells (B). Analysis of different proteins involved in both decay pathways 3'-5' and 5'-3' decay pathway showing differences detected in some proteins (n=4).

Comparable to previous results, Pat1b again showed a clear reduction in expression in *Lsm1* depleted samples (Figure 14A). Interestingly also expression of XRN1, the exonuclease of the 5'-3' decay pathway was reduced in *Lsm1^{neo/neo}* MEF cells, in contrast to DcpS levels, the decapping enzyme of the 3'-5' pathway that appeared elevated. Additional analyses did not identify changes in expression of Roquin-1 and Roquin-2, RCK, Edc4, DCP2 or *Lsm4*. In order to ensure that changes in expression was not cell-type specific but a consequence of *Lsm1* deletion, the same experiment was repeated with lysates derived from CD4⁺ T cells. Interestingly, differences in protein levels were similarly detectable also in this cell type (Figure 14B).

From these *in vitro* experiments it can be concluded that depletion of *Lsm1* did not affect P-body formation, the number of P-bodies in the cell or the localization of *Lsm4* to P-bodies. Nevertheless, its absence prevented interaction of *Lsm2* and *Lsm4* with Pat1b, changed the kinetics of induce histone mRNA degradation and reduced the cellular expression *Lsm1-7* associated Xrn1 and Pat1b proteins, while DcpS protein expression increased.

4.3 Consequences of the *Lsm1* knockout in the mouse

4.3.1 Global *Lsm1* deletion in the *Lsm1^{neo/neo}* mouse

The *in vitro* analyses suggested that *Lsm1* function in MEF cells could be compensated by other factors, when prototypic functions like P-body formation or histone mRNA decay were analyzed. We then searched for non-redundant functions in the *Lsm1^{neo/neo}* mouse. First, the efficient deletion was confirmed in a number of tissue samples of *Lsm1^{neo/neo}* mice. Endogenous levels of *Lsm1* were detectable in all wildtype spleen, brain, kidney, thymus and lung, and the corresponding band was missing in KO tissue samples (Figure 15).

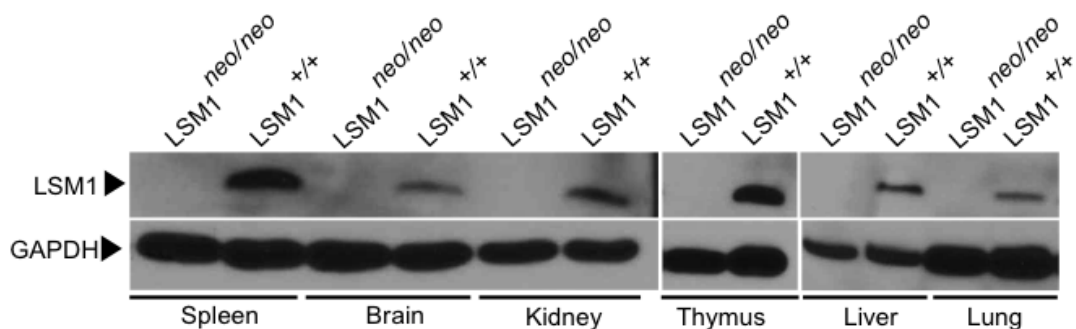


Figure 15: Efficient deletion of *Lsm1* in *Lsm1^{neo/neo}* mice.

Immunoblot showing *Lsm1* and GAPDH expression in different tissues of *Lsm1^{+/+}* and *Lsm1^{neo/neo}* mice. Protein lysates were prepared from different organs of the mice and analyzed by SDS-PAGE and immunoblotting. The protein band of *Lsm1* was missing in all organs of the *Lsm1^{neo/neo}* mouse, respectively. The experiment was repeated 3 times with newly prepared samples of the respective mouse.

Interestingly, homozygous female mice appeared sterile, whereas male *Lsm1^{neo/neo}* mice were fertile (data from 3 mating plugs). Another interesting observation is that mice with heterozygous or homozygous targeted *Lsm1* alleles were represented in significantly reduced frequencies (Figure 16).

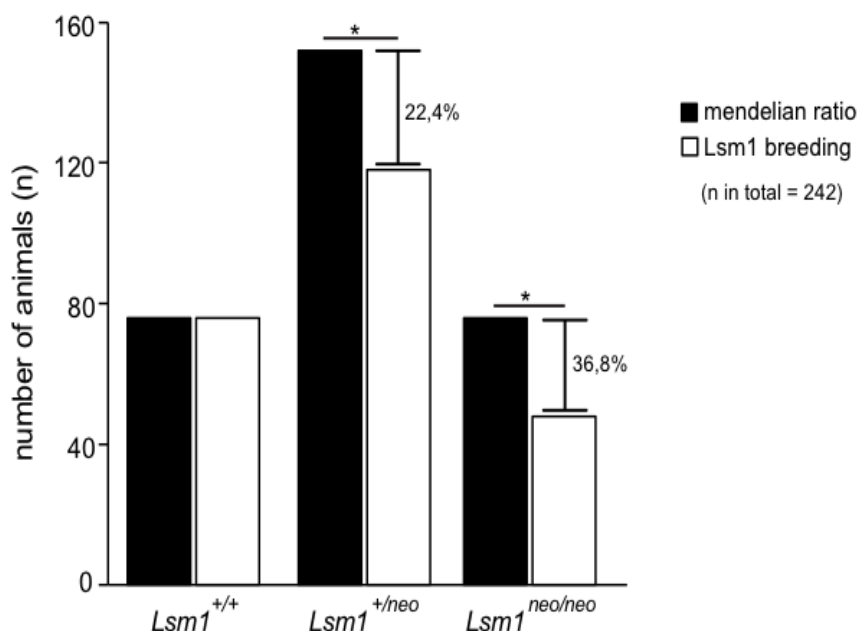


Figure 16: Genotypes of offspring from *Lsm1* breedings deviate from Mendelian distribution.

Number of animals resulting from heterozygous *Lsm1^{neo/+}* breedings, according to their genotypes. Expected Mendelian numbers (black bars) are compared to actual numbers (white bars). The numbers of animals carrying one KO allele or both KO alleles are reduced by 22,4% and 36,8%, respectively. Results were obtained from observation of 242 *neo/+* breedings. Error bars show SD and statistical analysis was performed by paired-t-test (ns: not significant, * $p < 0.05$, ** $p < 0.01$, *** $p < 0.005$).

The offspring of homozygous mice was reduced by 36,8%, heterozygous mice by 22,4% suggesting possible abnormalities during embryonic development caused by the deleted *Lsm1* gene (Figure 16). Interestingly, mice that were homozygous for *Lsm1* deletion, but survived, exhibited a significantly decreased body weight compared to litter mate control *Lsm1*^{+/+} mice (Figure 17A). To see whether the mice recovered, we weighted them again at the age of 8-10 weeks. Remarkably, results revealed that the phenotype remained significant until adulthood (Figure 17B).

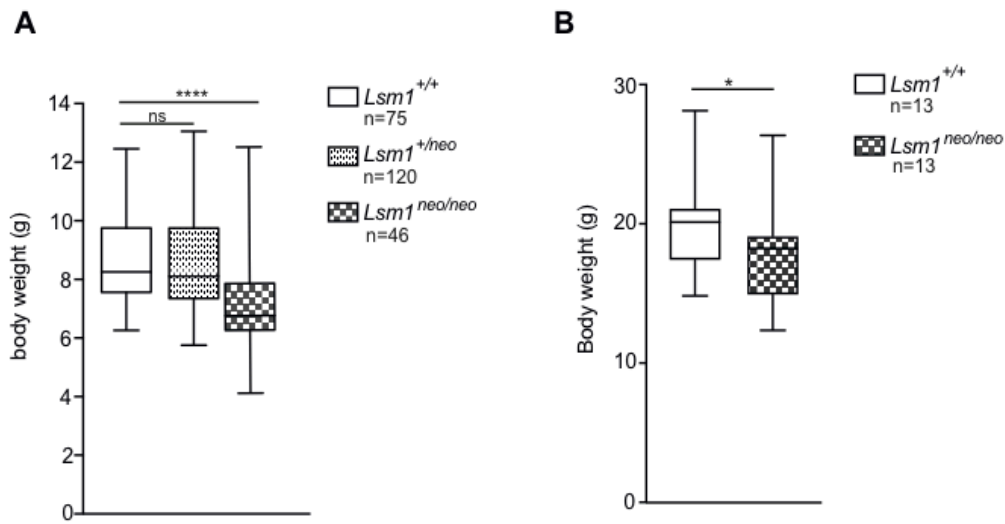


Figure 17: Body weights of *Lsm1*^{neo/neo} mice are significantly reduced.

The weight of *Lsm1*^{+/+}, *Lsm1*^{+/neo} and *Lsm1*^{neo/neo} mice were determined directly after weaning (**A**) or of *Lsm1*^{+/+} and *Lsm1*^{neo/neo} mice at the age of 8-10 weeks (**B**). Error bars show SD and statistical analysis was performed by paired-t-test (ns: not significant, **p*<0.05, ***p*<0.01, ****p*<0.005).

To gain insights into the potential role of *Lsm1* in different cell types, we measured *Lsm1* and *Lsm4* protein expression in extracts of several tissues of the mouse. As seen in Figure 18, *Lsm1* and *Lsm4* compared to GAPDH and Ubiquitin levels differed in various tissues of the mouse, being remarkably higher expressed in thymus and spleen.

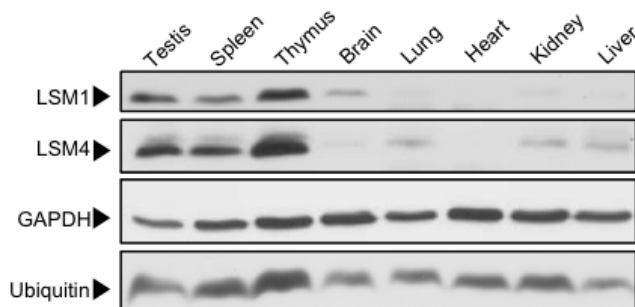


Figure 18: *Lsm1* expression is high in testis, spleen and thymus.

Western blot analysis of lysates of tissues from organs of a wildtype mouse. Immunoblot shows expression levels of the proteins *Lsm1*, *Lsm4* and the loading controls GAPDH and Ubiquitin. Experiment was performed by Dr. Kai Hoefig.

Based on these results we focused our investigation on the immune system. Interestingly, comparing wildtype and *Lsm1^{neo/neo}* mice, we did not find any changes in thymus weight or number of thymocytes as seen in Figure 19.

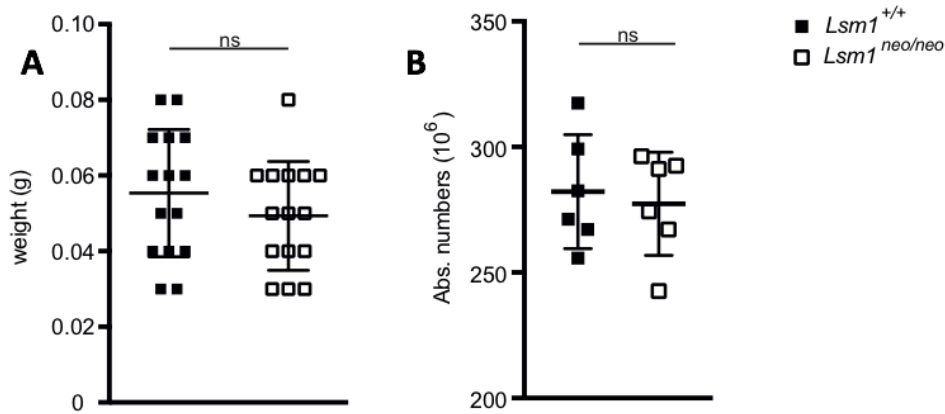


Figure 19: Thymus weight and thymocytes number of *Lsm1^{neo/neo}* mice are unchanged.

(A) Weight of thymi isolated from *Lsm1^{+/+}* and *Lsm1^{neo/neo}* mice and absolute thymocyte numbers **(B)**. Error bars show SD and statistical analysis was performed by paired-t-test (ns: not significant).

Next, we asked whether *Lsm1* deletion had any impact on the development of T cells. Frequencies of thymocytes derived from *Lsm1^{neo/neo}* were analyzed over the stages of double negative (DN) to double positive (DP) and single positives by staining with anti-CD4 and anti-CD8 antibodies. Flow cytometric results revealed no changes in any of the investigated stages as seen in the representative contour plot (Figure 20A) or in the compiled representation (Figure 20B).

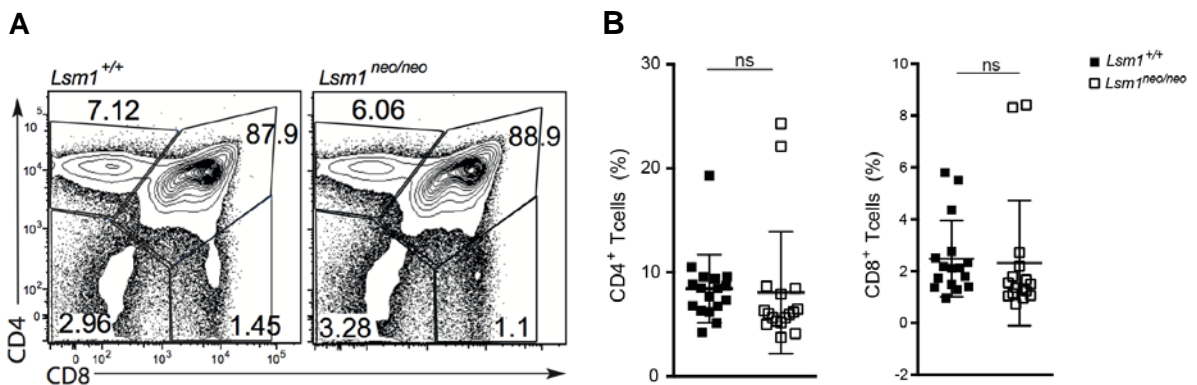


Figure 20: Deletion of *Lsm1* does not affect T cell development in the thymus.

(A) Representative contour plot showing the frequencies of CD4⁺ or CD8⁺ thymocytes in wildtype (left) and *Lsm1^{neo/neo}* mice (n=14). **(B)** Frequencies of CD4⁺ and CD8⁺ T cells in wildtype (black) and *Lsm1^{neo/neo}* (white). Error bars show SD and statistical analysis was performed by paired-t-test (ns: not significant).

One important subgroup of T cells generated in the thymus are regulatory T cells (Tregs). The impaired generation of Tregs can be the underlying cause of several autoimmune or auto-inflammatory diseases such as type-1 diabetes mellitus, thyroiditis, gastritis and the Crohn' disease (Ito et al., 2008). We investigated therefore also frequencies of Tregs in *Lsm1*-deficient and wildtype thymi. Intracellular staining of Foxp3, the marker of Tregs, was performed as described in the section 3.2.4.7, and the results revealed no abnormalities in frequencies of Foxp3⁺ T cells compared to wildtype animals (Figure 21).

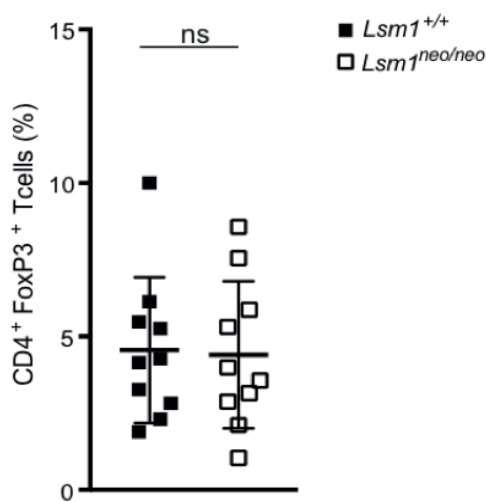


Figure 21: Frequencies of regulatory T cells in thymi of *Lsm1*^{neo/neo} mice are normal.

Frequencies of CD4⁺ T cells expressing Foxp3 intracellularly. Results are shown for wildtype (black) and *Lsm1*^{neo/neo} (white). Error bars show SD and statistics were performed using paired-t-test (ns: not significant).

High protein levels of *Lsm1* were detected also in the spleen of *Lsm1*-deficient mice, we therefore investigated this organ in more detail. Flow cytometric analysis of a variety of peripheral hematopoietic lineages followed and was performed according to the staining protocol described in section 3.2.4.7. Analyses included the investigation of frequencies of CD4, CD8, Tregs, total B cells, follicular B cells or marginal zone B cells (MZB) as well as dendritic cells, NKT and NK cells. In comparison with littermate wildtype control animals none of this cell types exhibited changes in frequencies as shown in Figure 22.

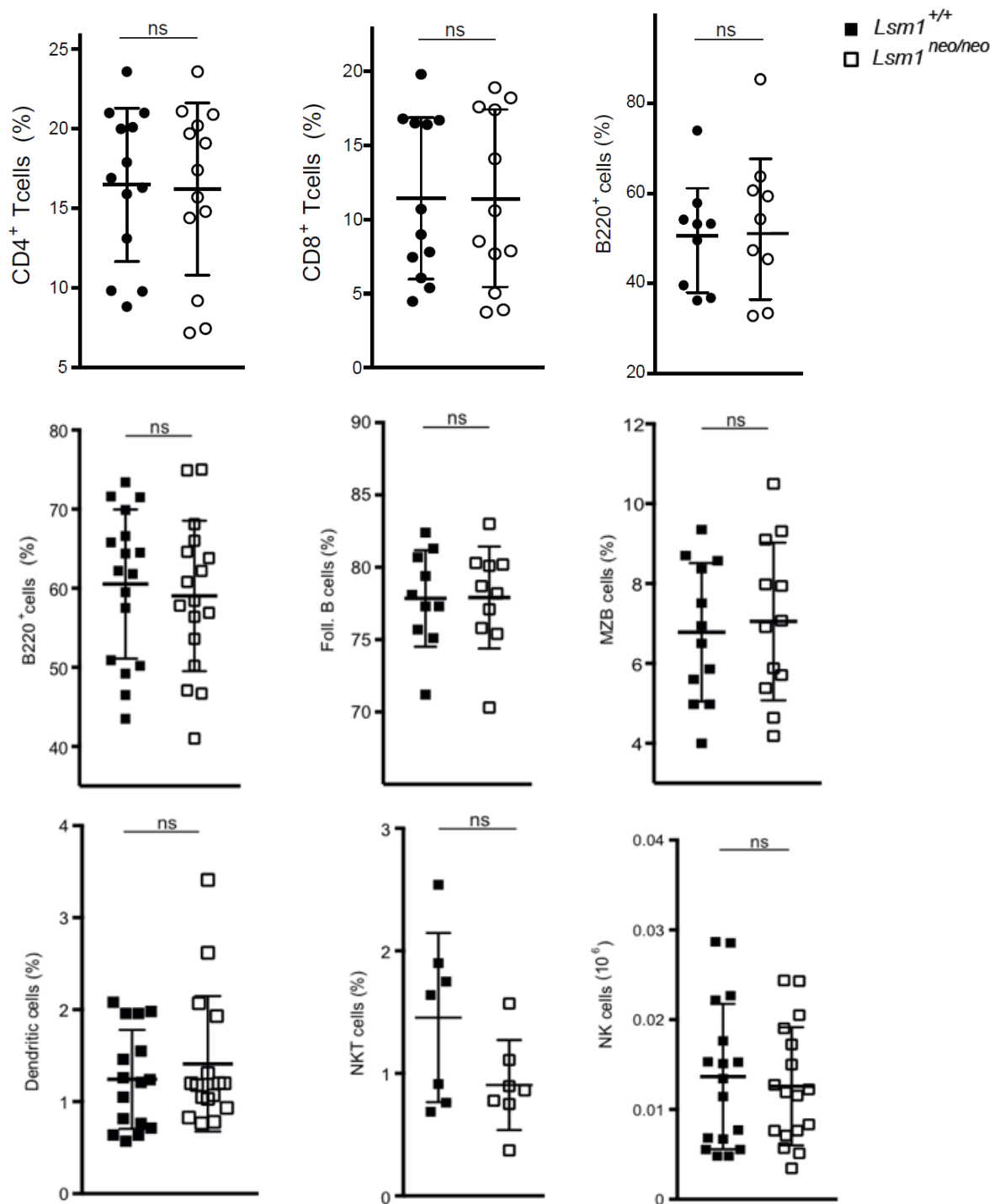


Figure 22: The frequencies of different hematopoietic lineages are not changed in splenocytes of $Lsm1$ -deficient mice.

Frequencies of CD4⁺ T cells (upper panel left), CD8⁺ T cells (upper panel middle), Tregs (upper panel right), total B cells, follicular B cells and MZB cells (middle panel), dendritic cells (lower panel left), NKT cells (lower panel middle) and NK cells (lower panel right) of wildtype (black) and $Lsm1^{neo/neo}$ (white) mice. Error bars show SD and statistical analysis was performed by paired-t-test (ns: not significant).

More striking were the observation of enlarged spleens of *Lsm1^{neo/neo}* mice that were already noticeable by visual inspection, particularly in light of the reduced body weight of the mice. Moreover, these mice revealed significantly increased numbers of splenocytes compared to control animals (Figure 23A). Splenomegaly was confirmed by weighting spleens of investigated mice and was highly significant compared to control animals (Figure 23B).

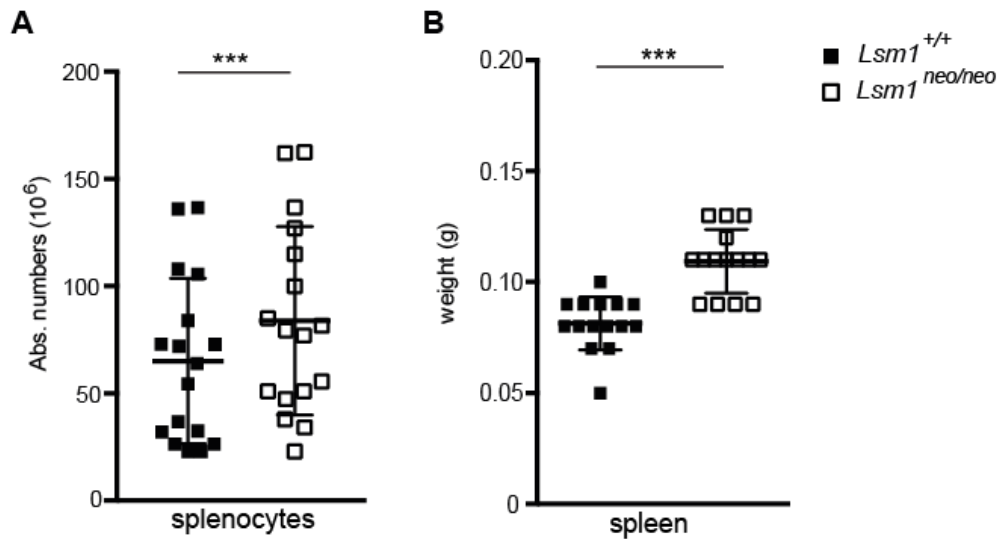


Figure 23: Spleen weights and splenocyte numbers are increased in *Lsm1*-deficient mice.

(A) Weight of spleens and absolute splenocyte numbers **(B)** of wildtype (black) and *Lsm1^{neo/neo}* (white) mice as measured in 8-10 weeks old animals. Error bars show SD and statistical analysis was performed by paired-t-test (ns: not significant, * $p < 0.05$, ** $p < 0.01$, *** $p < 0.005$).

This observation was already a strong indication of a possible dysregulation of the immune system and led us to investigate phenotypes connected to the development of autoimmunity. We next analyzed the activation status of T cells in *Lsm1*-deficient mice. Indeed, we found excessive T cell activation in CD4⁺ as well as CD8⁺ T cells (Figure 24A). Notably, both subsets displayed increased frequencies of effector-like T cells accompanied by a significantly reduced frequency of naïve T cells and almost unchanged frequencies of memory-like T cells (Figure 24B).

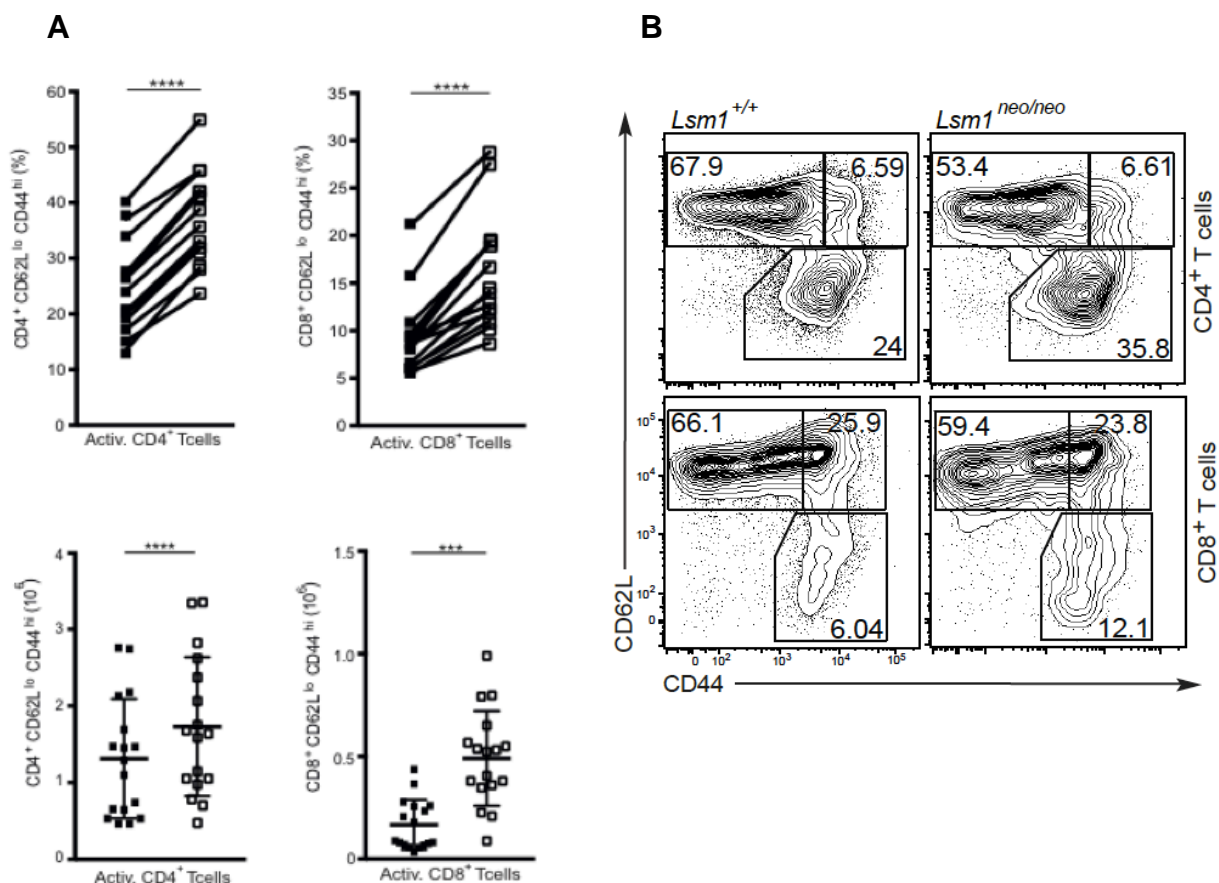


Figure 24: Lsm1-deficient CD4⁺ and CD8⁺ T cells show a phenotype of spontaneous activation.

(A) Relative (upper panel) and absolute (lower panel) numbers of effector-like CD4⁺ T cells and CD8⁺ T cells. (B) Representative contour plots of CD62L and CD44 stainings, gated on CD4⁺ T cells (upper panels) or CD8⁺ T cells (lower panels). Flow cytometric analysis performed in wildtype (black) and Lsm1^{neo/neo} (white) 8-10 weeks old animals. Error bars show SD and statistical analysis was performed by paired-t-test (ns: not significant, *p<0.05, **p<0.01, ***p<0.005).

4.3.2 Role of Lsm1 in CD4⁺ T cells

4.3.2.1 Stable expression of Lsm1 protein in activated CD4⁺ T cells

Due to the observed spontaneous activation of T cells in Lsm1-deficient mice, we speculated about a special role of Lsm1 in these cells. We first analyzed the expression level of Lsm1 during the process of T cell activation in wildtype CD4⁺ T cells. Two different types of *ex vivo* stimulations were employed: PMA/Ionomycin and α -CD3/CD28. By using PMA/Ionomycin, cells were subjected to a strong and unspecific stimulation. PMA diffuses into the cytoplasm and activates the Protein kinase C (PKC) and Ionomycin, as an ionophor triggers calcium influx. Because the two compounds act directly in the cytoplasm, bypassing stimulation through surface receptors, they

evoke maximal stimulation. Protein expression was measured here after 0, 30, 60, 90 and 120 minutes of stimulation (Figure 25A). For a more physiological stimulation, isolated T cells were subjected to α -CD3/CD28 mix. Expression levels were determined here after 6 and 24 hours of activation (Figure 25B). Protein level of I κ BNS was followed and served as control for the efficiency of stimulation (Fiorini E et al, 2002).

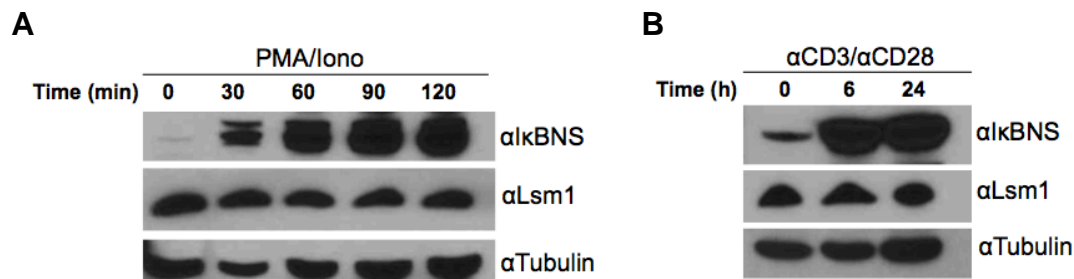


Figure 25: Lsm1 protein expression during activation is unchanged.

Immunoblot showing expression of Lsm1 protein during activation with PMA/Ionomycin (A) or α -CD3/CD28 (B). I κ BNS served as control of T cell activation and Tubulin as loading control in both experiments. Each experiment was performed twice.

After 30min of stimulation, I κ BNS protein levels increased as expected and reached highest amounts after 60min to then remain stable for the following 90 and 120min (Figure 25A). In contrast, Lsm1 protein levels remained unchanged over the entire period of time. Similar results were achieved when cells were stimulated with α -CD3/CD28, and Lsm1 expression was stable even after 24h of stimulation (Figure 25B).

4.3.2.2 Lsm1-deficient CD4⁺ T cells proliferate normally

Next, we asked whether proliferation of T cells was affected by the absence of Lsm1. To answer this question, we labeled cells with two different proliferation dyes and controlled the results by “dye swap”. By labeling cells of the analyzed genotypes, this method circumvents the culturing of two genotypes in different wells to minimize experimental variations. We isolated CD4⁺ T cells from wildtype and Lsm1-deficient mice, cultured them under Th0 (Figure 26A) or Th1 (Figure 26B) conditions and stained them with CFSE or eFLuro450 according to the protocols described in section 3.2.4.9. With each cell division the proliferation dye is diluted by a factor of two

resulting in a new peak with reduced fluorescence. Dashed graphs represent unstimulated and thereby undivided T cells containing the entire amount of proliferating dye. Histograms with the overlay of wildtype and KO showed no significant differences in the progression of the cell population through each single cell division.

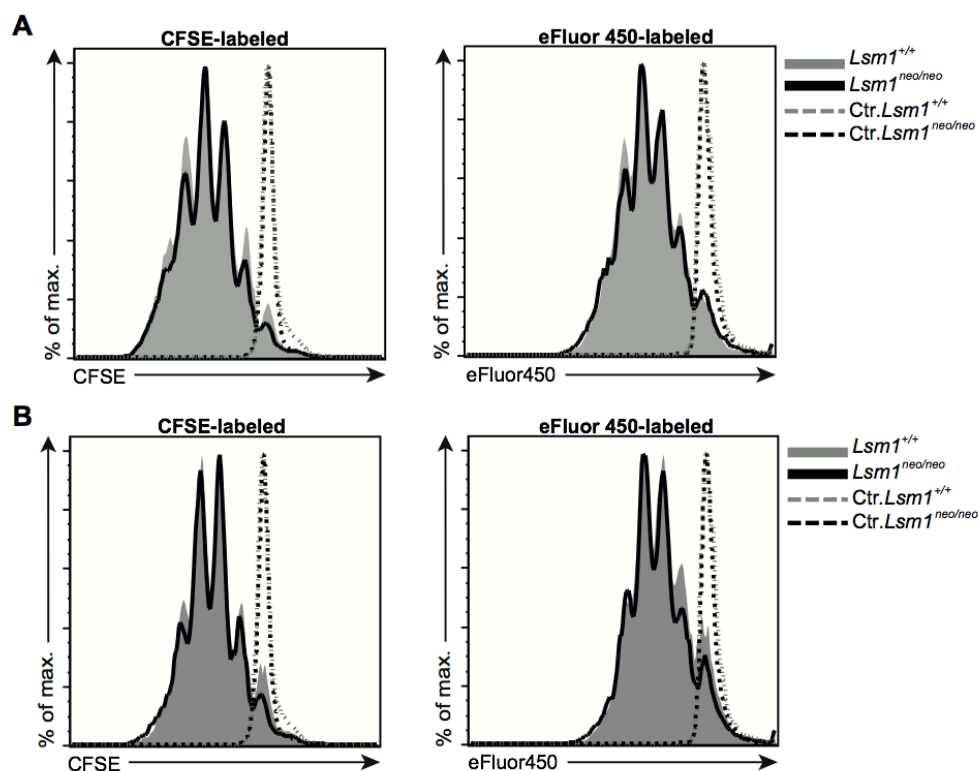


Figure 26: Proliferation of CD4⁺ T cells is unchanged after deletion of Lsm1.

Histograms displaying proliferation analyses of wildtype and Lsm1-deficient CD4⁺ T cells using CFSE and eFluor450 as proliferation dyes. Single peaks resulting from proliferation-dye dilution after each cell division represent single cell populations. Dashed lines represent control cells analyzed at the first day of experiment. Wildtype CD4⁺ T cells (gray) and Lsm1^{neo/neo} CD4⁺ T cells (black) were stained with different dyes and cultured in the same well under (A) Th0 or (B) Th1 conditions. Representative overlay histograms of 3 independent experiments.

4.3.2.3 T cell metabolism is unchanged in the absence of Lsm1

T cells change their metabolic profiles during activation and differentiation and can switch from oxidative phosphorylation to aerobic glycolysis (H. Chen, Yang, Zhu, & Zhao, 2015). Importantly, Lsm1 was connected to the regulation of the glycolysis process in yeast cells through its binding to mRNAs encoding enzymes of this metabolic pathway such as *pgk1* (Chowdhury et al., 2014). We therefore speculated about changes in the metabolic programs of T cells leading to the observed activation.

By using the seahorse approach, we analyzed the metabolic fitness of *Lsm1*-deficient $CD4^+$ T cells and control cells. For this purpose, we cultivated wildtype and *Lsm1*-deficient $CD4^+$ T cells for 48h under Th0 conditions as described in section 3.2.4.10. Results are shown in figure 27 and included measured values of extracellular acidification rate (ECAR) and oxidative consumption rate (OCR), as indicators of glycolysis or oxidative phosphorylation, respectively.

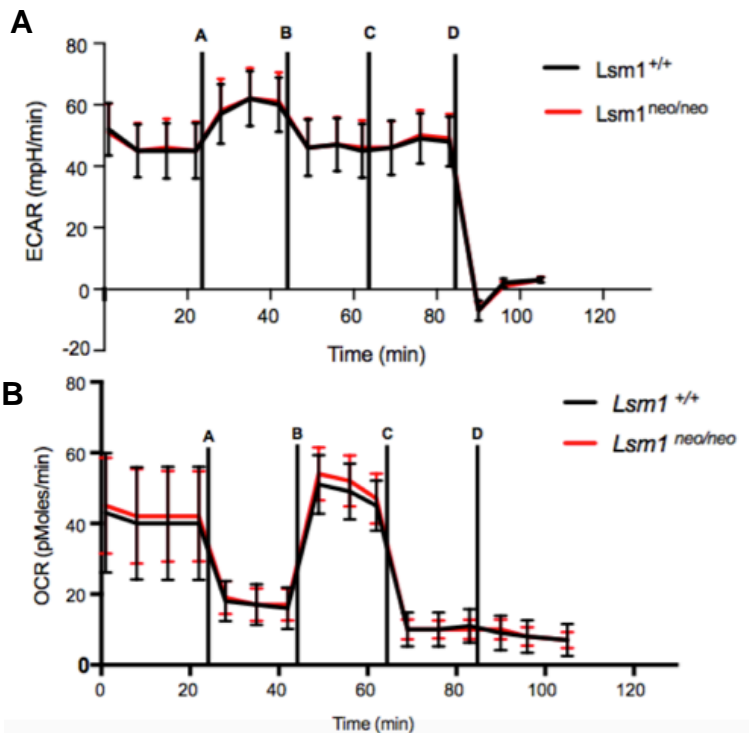


Figure 27: The metabolic program of $CD4^+$ T cells is not altered in the absence of *Lsm1*.

Seahorse measurements showing (A) extracellular acidification rates (ECAR) and (B) oxygen consumption rate (OCR) of wildtype (black) and *Lsm1*^{neo/neo} (red) $CD4^+$ T cells. Experiments were performed in cooperation with the group of Dr. Martin Jastroch (Helmholtz Zentrum Garching). Representative results of 3 biological and 3 technical replicates of wildtype and *Lsm1*^{neo/neo} are shown.

In this experimental setup the compounds Oligomycin, FCCP, Rotenone/Antimycin and 2-GC were serially injected. Oligomycin (A) and Rotenone/Antimycin (C) are inhibitors of electron transport chain complexes in the mitochondrial inner membrane. Injection of these compounds led to the decrease in OCR values (Figure 27). FCCP is an uncoupler that makes cells use maximum of oxygen. Its injection (B) resulted in elevated OCR values. Finally, 2-GC, a glucose analogue used for investigation of the glycolysis process in the cell was injected (Figure 27). All in all, the ECAR and OCR values measured in all triplets of *Lsm1*-deficient cells did not change compared to control cells.

4.3.2.4 Lsm1-deficient CD4⁺ T cells differentiate preferentially towards Th1

Because neither proliferation, nor metabolism of CD4⁺ T cells was affected, we wondered whether the differentiation programs of CD4⁺ T cells were influenced by the absence of Lsm1. To answer this question differentiation of CD4⁺ T cells was investigated *ex vivo* as described in 3.2.4.6. Interestingly, the results revealed a clear increase in IFN- γ production under Th0 and Th1 conditions in the absence of Lsm1 (Figure 28A/B). This result suggested that naïve Lsm1-deficient CD4⁺ T cells clearly preferred differentiation towards Th1 (Figure 28C).

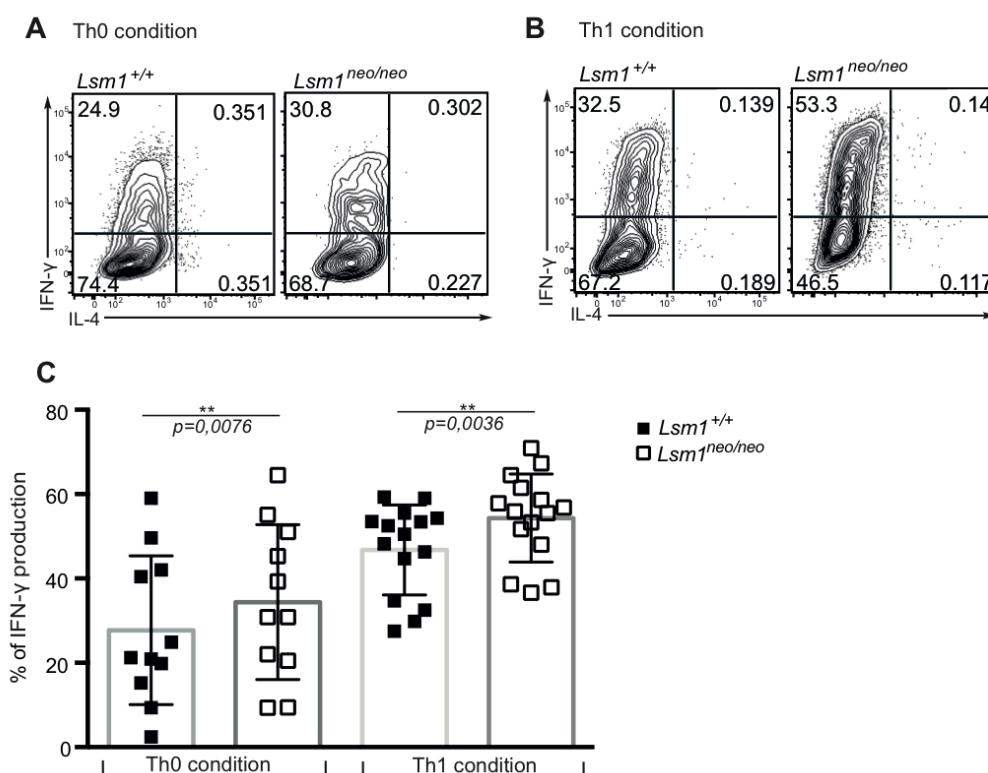


Figure 28: Lsm1-deficient CD4⁺ T cells differentiate preferentially towards Th1.

Representative contour plot of differentiation experiments of naïve CD4⁺ T cells isolated and activated with α -CD3/CD28 under Th0 (A) or Th1 (B) polarizing conditions. Results represent intracellular flow cytometry staining of the cytokines IFN- γ and IL-4 in wildtype and Lsm1-deficient CD4⁺ T cells. (C) Frequencies of IFN- γ producing cells in each single experiment are represented by black (wildtype) and white (*Lsm1*^{neo/neo}) dots ($n=11$ for Th0 and $n=14$ for Th1). Statistical analysis was performed by paired-t-test (ns: not significant, * $p<0.05$, ** $p<0.01$, *** $p<0.005$).

Analysis of Th2 and Th17 conditions, by contrast, did not show any changes in the respective cytokine production. Here, expression of IL-4 (Figure 29A) and IL-17 (Figure 29B) remained unchanged when compared to wildtype CD4⁺ T cells.

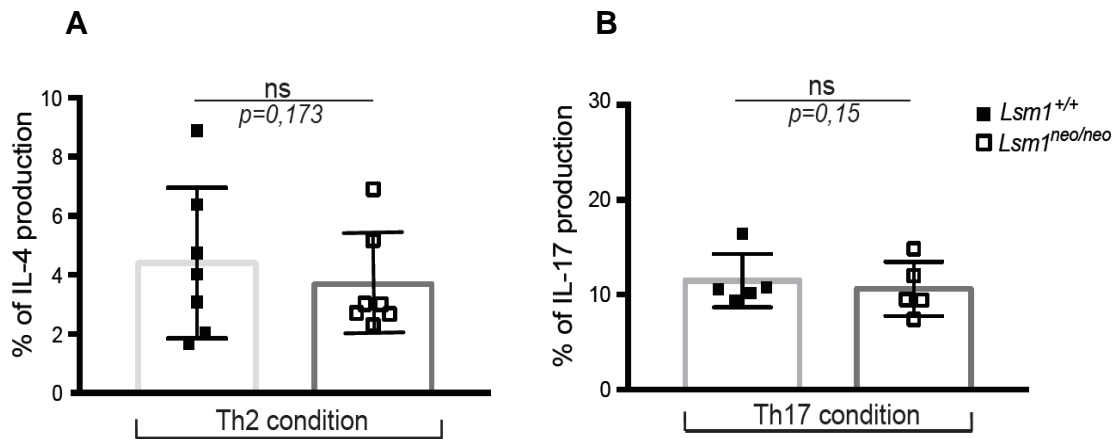


Figure 29: No changes in differentiation program of *Lsm1*-deficient CD4⁺ T cells under Th2 or Th17 conditions.

Frequencies of IL-4 (A) or IL-17 (B) production in intracellular stained wildtype (black) and *Lsm1*-deficient (white) CD4⁺ T cells for the cytokines IL-4 and IL-17, respectively.

4.3.2.5 RNA-Sequencing to identify direct *Lsm1* targets in CD4⁺ T cells

Deletion of *Lsm1* in CD4⁺ T cells resulted in a preferential differentiation of these cells towards Th1 *in vitro*. We hypothesized this bias to be caused by a possible deregulation of mRNA transcripts in these cells. We first analyzed *Ifng* mRNA expression in *Lsm1*-deficient CD4⁺ T cells and found a moderate overexpression over the wildtype control (Figure 30).

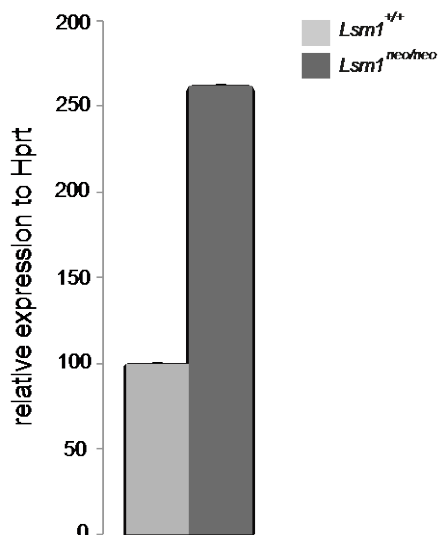


Figure 30: Overexpression of *Ifng* mRNA in *Lsm1*-deficient CD4⁺ T cells.

Relative expression of *Ifng* mRNA measured in *Lsm1*-deficient CD4⁺ T cells and CD4⁺ T cells of control wildtype mice via qPCR (n=4).

This detected overexpression of the *Ifng* mRNA in the absence of *Lsm1* encouraged us to search for more mRNA targets that might be directly or indirectly regulated by *Lsm1*. We therefore performed next generation sequencing in CD4⁺ T cells (Figure 31). We tested mRNA differences in *Lsm1*-deficient cells that were subjected to Th1 polarizing conditions for 48h. Samples were sent for deep sequencing and results are plotted in Figure 31 and Table 24.

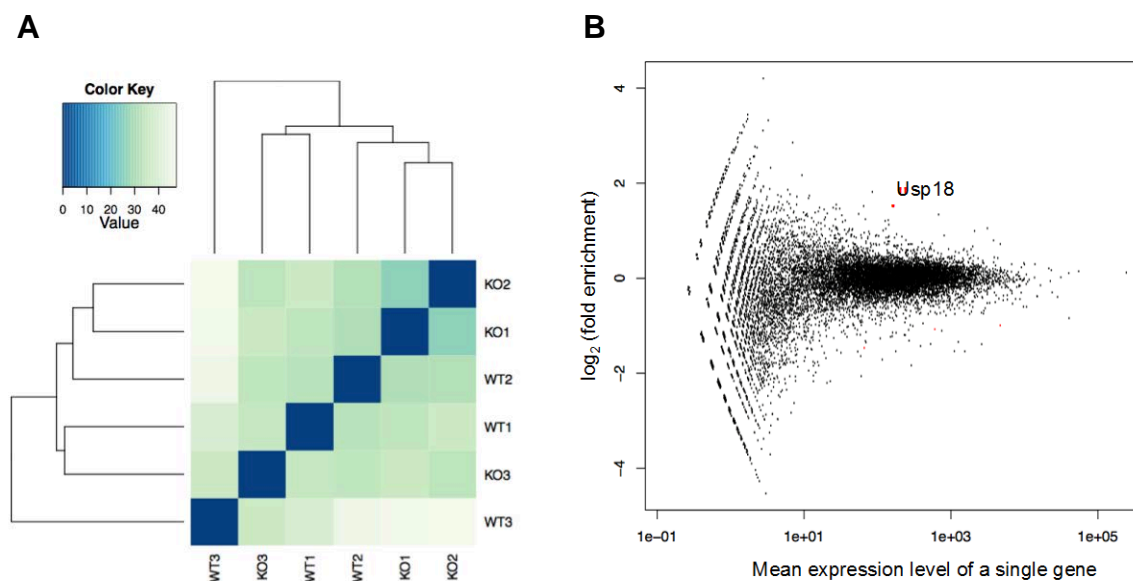


Figure 31: RNA sequencing to analyze gene expression in *Lsm1*-deficient Th1 cells.

CD4⁺ T cells isolated from wildtype and *Lsm1*-deficient mice, cultured under Th1 conditions for 48 hours and collected in trizol to be sent for RNA purification and library preparation and sequencing to the group of Blum (Gene Center, LMU Munich). **(A)** Dendrogram showing the extent of differences between the triplicates in wildtype- and *Lsm1*^{neo/neo} samples and **(B)** expression pattern of all investigated genes. Mean expression level of each single gene plotted against log₂ fold change between wildtype and *Lsm1*^{neo/neo} (one dot represents one gene). *Usp18* showed the highest fold change expression in this screen. Results of the NGS approach were bioinformatically analyzed with the help of Alexander Graf from AG Blum.

The dendrogram displays the similarity between the analyzed samples. According to the color key, two samples of knockout genotype exhibited highest similarities to one another, but were more different from the third replica compared to two wildtype samples (Figure 31A). The lack of consistency in genotype clustering may be explained by the small differences of expression of genes between knockout and wildtype samples (Figure 31B). Surprisingly, the total number of genes with significant changes in expression level was only 42 (Table 24). The top target candidate was the gene *Usp18*.

Table 24: List of potential *Lsm1* targets in *Th1* differentiated *CD4⁺* T cells. Light grey: significantly upregulated mRNA transcripts in *Lsm1*-deficient *CD4⁺* T cells compared to wildtype-control. Dark grey: significantly downregulated mRNA transcripts. Experiment was performed using 3 triplicates of each genotype.

| Gene | Gene-ID | fold change | Description |
|--------------|--------------|-------------|---|
| Usp18 | 24110 | 1.48 | Ubiquitin specific peptidase 18 |
| Atp2b4 | 381290 | 1.38 | ATPase, Ca ⁺⁺ transporting plasma membrane 4 |
| Mctp2 | 244049 | 1.22 | Multiple C2 and transmembrane domain containing 2 |
| Arl4c | 320982 | 1.00 | ADP-ribosylation factor-like 4C |
| Pde4d | 238871 | 0,78 | Phosphodiesterase 4D, cAMP specific |
| Angptl2 | 26360 | -1.62 | Angiotensin-like 2 |
| Akr1c13 | 27384 | -1.38 | Aldo-keto reductase family 1, member C13 |
| Pi15 | 94227 | -1.25 | Peptidase inhibitor 15 |
| Zfp457 | 431706 | -1.24 | Zinc finger protein 457 |
| Gpr83 | 14608 | -1.21 | G protein-coupled receptor 83 |
| Ccl3 | 20302 | -1.11 | Chemokine (C-C motif) ligand 3 |
| Cd52 | 23833 | -0.98 | CD52 antigen |
| Rnu6 | 19862 | -0.91 | U6 small nuclear RNA |
| Tnf | 21926 | -1.06 | Tumor necrosis factor |
| Snord83b | 100302601 | -0.93 | Small nucleolar RNA, C/D box 83B |
| Ccl4 | 20303 | -1.19 | Chemokine (C-C motif) ligand 4 |
| Rn4.5s | 19799 | -0.89 | 4.5S RNA |
| Deb1 (SS18) | 26901 | -0.97 | Chromatin remodeling complex |
| Tmem8b | 242409 | -0.79 | Transmembrane protein 8B |
| Rab26os | 75614 | -0.88 | ncRNA and member of RAS oncogene family |
| Snod49a | 100217455 | -0.97 | Small nucleolar RNA, C/D box 49A |
| Loxl2 | 94352 | -0.94 | Lysyl oxidase-like 2 |
| Gm4841 | 225594 | -0.98 | Predicted gene 4841 |
| Hist1h2bp | 319188 | -1.01 | Histone cluster 1, H2bp |
| Tjp2 | 21873 | -1.1 | Tight junction protein 2 |
| Naa38 | 78304 | -0.70 | N(alpha)-acetyltransferase 38 |
| Eny2 | 223527 | -0.72 | ENY2 transcription and export complex 2 subunit |
| Slc7a14 | 241919 | -0.84 | Solute carrier family 7, member 14 |
| Tmem69 | 230657 | -0,74 | Transmembrane protein 69 |
| Ap3s1 | 11777 | -0,64 | Adaptor-related protein complex 3, sigma 1 subunit |
| Rmrp | 19782 | -0,83 | RNA component of mitochondrial RNAase P |
| Rnu1b6 | 19847 | -0,84 | U1b6 small nuclear RNA |
| Gm6455 | 623849 | -1,34 | Predicted gene 6455 |
| Gtf2h2 | 23894 | -0,64 | General transcription factor II H, polypeptide 2 |
| Lsm3 | 67678 | -0,69 | Sm like protein 3 |
| Gm8210 | 666642 | -0,73 | Predicted pseudogene 8210 |
| Hist1h4j | 319159 | -0,69 | Histone cluster 1, H4j |

Elevated expression level of Usp18 was evaluated by qPCR measurements. One representative qPCR is shown in Figure 32A. Next we asked whether the Usp18 mRNA transcript showed changes in the length of their poly(A) tails. In theory, mRNAs that were deadenylated but could not be degraded due to lack of Lsm1-7 function should accumulate in the cell as oligoadenylated mRNA transcripts. We tested the possible accumulation of oligoadenylated Usp18 mRNA transcripts by performing poly(A) tail analysis. Key steps of this method are the addition of guanosine and inosine residues to the 3' ends of all poly(A) tail containing RNAs, the reverse transcription of the tailed-RNAs using the newly added G/I tails as starting sites and the PCR amplification using two different primer sets. The first primer set is designed to detect the gene-specific sequence (specific PCR). The second primer set consists of the gene-specific forward primer and a supplied universal reverse primer that amplifies the gene-of-interest with its poly(A) tail (tail PCR). The experiment is controlled on the level of reverse transcription. The reverse transcription sample either contained the RT enzyme mix (RT+) or nuclease-free water instead (RT-). Because overexpression of Usp18 was detected in CD4⁺ T cells that differentiated under Th1 polarizing conditions for 48hours, we repeated differentiation under these conditions and used samples for poly(A) tail determination (Figure 32B).

As expected, both specific PCR samples in wildtype and *Lsm1^{neo/neo}* showed specific bands for the *Usp18* encoded mRNA product expected for the designed primers (specific PCR, RT+). Taking a more detailed look at the tail PCR products in wildtype and *Lsm1^{neo/neo}* samples revealed that all detected bands; representing different oligoadenylated Usp18 mRNA transcripts are comparable (Figure 32B). Importantly, both negative controls of tail PCRs did not show corresponding bands, pointing to a reliable result. The overexpression of Usp18 mRNA and unchanged poly(A) tail lengths of the encoding mRNA transcripts in the absence of Lsm1 pointed out that the decay process was rather unaffected. Importantly, overexpression of Usp18 in Lsm1-deficient CD4⁺ T cells might be linked to the upregulation of *Ifng* mRNA detected in the same cells, since Usp18 is known to be an *Ifng*-regulated gene (Santin et al., 2012). Different mRNA amounts might be therefore the result of induced transcription rather than changes in the decay process.

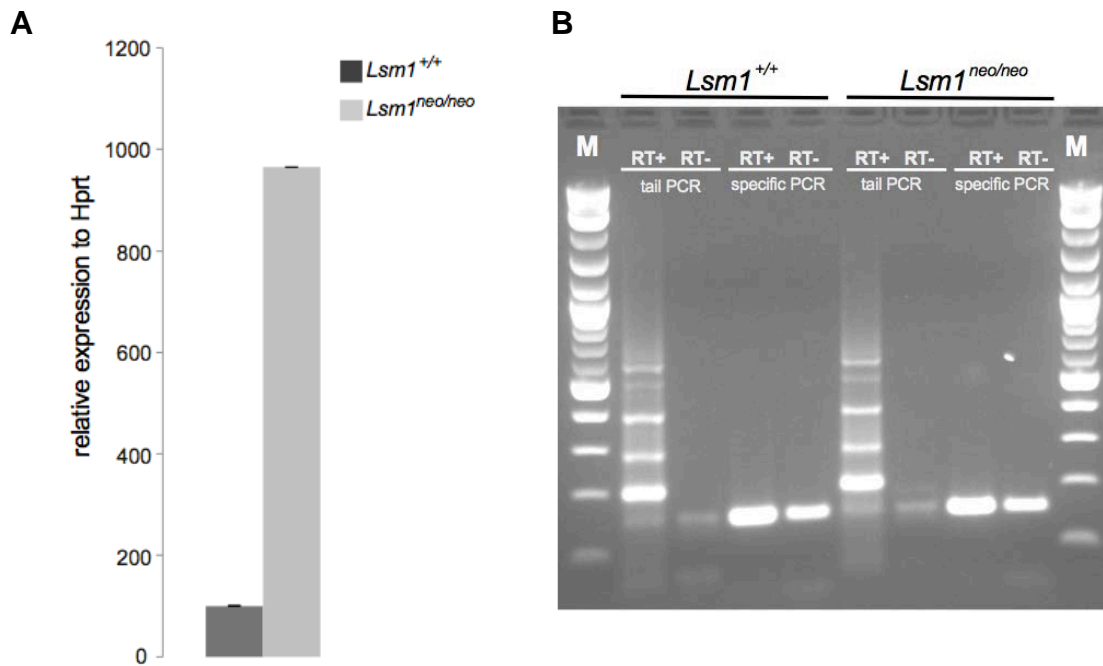


Figure 32: Usp18 is overexpressed in the absence of Lsm1.

(A) Representative diagram of 4 independent experiments with the relative expression of Usp18 mRNA in CD4⁺ T cells, differentiated for 48h towards Th1 (dark grey: wildtype; grey: Lsm1^{neo/neo}). **(B)** Poly(A) tail determination assay showing poly(A) tail lengths of Usp18 mRNA in Th1 differentiated CD4⁺ T cells. Specific PCR produced a specific band of Usp18 mRNA with a product size of 153bp. The tail PCR was performed using a designed forward primer and a supplied reverse primer to generate the gene-of-interest including the poly(A) tail. The fragment size between the RV primer and AATAA was 41bp and represents together with the product size of the gene-of-interest the lowest bands in the tail PCR (RT+). The four bands on top resulted from different oligo(A) tails lengths of the Usp18 mRNAs. qPCR was performed 5times each with 3 technical replicates; poly (A) tail experiment 2 times.

In summary, the observed spontaneous activation of CD4⁺ T cells in the absence of Lsm1 could not be explained by the proliferation or the metabolism of these cells. Although, *in vitro* differentiation experiments revealed changes in the Th1 differentiation program of these cells, we could not find specific targets by RNA sequencing that might explain this phenotype. We speculated about a possible compensation for the absence of Lsm1 over time leading to the restoration of the original condition in the cell and therefore decided to examine effects shortly after the induced acute conditional deletion of Lsm1.

4.3.2.6 Reduction of P-body numbers after acute deletion of Lsm1 in CD4⁺ T cells

Since the best characterized function for Lsm1 in yeast and HeLa cells was described in its involvement in P-body formation as was introduced before and because previously performed experiments revealed no influence of Lsm1 on the process of P-body formation 4.2.2, we decided to analyze P-body formation now directly after Lsm1 deletion. For this purpose, I crossed *Lsm1^{fl/fl}* mice with *CD4Cre-Ert2* mice in order to generate *Lsm1^{fl/fl}; CD4Cre-Ert2* mice. CD4⁺ T cells of these mice could be treated with tamoxifen, resulting in the acute deletion of Lsm1 ex vivo. Dr. Gesine Behrens analyzed P-body formation in these CD4⁺ T cells by using antibodies against Lsm1 and the P-body marker RCK. As expected, Lsm1 signal was reduced upon tamoxifen treatment (Figure 33A). Interestingly, number of P-bodies that is represented by the counts for RCK was reduced in the tamoxifen treated sample indicating a positive impact of Lsm1 on the formation of P-bodies (Figure 33B). Although the second experiment displayed in Figure 33C showed a milder effect, the tendency of disappearing P-bodies in the absence of Lsm1 was clearly detectable.

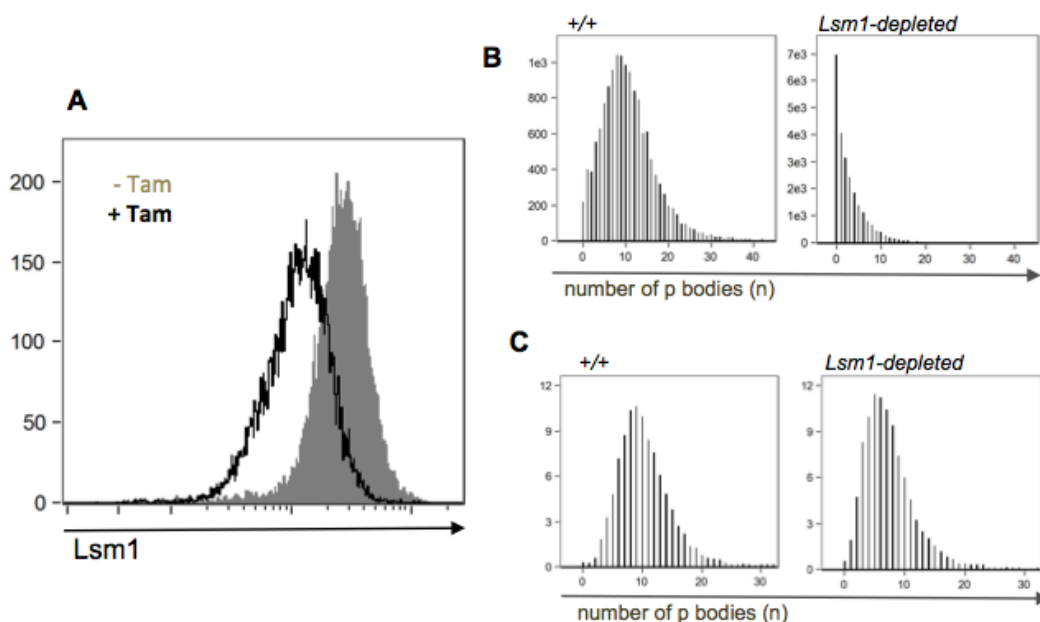


Figure 33: Reduced P-body numbers upon acute deletion of Lsm1.

(A) Histogram showing expression of intracellularly stained Lsm1 protein in CD4⁺ T cells isolated from *Lsm1^{fl/fl}; CD4Cre-Ert2* mice and subjected to tamoxifen (black) or left untreated (grey) for 24h, then stimulated with α -CD3/CD28 for 40h and finally incubated in IL-2 containing medium for additional 2-3 days. For determination of the number of P-bodies, cells were treated as described in (A) and were subsequently stained with DAPI and antibodies against RCK and Lsm1. (B) First experiment showing counts of RCK signals in wildtype and Lsm1-depleted cells (C) Repetition of experiment described in (B). Staining of Lsm1 was performed using the in-house produced antibody 5F3. Both Experiments were performed by Dr. Gesine Behrens with the help of Juliane Klein.

These last experiments showing the influence of *Lsm1*-deletion on P-body formation were very promising and pointed to the importance of this experimental setup for the investigation of *Lsm1* functions. Unfortunately, the generation of the *Lsm1^{f/f}; CD4Cre-Ert2* mice was only reached in the final phase of my project, therefore experiments to examine RNA expression levels in tamoxifen treated cells are still ongoing.

4.3.3 Autoimmune phenotype of *Lsm1*-deficient mice

Spontaneous activation of T cells in *Lsm1*-deficient mice prompted us to investigate whether differentiation into follicular helper T cells (T_{FH}) in vivo was also altered in the absence of *Lsm1*. T_{FH} cells constitutively express the B cell follicle homing receptor CXCR5 and can be distinguished from other $CD4^+$ T cells by co-staining of this receptor with the surface marker PD-1. Staining of splenocytes isolated from *Lsm1^{+/+}* and *Lsm1^{neo/neo}* allowed quantification of frequency and numbers of T_{FH} cells that were highly increased compared to control mice (Figure 34A and 34C).

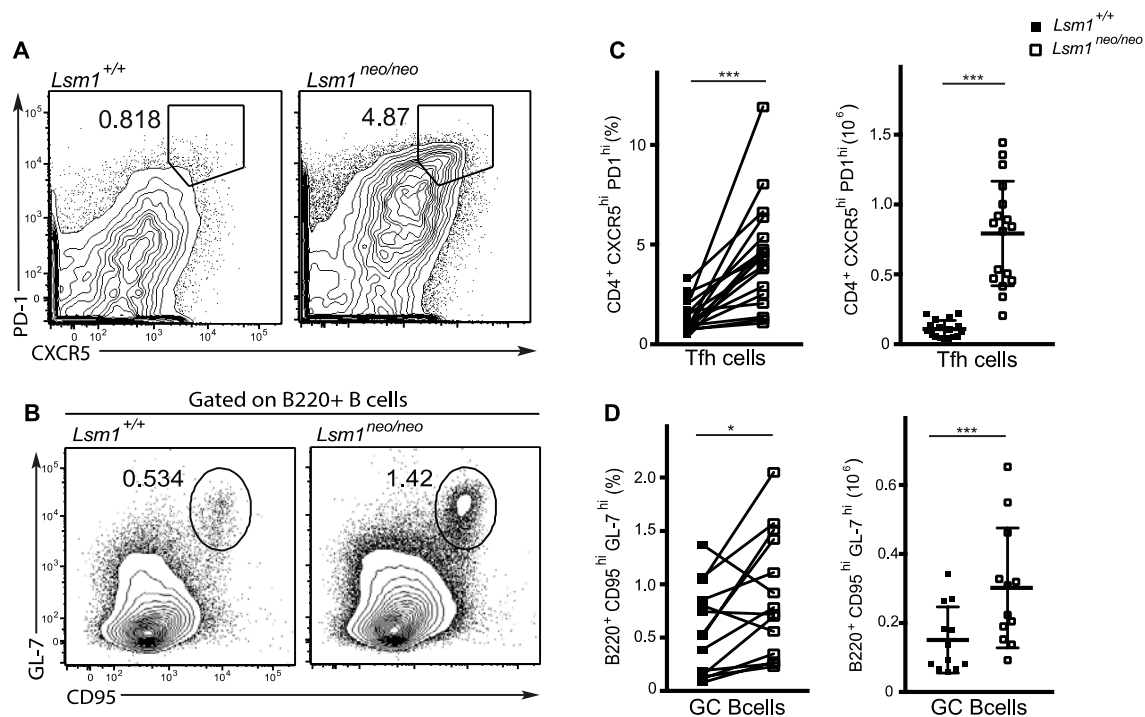


Figure 34: Increased frequencies and numbers of T_{FH} and GC B cells in spleens from *Lsm1*-deficient mice.

(A) Representative contour plots of follicular helper T cells ($PD-1^{hi}$ and $CXCR5^{hi}$), pre-gated on $CD4^+ B220^-$ cells. **(B)** Representative contour plots of germinal center B cells ($GL-7^{hi}$ $CD95^{hi}$) staining of B cells. Cumulative representation of flow cytometric analysis comparing wildtype (black) and $Lsm1^{neo/neo}$ (white) 8-10 weeks old animals. Frequencies or absolute cell numbers of **(C)** T_{FH} cells and **(D)** GC B cells are shown. Error bars show SD and statistical analysis was performed by paired-t-test (ns: not significant, * $p < 0.05$, ** $p < 0.01$, *** $p < 0.005$).

Since T_{FH} cells regulate the differentiation of antigen-specific B cells, we suspected that this increase in T_{FH} cells might result in higher cell numbers of GC B cells. Interestingly, GC B cells were indeed significantly increased over the control (Figure 34B). This was similarly the case for frequencies and cell number (Figure 34D). In addition, accumulation of T_{FH} cells can promote uncontrolled autoantibody production (Nakayamada & Tanaka, 2016). We therefore used indirect immunostaining of HEp-2 cells to examine sera of *Lsm1*-deficient mice and their wildtype littermates for the presence of autoantibodies. Sera from mice with different ages (12, 15, and 18 weeks old) were incubated on HEp-2 cell slides and probed with a fluorescent secondary antibody as described in section (3.2.4.12.). Two different positive controls and one negative control were included. Serum from *MRL-lpr* mice served as one positive control. These mice are homozygous for the lymphoproliferation-inducing spontaneous mutation in the Fas gene (*Fas^{lpr}*) and develop a systemic lupus erythematosus (SLE) phenotype. The sera of *sanroque* mice were used as another positive control. To exclude false positive signals, serum from a NOD scid gamma (*NSG*) mouse served as a negative control. These mice lack mature T cells, B cells and natural killer (NK) cells and are not able to produce any antibodies. In contrast to the wildtype mice, sera from *Lsm1*-deficient mice showed already at the age of 12 weeks a clear signal proving the presence of autoantibodies (Figure 35). Results belonging to the negative and wildtype control are not shown since obtained images did not show any signal and were therefore black.

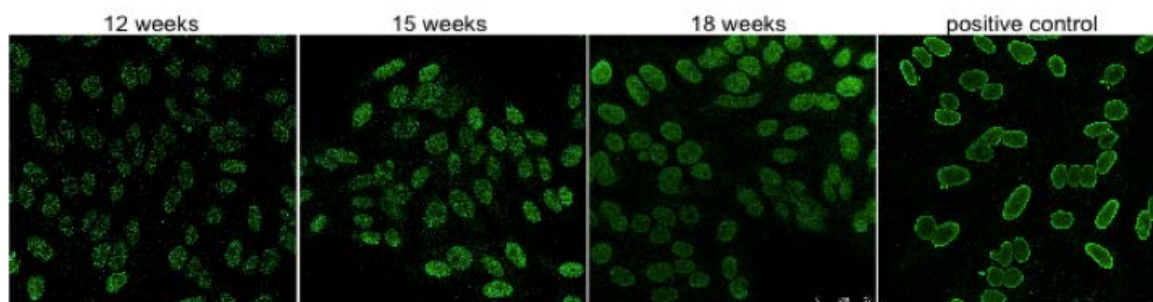


Figure 35: *Lsm1*-deficient mice have anti-nuclear autoantibodies in their sera.

Indirect immunofluorescence microscopy showing the detection of autoantibodies on HEp-2 cells. Each panel represents sera from individual animals carrying the *Lsm1^{neo/neo}* genotype. Serum of the *san/san* mouse was used as positive control and is shown far right.

Interestingly, the signals became stronger in the samples of 15 weeks and 18 weeks old mice implying an increase in autoantibody production in aging mice. We therefore addressed the question at which age autoantibodies appeared in *Lsm1*-deficient mice. To exclude differences in signal strengths on the same slide that might occur through the staining procedure, three different areas from the same slide were selected to determine the mean of detected signal. Significant differences between *Lsm1*^{+/+} and *Lsm1*^{neo/neo} could be detected in sera of mice that were at least 11 weeks old. Younger mice did not show significant signals (Figure 36).

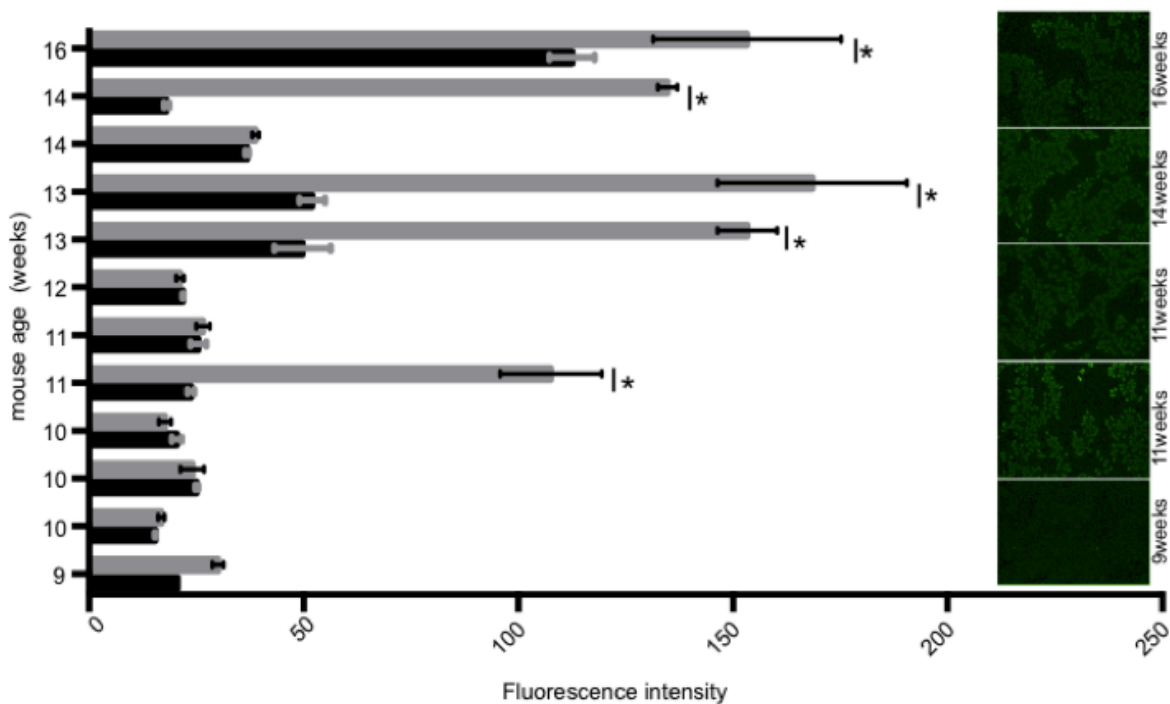


Figure 36: Age-dependent development of autoantibodies in sera from *Lsm1*-deficient mice.

Indirect immunofluorescence for the detection of anti-nuclear antibodies using HEp-2 cells for the analysis of sera isolated from *Lsm1*-deficient mice of different ages. Each bar represents the average of 3 different areas detected on the same slide. Error bars show SD and statistical analysis was performed by paired-t-test (ns: not significant, * $p < 0.05$, ** $p < 0.01$, *** $p < 0.005$). Quantification was performed in cooperation with the imaging core facility of the BMC at the LMU.

4.3.3.1 Comparing autoimmune phenotypes of *Lsm1*^{neo/neo} and *sanroque* mice

Together, the analysis of the *Lsm1*^{neo/neo} mouse demonstrated the development of an autoimmune phenotype causing splenomegaly, spontaneous T cell activation, higher frequencies and cell numbers of T_{FH} cells and GC B cells as well as the presence of high affinity anti-nuclear antibodies in the sera. These autoimmune phenotypes resembled the *Sanroque* mouse-model that is also investigated in our group. We therefore

compared both mouse models for T cell activation (Figure 37A) and accumulation of T_{FH} cells (Figure 37B) and GC B cells (Figure 37C) as well as Th1 differentiating of naïve CD4⁺ T cells (Figure 37D). In all phenotypes examined, the *Lsm1*-deficient mouse showed similar but intermediate phenotypes between wildtype and the *sanroque* mouse.

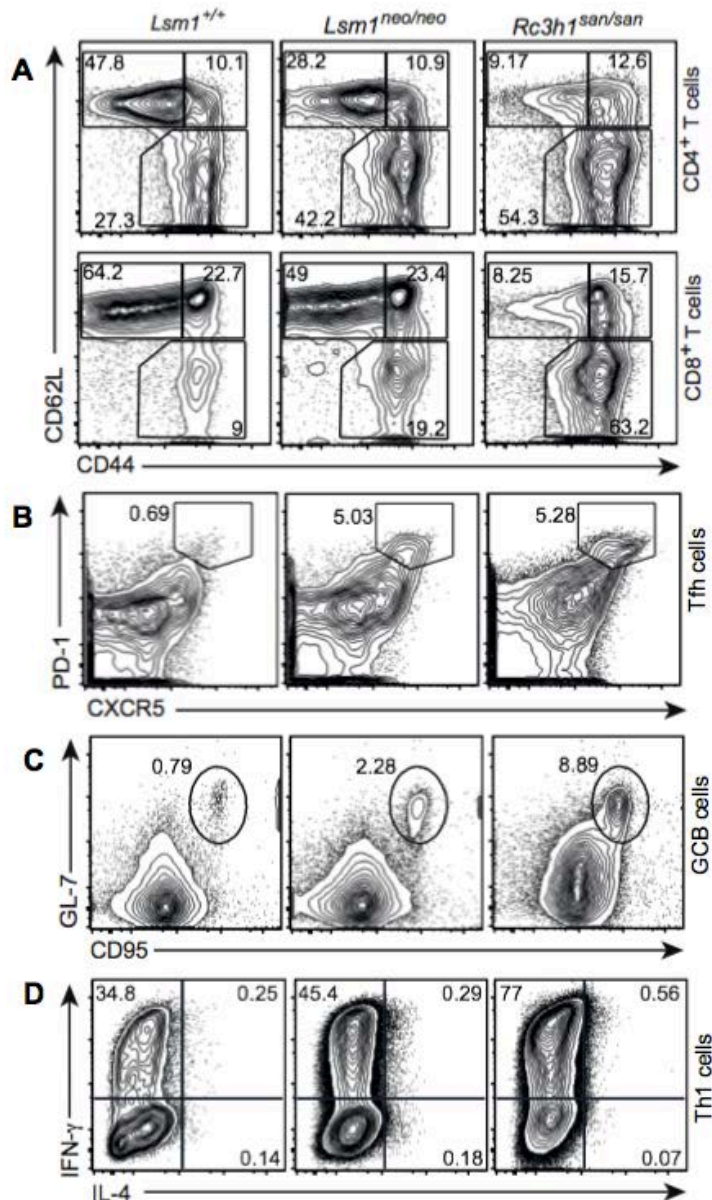


Figure 37: *Lsm1*-deficiency causes less severe phenotypes than observed in the *sanroque* mouse.

Representative contour plots of (A) CD62L and CD44 stained splenocytes, gated on CD4⁺ T cells (upper plots) or CD8⁺ T cells (lower plots); (B) follicular helper T cells (PD-1^{hi} and CXCR5^{hi}), pre-gated on CD4⁺ B220; (C) germinal center B cells (GL-7^{hi} CD95^{hi}) and (D) CD4⁺ T cells cultured under Th1 conditions. Flow cytometric analysis performed in splenocytes from wildtype (left); *Lsm1*^{neo/neo} (middle) and *san/san* animals (right).

In conclusion these data suggested that *Lsm1* or Roquin-1^{san} proteins work in the same or similar pathways to prevent the development of autoimmunity.

4.3.4 Conditional deletion of *Lsm1* in T cells

To investigate whether the autoimmune phenotype of *Lsm1^{neo/neo}* mice was T cell intrinsic, we generated *Lsm1^{fl/fl}* mice and crossed them with *CD4Cre* transgenic mice to generate *Lsm1^{fl/fl}; CD4Cre* mice. In these mice, the expression of the Cre-recombinase takes place upon activation of CD4 *cis*-regulatory regions. Therefore, Cre-mediated excision of the loxP site flanked *Lsm1* exon 2 and 3 was expected to start already in the double positive thymocyte stage and be present in CD4⁺ and CD8⁺ T cell lineages. Successful Cre-mediated deletion in T cells was verified by Western blot analysis. *Lsm1* protein expression was almost absent in peripheral CD4⁺ T cells of *Lsm1^{fl/fl}; CD4Cre* mice when compared to the *Lsm1^{fl/fl}* levels. A weak residual band was likely to be the result of incomplete purification (Figure 38).

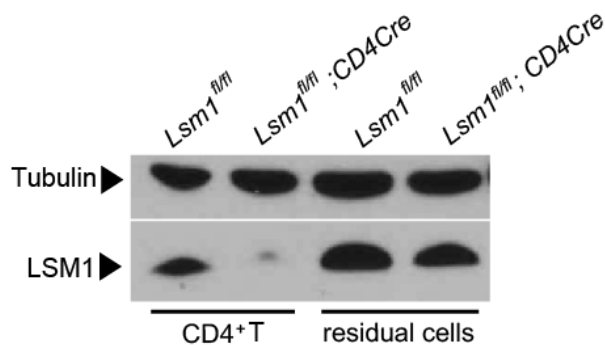
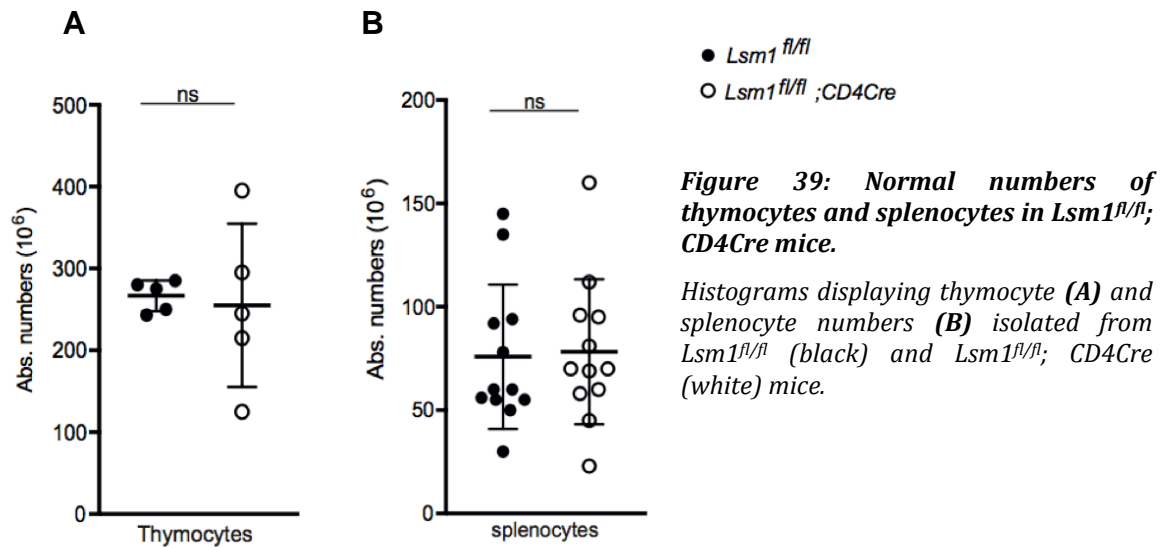


Figure 38: Confirming absence of *Lsm1* protein in CD4⁺ T cells from *Lsm1^{fl/fl}; CD4Cre* mice.

Immunoblotting of lysates derived from CD4⁺ T cells isolated from *Lsm1^{fl/fl}* and *Lsm1^{fl/fl}; CD4Cre*. CD4⁺ T cells were bead-enriched from splenocytes derived from *Lsm1^{fl/fl}* and *Lsm1^{fl/fl}; CD4Cre* mice and both fractions, CD4⁺ T cells and residual cells, which remained in the supernatant after selection with beads were compared by immunoblotting with 5F3 antibody against *Lsm1* and the loading control anti-tubulin (n=3).

When examining *Lsm1^{fl/fl}; CD4Cre* mice, it was noticeable that spleen sizes of these mice were not enlarged, as this was the case for the *Lsm1^{neo/neo}* mouse. This was also reflected in normal numbers of thymocytes or splenocytes (Figure 39A/B).



Similarly to $Lsm1^{neo/neo}$ mice, the frequencies of CD4⁺ and CD8⁺ T cells as well as frequencies of B cells were unchanged (Figure 40).

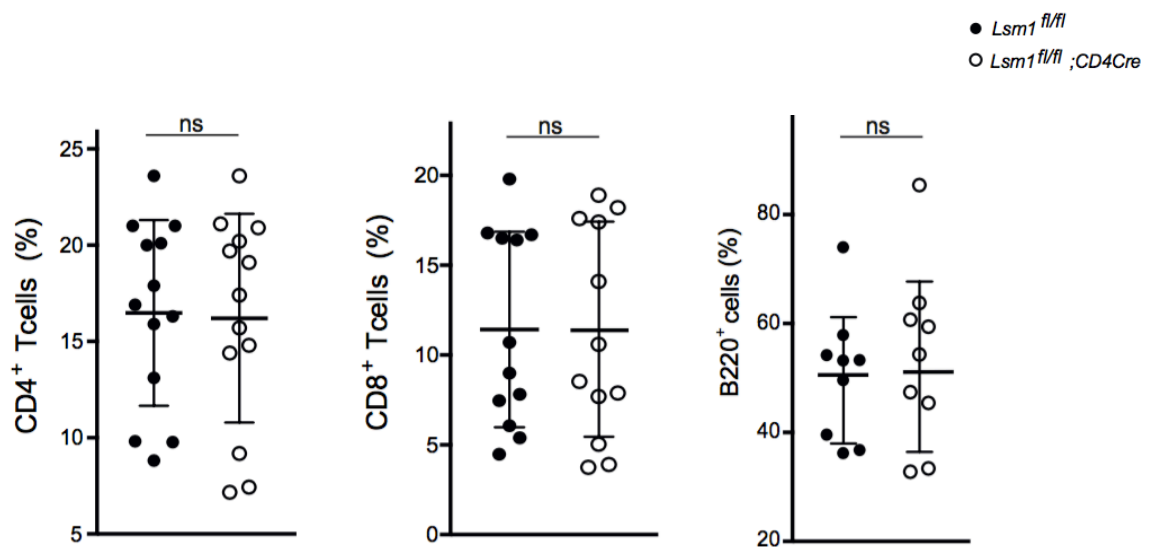


Figure 40: Absence of $Lsm1$ in T cells does not affect frequencies of T cells or B cells.

Flow cytometric analysis of splenocytes isolated from $Lsm1^{fl/fl}$ (black) and $Lsm1^{fl/fl}; CD4Cre$ mice (white) stained with antibodies against CD4 (left) or CD8 (middle) or against the B cell marker B220 (right). Statistical analysis was performed with the paired t-test.

Finally, the activation of CD4⁺ and CD8⁺ T cells as well as the frequencies of T_{FH} cells were addressed in these mice. Notably, frequencies of activated CD4⁺ T cells were increased similar to $Lsm1^{neo/neo}$ mice, and also T_{FH} cells exhibited a significant increase in frequencies (Figure 41A and Figure 41B). In contrast, significant activation of CD8⁺ T cells that was detected in $Lsm1^{neo/neo}$ mice did not occur upon conditional deletion in $Lsm1^{fl/fl}; CD4Cre$ mice (Figure 42).

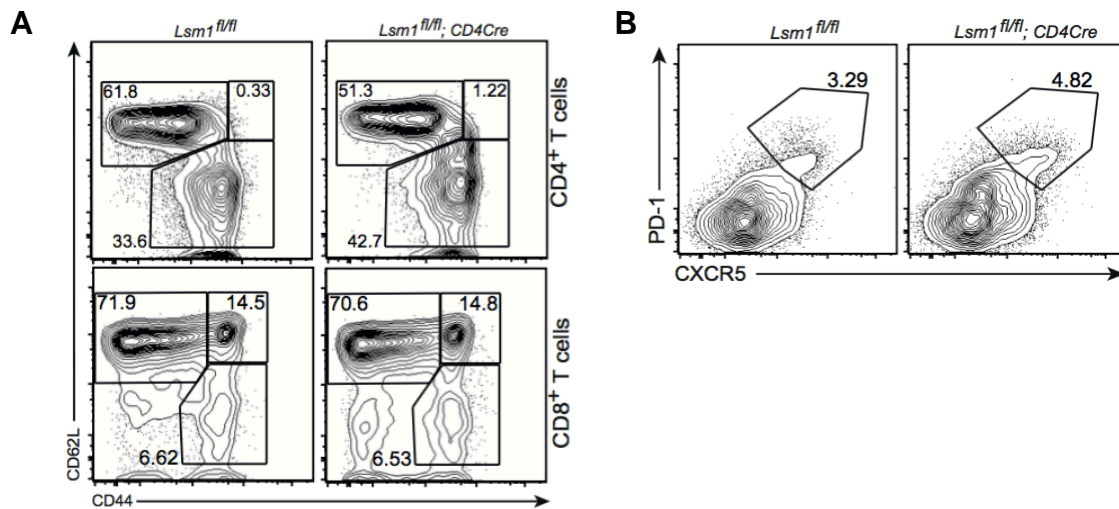


Figure 41: Elevated frequencies of activated CD4⁺ T cells and T_{FH} cells in *Lsm1^{fl/fl}; CD4Cre* animals.

(A) Representative contour plots of CD62L and CD44 stainings, gated on CD4⁺ T cells (upper plots) or CD8⁺ T cells (lower plots) and Follicular helper T cells (PD-1^{hi} and CXCR5^{hi}), pre-gated on CD4⁺ B220⁺ **(B)**. Flow cytometric analysis performed in *Lsm1^{fl/fl}* and *Lsm1^{fl/fl}; CD4Cre* animals at the age of 8-10 weeks.

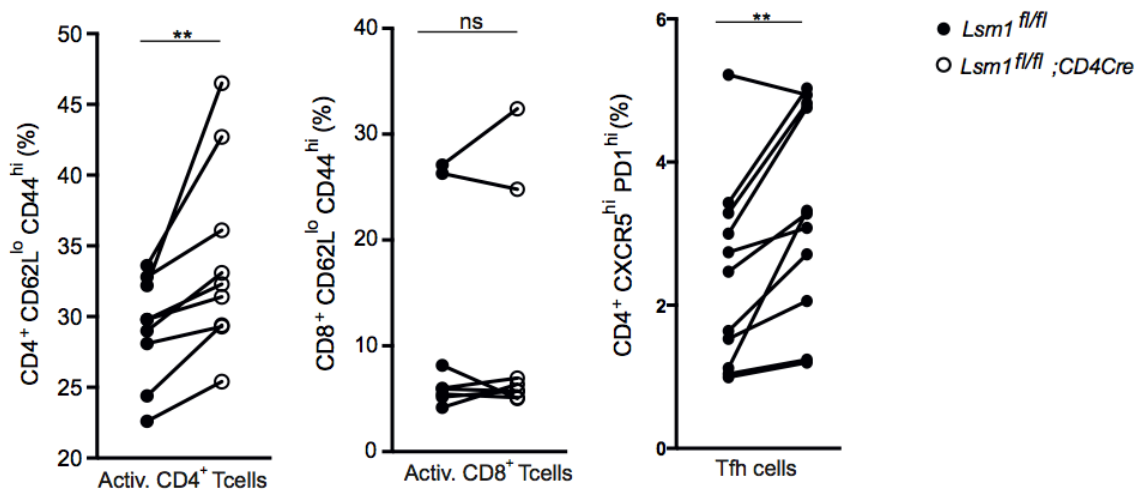


Figure 42: *Lsm1^{fl/fl}; CD4Cre* mice confirm cell-intrinsic activation of CD4⁺ T cells and T_{FH} accumulation upon deletion of *Lsm1*.

Flow cytometric analysis performed on splenocytes from *Lsm1^{fl/fl}* (black) and *Lsm1^{fl/fl}; CD4Cre* mice (Servaes et al.) at the age of 8-10 weeks. Frequencies of activated CD4⁺ T cells (left), CD8⁺ T cells (middle) and T_{FH} cells (right) are displayed. Statistical analysis was performed by paired t-test (ns: not significant, * $p < 0.05$, ** $p < 0.01$, *** $p < 0.005$).

These results demonstrate that T cell-intrinsic changes are the origin of autoimmunity in *Lsm1*-deficient mice; however contributions from other cell-types cannot be excluded.

4.4 Testing candidate interactors of Lsm1

4.4.1 Lsm1 interacts with 4E-T but not Roquin proteins

In order to understand the link between the absence of Lsm1 and the development of autoimmunity in the mouse, we started to investigate interaction partners of Lsm1 in MEF and T cells. Because of the phenotype-similarity to the RNA-binding protein Roquin, we hypothesized a common pathway or even direct interaction of both proteins. To address this question, we performed immunoprecipitation experiments using antibodies against Lsm1 or Roquin, respectively (see 0). Lysates derived from Lsm1 KO MEF cells served as control (Figure 43A). Similarly, we used Roquin1/2 DKO cells as a negative control for IPs of Roquin (Figure 43B). As expected no Lsm1 band was detected in the IP performed in extracts of Lsm1-deficient cells (Figure 43A). Remarkably, even the strong immunoprecipitation of Lsm1 from wildtype extracts did not show co-immunoprecipitation of Roquin-1 or Roquin-2 (Figure 43A). Also bands corresponding to the proteins RCK or DCP2 were not detectable. Interestingly, a slight signal for the 4E-T protein was present in wildtype but not in KO samples. In line with this, 4E-T was already shown to interact with the Lsm1-7-Pat1 complex by binding to Lsm2 (Nishimura et al., 2015).

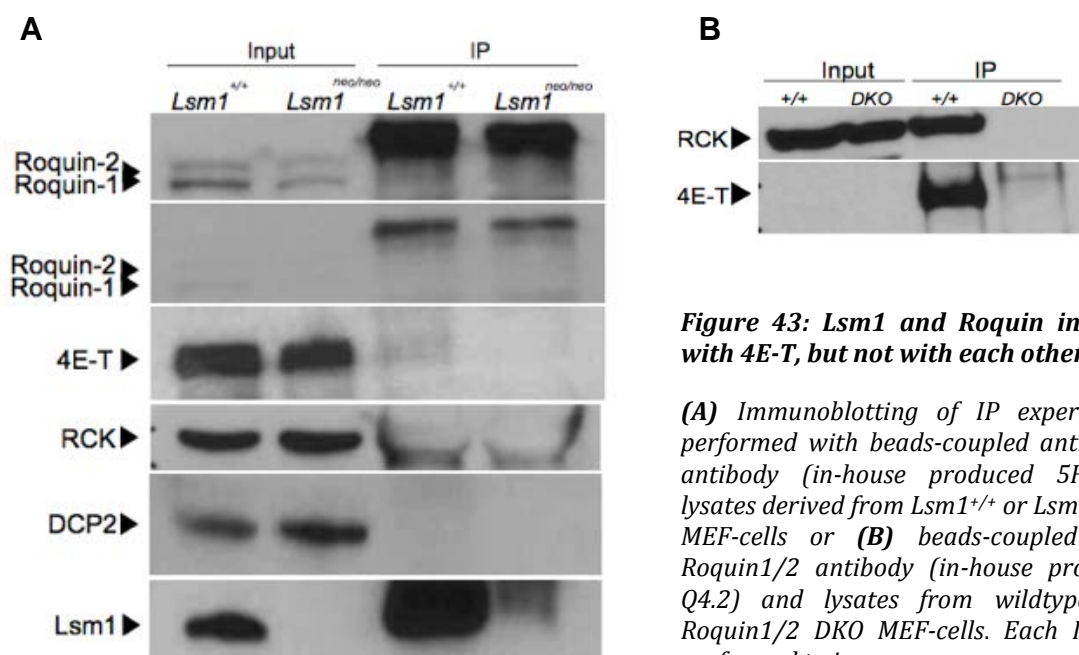


Figure 43: Lsm1 and Roquin interact with 4E-T, but not with each other.

(A) Immunoblotting of IP experiments performed with beads-coupled anti-Lsm1 antibody (in-house produced 5F3) in lysates derived from Lsm1^{+/+} or Lsm1^{neo/neo} MEF-cells or **(B)** beads-coupled anti-Roquin1/2 antibody (in-house produced Q4.2) and lysates from wildtype and Roquin1/2 DKO MEF-cells. Each IP was performed twice.

Interestingly, Roquin IP using Q4.2 coupled antibody revealed an even more prominent band when blotted against 4E-T (Figure 43B). Roquin signals are not blotted in Figure 43B, since films showed here undefined bands due to a black background. Still, pulldown of Roquin1/2 was considered successful since RCK was detectable in the wildtype IP.

4.4.2 Cnot4 and 4E-T are newly identified interaction partners of Lsm1

The identification of 4E-T as an interaction partner of Lsm1 as well as Roquin-1 or Roquin-2 led to the general question whether other proteins function together with Lsm1 in T cells. For answering this question, we employed the so-called BioID method that was recently demonstrated for screening of proteins that are in proximity of the protein-of-interest within living cells (Roux, Kim, & Burke, 2013). The advantage of this method is the capability to detect all proteins in very short distance (approximately 10 nm) to the protein of interest. This is achieved by expressing fusion proteins that carry the protein of interest and a promiscuous form (BirA*) of the bacterial biotin ligase BirA. This enzyme activates biotin but does no longer conjugate the activated biotin to specific targets, instead releases it for the unbiased labeling of proximal endogenous proteins. To identify proteins in close distance to Lsm1, I cloned the BioID constructs, BirA*-Lsm1 and BirA*-GFP and performed the first try-out analysis on isolated CD4⁺ T cells. Dr. Gesine Behrens, a postdoc in our group, then performed the final BioID experiment according to the protocol described in 3.2.4.8. Briefly, Dr. Behrens isolated CD4⁺ T cells from Lsm1^{fl/fl};CD4Cre mice, stimulated them for 40h with α -CD3/CD28 and transduced them with either BirA*-GFP or BirA*-Lsm1. After stringent cell lysis and protein denaturation, biotinylated proteins were affinity purified using streptavidin beads. Samples were then used either for western blot analysis or mass spectromic analysis. Western blotting was performed using an α -biotin antibody in order to control for the specific pull-down of BirA*-Lsm1 (Figure 44). Although, protein bands for BirA*-Lsm1 and the control BirA*-GFP were still detectable in lysates after pull down (Apd), a more prominent band was present in protein eluate after capture with streptavidin beads indicating a successful pulldown (Figure 44).

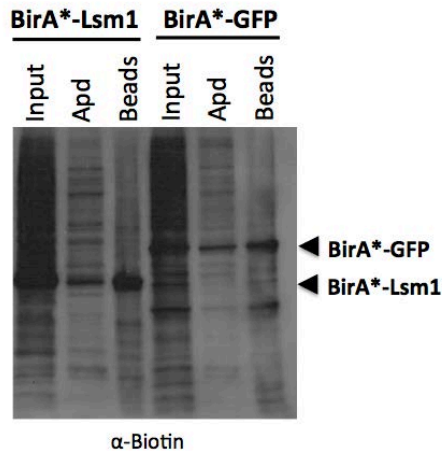


Figure 44: Biotinylation and capture of biotin-conjugated proteins.

Western blot showing input lysates, lysates after pull down (Apd) and the eluted proteins from beads incubated with lysates from BirA*-Lsm1 and BirA*-GFP transduced CD4⁺ T cells, respectively. Protein bands were visualized with a primary α -biotin specific antibody.

As mentioned above, samples were also subjected to mass spectrometric (MS) analysis. MS data was generated based on the peptide intensity measured in each sample. In the step of data processing, proteins identified in the BirA*-GFP negative control were subtracted from the large list of potential interactome components to narrow down to a list of potential Lsm1 interactors with higher confidence. Results of the statistical analysis of the calculated BirA*-Lsm1/BirA*-GFP ratio are listed in Figure 45A and are schematically shown in Figure 45B. Interestingly, highest scores were measured for the protein CNOT4. In addition, Lsm2 and Lsm4 as well as Pat1b could be identified in this screen.

A

| Protein | Ratio | |
|--------------|--------------------------|---------------------|
| | BirA*-Lsm1/ BirA*-GFP | T-test (p-value) |
| Cnot4 | 26.2 | 0,0448 |
| Lsm2 | 21.8 | 0,0089 |
| Ddb1 | 19.2 | 0,0002 |
| Cks2 | 12.7 | 0,0001 |
| Lsm4 | 10.3 | 0,0134 |
| Idi1 | 9.8 | 0,0064 |
| Psmb8 | 9.5 | 0,0020 |
| Pat1b | 9.4 | 0,0106 |

B

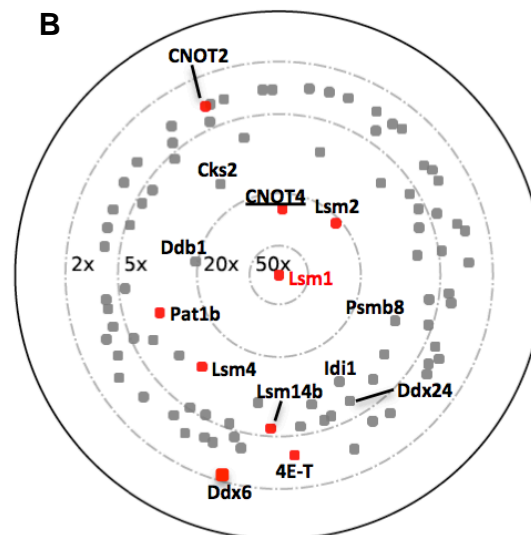


Figure 45: Proteins identified using proximity-dependent biotinylation (BioID).

(A) Peptide counts in BirA*-Lsm1 transduced samples were normalized to the negative control BirA*-GFP. Proteins with significantly enriched peptide counts and calculated p-values are shown. **(B)** Schematic representation of all identified proteins (one protein=one dot) with >2x peptide counts over the BirA*-GFP control placed around the Lsm1 protein in the center according to the determined ratio BirA*-Lsm1/BirA*-GFP. Dots corresponding to proteins that are known to be involved in the decay process of mRNA transcripts are highlighted in red. Experiment was performed by Dr. Gesine Behrens using 4 replicates. Mass spectrometry and data analysis were performed by Steffi Hauck.

5 Discussion

In this research project, the main objective was to analyze the role of Lsm1 in the mouse system. I started by investigating known functions of Lsm1 that were previously described in other cellular systems, most prominently in yeast. The focus was set here on the consequences of Lsm1-depletion in MEF and T cells. A second goal of this study was the biological phenotyping of the immune system of Lsm1-deficient mice. In the following, my achieved results are discussed.

I addressed the question how the absence of Lsm1 influenced the remaining Lsm proteins in the cytoplasm. Importantly, the Lsm2-7 subunits are shared by two Lsm complexes in the cell: the cytoplasmic Lsm1-7 complex as well as the Lsm2-8 complex that is located in the nucleus (**Figure 2**). Interestingly, a previous study showed that depletion of Lsm8 in human cells resulted in the relocalization of Lsm4 and Lsm6 to the cytoplasm indicating that Lsm8 is essential for the nuclear localization of Lsm4, Lsm6 and most likely of all Lsm2-7 proteins (Novotny et al., 2012). By analogy, I expected Lsm1 to regulate the localization or stability of Lsm2-7 subunits. In contrast, I could not find any changes in expression or localization of Lsm4 in Lsm1-depleted MEF cells when compared to wildtype counterparts (**Figure 11**). Lsm4 was found similarly expressed in wildtype and *Lsm1^{neo/neo}* cells as well as in cytoplasmic and nuclear fractions of these, demonstrating that cytoplasmic Lsm2-7 components did most likely not change their localization in the absence of Lsm1. Moreover, Lsm4 was still present in P bodies that also formed in an unchanged frequency per cell. This demonstrates that Lsm1 is not essential for the localization of Lsm1-7 proteins to the cytoplasm or P bodies. A likely explanation for Lsm2-7 proteins not translocating to the nucleus is that only Lsm8 carries the required nuclear localization signal (Reijns, Auchynnikava, & Beggs, 2009). Lsm8 was found unchanged in Lsm1-deficient cells (**Figure 11B**) therefore its limited availability may prevent formation of additional Lsm2-8 complexes in Lsm1 knockout cells. Despite these potential explanations it was not expected to find Lsm4 enriched in P bodies (**Figure 11A**). Generally, little is known about how Lsm1-7 complexes contribute to P body formation. It has only been shown that this complex can assemble without binding to RNA, suggesting the existence of pre-assembled rings in the cytoplasm (Achsel et al., 1999; Mayes et al.,

1999; Vidal et al., 1999). Experiments from the Lührmann group suggested an interdependence of the P body components for accumulation in P bodies. By using RNAi against mRNA degradation factors in HeLa cells they showed, inter alia, that the knockdown of eIF4E-T or RCK resulted in the redistribution of Lsm1 in the cytoplasm, suggesting the formation of a larger mRNP complex with these factors that is then targeted to P bodies (Andrei et al., 2005). Another study from Zaric and colleagues showed that particular sequence elements in the Lsm subunits define the interaction of the entire complex with effector proteins such as Xrn1 or Dcp1/2 and with its target mRNA (Zaric et al., 2005). Of note these studies interpret their data on the basis of Lsm1-7 complex formation being required for P body formation, as it was previously demonstrated by knockdown approaches (Andrei et al., 2005; Chu & Rana, 2006; Kedersha et al., 2005; Stoecklin et al., 2006; Vindry et al., 2017). The fact that I found Lsm4 in P bodies in the absence of Lsm1 may suggest the assembly of a heterohexameric Lsm2-7 complex that retains its ability to localize to P bodies or that another unknown component can substitute for Lsm1 leading to the enrichment of Lsm4 in P bodies. As was suggested from the crystal structure of the Lsm1-7-Pat1 complex, the Lsm1-7 complex is expected to assemble from hetero-oligomeric building blocks: Lsm2-3 that corresponded to the nuclear SmD1-D2, Lsm6-5-7 corresponding to SmF-E-G and Lsm4-1 similar to SmD3/B (Sharif & Conti, 2013). This pre-assembly of heterodimeric and heterotrimeric sub-complexes that are then put together into one Lsm1-7 ring was shown *in vitro* by several groups (Kambach et al., 1999; Zaric et al., 2005). Electron microscopy investigating complex formation *in vitro* demonstrated ring-shaped structures of the subcomplexes Lsm2-3 and Lsm5-6-7 in addition to the Lsm1-7 and Lsm2-8 complexes (Zaric et al., 2005). These observations argue against the formation of a heterohexameric Lsm2-7 complex or substitution of only Lsm1, since Lsm4 cannot be integrated into subcomplexes in the absence of Lsm1. Complex formation with other Lsm-subunits is highly unlikely since only eubacteria and archaea are known to build homohexamers or homoheptamers, whereas eukaryotes form only heteroheptameric rings (Khusial, Plaag, & Zieve, 2005). My favorite hypothesis therefore is that in cells lacking Lsm1 Lsm4 might be present in P bodies due to associations with other proteins without being part of any Lsm complex. This idea is further supported by the fact that Lsm4 did not interact with Pat1b in the absence of Lsm1 (**Figure 13**). It is important to mention in this context that Chowdhury and colleagues reported the necessity of Pat1b interaction for the Lsm1-7 ring to bind to target mRNAs (Chowdhury et al., 2014). In their study, they demonstrated the

failure of the Lsm1-7 ring to effectively bind the *PGK1* and *MFA2* mRNAs by itself and only the association with Pat1b enabled binding of target mRNAs. Most importantly, P bodies require mRNAs for assembly since treatment with RNase A led to the disruption of P bodies (Teixeira et al., 2005). The localization of Lsm4 to P bodies and the simultaneous failure to interact with Pat1b in the absence of Lsm1 point to a molecular property of Lsm4 that is independent from its so far described function within the Lsm1-7 complex. Lsm4 could either be part of or direct the assembly of mRNPs into P-bodies by facilitating physical interaction between different mRNPs (Decker, Teixeira, & Parker, 2007; Reijns, Alexander, Spiller, & Beggs, 2008). Interestingly, the C-terminal Glutamine/Asparagine (Q/N)-rich domain of Lsm4 was suggested to promote the assembly of P bodies (Decker et al., 2007; Kedersha et al., 2005). My findings suggest that this property of Lsm4 is functional without being integrated into an Lsm1-7 ring.

Within the course of this project it was often difficult to decide whether and how far to pursue the investigation of compensatory changes in the absence of Lsm1 or to rather try to identify novel non-redundant roles. Previous studies that investigated the effect of Lsm1 on P body formation demonstrated a significant reduction of P body numbers upon Lsm1 knockdown (Andrei et al., 2005; Chu & Rana, 2006; Kedersha et al., 2005; Stoecklin et al., 2006; Vindry et al., 2017). By contrast, when I examined P body formation in Lsm1-deficient MEF and T cells I could not notice any changes in P body frequency per cell (**Figure 10; Figure 12**). The most plausible explanation seemed to be that the published data described the reduction of P body numbers after transient knockdown of Lsm1. Cells that lack a protein from their beginning, as it was the case for the present study on the *Lsm1^{neo/neo}* MEF cells, might be able to compensate, whereas in knockdown approaches, this adaptation may not be achieved in a short period of time. This hypothesis is further supported by the observation of reduced expression of two important players in the 5'-decay pathway, Pat1b and XRN1 in Lsm1-deficient MEF cells compared to wildtype counterparts (**Figure 14A**). Moreover, adaptation through compensation seemed to be a logical explanation since also DcpS, the scavenger protein that performed the decapping step in the 3'-5' pathway was overexpressed and strikingly similar results were obtained in T cells (**Figure 14B**). Although, this altered protein expression per se does not necessarily mean a shift towards the optional 3'-5' decay pathway, these changes were Lsm1-dependent, and should be addressed in more detail in the future. Altogether, these data suggest

compensatory changes in the Lsm1-deficient mouse cells, most probably through the 3'-5' decay pathway. To obtain definite proof how the absence of Lsm1 alters mRNA decay, one could for example perform a Pat1b PAR-Clip experiment in extracts from Lsm1-KO cells in comparison to WT counterparts, however, such an experiment exceeded the scope of this study.

In previous studies, the Lsm1 subunit could be coimmunoprecipitated with the stem-loop-binding protein (SLBP) in HeLa cells and its experimental downregulation resulted in stabilization of histone mRNA transcripts (Mullen & Marzluff, 2008). In addition, it was shown to interact with the exonuclease Eri1 (Hoefig et al., 2013). Thus, Lsm1 is believed to be involved in the degradation process of histone mRNAs. Based on these data, when analyzing histone mRNA decay in MEF cells, I expected the accumulation of oligo-uridylated histone mRNA transcripts in *Lsm1^{neo/neo}* when compared to WT MEF cells. However, qPCR measurements after HU-treatment revealed an unchanged induced reduction of all tested histone mRNA transcripts in knockout and WT cells (**Figure 7**). This finding led to the question, whether the known functions of Lsm1 were not conserved in the mouse. However, a number of observations in this study argue against this possibility. Although, histone mRNA levels were similarly reduced at the end of the HU treatment, I could detect a moderate delay in all tested histone mRNA transcripts during the kinetic (**Figure 9**). Furthermore, based on the hypothesis that expected changes were not detectable due to the adaptation of the cell to the absence of Lsm1 over time, P body numbers were determined in induced acute Lsm1-deleted T cells. In fact, these cells showed a clear reduction of P bodies frequencies when compared to WT control (**Figure 33**). In line with previously described observations made on the Lsm1-7 ring formation, these findings suggest rather a compensation in the Lsm1 knockout situation that is most probably not achieved during the short time interval of knockdown approaches. In regard to early studies by Ross and colleagues, suggesting that degradation of histone mRNAs proceeds 3'-5' and considering the results of experiments performed by Mullen and Marzluff in 2008 demonstrating degradation of individual histone mRNA molecules from both ends, I hypothesize that again compensation might be achieved in Lsm1-deficient cells through the 3'-5' pathway (Mullen & Marzluff, 2008; Ross, Peltz, Kobs, & Brewer, 1986). Importantly, also in human cells, degradation of histone mRNAs was shown to take place 3'-5' with the help of the exonuclease PM/Scl-100 that is associated with the exosome pointing to the conservation of this optional pathway throughout different species (Slevin et al., 2014). Moreover, the 3'-5' decay

pathway targets not only histone mRNA transcripts but in addition, and similar to the Lsm1-7 complex, also oligoadenylated and oligouridylated mRNA transcripts (Norbury, 2010). This indeed might be the cause for the almost unchanged transcriptome of Lsm1-deficient T cells in the present study (**Table 24**). Interestingly, deletion of the two TUTases TUT4 and TUT7 that perform the crucial task of uridylating mRNA transcripts to mark them for degradation did surprisingly not result in drastic phenotypes in somatic cells as was initially assumed. Strikingly, deletion in oocytes caused the accumulation of transcripts with very short poly(A) tails. The group of Dónal O'Carroll could show that this was crucial for oocyte maturation and fertility (Morgan et al., 2017). Importantly, we similarly noticed sterility of Lsm1-deficient female mice. These parallels underlie the idea of possible compensation of Lsm1 in MEF cells and suggest the investigation of the role of Lsm1 in oocytes.

Another possibility of how mouse cells could adapt to the absence of Lsm1 may relate to a more general redundancy of mRNA decay pathways in mammalian cells, which may not exist to a similar extent in yeast. In addition to Dcp2 that is responsible for decapping and that is recruited by Lsm1-7 to the 5' end of target mRNAs, other mRNA decapping enzymes (e.g. Nudt16) could be identified in mammalian cells (Song, Li, & Kiledjian, 2010). This suggests additional ways of mRNA decapping and subsequent degradation through the 5'-3' pathway. Consistent with this hypothesis, the knockout of Dcp2 had no adverse effects in mice. In addition, Dcp2 was not expressed in all tissues of WT mice and was also absent in the human liver, suggesting the presence of other decapping enzymes in these tissues (Song et al., 2010). The discussed redundancy may explain the minor changes in the cellular transcriptome in the absence of Lsm1, but it may also be considered that Lsm1 may function in a previously unrecognized way. It appears reasonable to assume that Lsm1 could play a role e.g. in the translational control of target mRNAs. This idea is supported by the fact that also other P body factors such as Pat1 and RCK, are activators of mRNA decapping but at the same time also repress translation (Bouveret et al., 2000; J. Coller & Parker, 2005; Minshall & Standart, 2004; Tharun & Parker, 2001). It was found that overexpression of Pat1 resulted in the general translational repression of yeast mRNA and depletion of both Pat1 and RCK derepressed translation (J. Coller & Parker, 2005). Importantly, the identification of CNOT4, as a potential new interaction partner of Lsm1 in the BioID experiment performed by Dr. Gesine Behrens further supports this idea (**Figure 45**). Experiments in human cells showed that CNOT4 was able to specifically recognize

mRNAs with stalled ribosomes and to recruit the decapping machinery to initiate degradation of these mRNAs (Lau et al., 2009). It remains to be determined whether Lsm1 indeed plays a role in the regulation of translation and which mRNAs are targeted in this case. These questions might be solved by future polysome profiling or ribosome footprint analyses in WT and Lsm1 KO cells.

Concluding, based on the molecular findings, this study clearly shows that Lsm1 function in mammalian mRNA decay pathways is more complex than it was expected based on studies in yeast. Future research efforts addressing the redundancy as well as possible new functions of Lsm1 in the regulation of translational may provide important insights.

The most surprising finding of this study was that Lsm1-deficient mice developed signs of autoimmunity. *Lsm1^{neo/neo}* mice exhibited splenomegaly (**Figure 23**), spontaneous activation of CD4⁺ and CD8⁺ T cells (**Figure 24**) as well as an accumulation of T_{FH} cells and GC B cells (**Figure 34**). The finding that confirmed the development of autoimmunity in Lsm1-deficient mice was the detection of autoantibodies in their sera (**Figure 35**; **Figure 36**). These results led to the question, which cells of the hematopoietic system might be affected and causal for the observed changes. In this respect I examined the possibility of a T cell-intrinsic induction of autoimmunity. Interestingly, analyses of the *Lsm1^{fl/fl}; CD4Cre* mice revealed activation of CD4⁺ T cells that exceeded the basal levels in control animals (**Figure 41**), and the same holds true for frequencies of T_{FH} cells (**Figure 42**). Although these frequencies did not increase to the same extent as in the complete KO mouse, they were significantly higher than in control mice. The frequencies of activated CD8⁺ T cells, by contrast, remained unchanged in the *Lsm1^{fl/fl}; CD4Cre* mouse. Considering the weaker increase in frequencies of activated CD4⁺ T cells and T_{FH} cells compared to the *Lsm1^{neo/neo}* mouse, it was assumed that there is very likely in addition to a clear T cell-intrinsic contribution also another cell type that participated to the autoimmune phenotype in the complete KO mouse. Generally, three professional antigen-presenting cells are believed to activate CD4⁺ T cells: macrophages, B cells and dendritic cells. Whether or not DCs, macrophages or B cells exhibited changed priming properties in the absence of Lsm1 is not clear yet. Nevertheless, spontaneous activation of CD4⁺ T cells in the *Lsm1^{fl/fl}; CD4Cre* mice pointed to a T cell-intrinsic potential that I aimed to investigate in more detail. First, I examined the differentiation of Lsm1-deficient CD4⁺ T cells. Interestingly, they spontaneously differentiated into

Th1 cells even in the absence of polarizing cytokines indicating that deletion of *Lsm1* influenced the T cell differentiation program *ex vivo* (**Figure 28**). In contrast, there were no preferences in differentiating towards Th2 or Th17 (**Figure 29**). Elevated levels of IFN- γ in *Lsm1*-deficient CD4⁺ T cells was a promising observation and we pursued the question how it came about. The overexpression of IFN- γ was previously, *inter alia*, connected to the T cell metabolism. Erika Pearce and her group studied the effect of overexpression of IFN- γ in connection to the metabolic state of the cell and could show full IFN- γ effector cytokine production correlated with and required a cellular commitment to aerobic glycolysis and IFN- γ production was strongly decreased when cells were forced into the metabolic program of oxidative phosphorylation (Chang et al., 2013). Interestingly, another study in yeast could demonstrate that *Lsm1* regulated mRNAs that encoded almost all enzymes of the glycolysis pathway (Li et al., 2013). Thus, I hypothesized that a causal link between overexpression of IFN- γ and the lack of *Lsm1* was based on a different choice of metabolic program in *Lsm1*-deficient T cells. When analyzing the metabolism of *Lsm1*-deficient CD4⁺ T cells, however, I found the two major processes of T cell metabolism, oxidative phosphorylation and glycolysis not affected by the absence of *Lsm1* (**Figure 27**). These data allowed me to disprove the hypothesis and therefore propose the reasons for increased levels of IFN- γ simply due to changes in mRNA levels. Indeed, the mRNA levels of *Ifng* in *Lsm1*-deficient CD4⁺ T cells were increased compared to control cells (**Figure 30**). However, whether the *Ifng* mRNA is a direct target of *Lsm1* or whether its accumulation was due to a secondary effect needs to be addressed in the future. Generally, IFN- γ production was shown to occur in low levels even in the absence of infections and being important for diverse biological processes (Gough, Messina, Clarke, Johnstone, & Levy, 2012; Hata et al., 2001). Very tight regulation of the low expression levels of IFNs in general is of great significance since perturbations cause pathologies such as autoimmune diseases and cancer (Crowl, Gray, Pestal, Volkman, & Stetson, 2017).

To understand the link between the absence of *Lsm1*, as part of an RNA-binding complex that was so far only described in the decay process of mRNAs and the development of autoimmunity was challenging. One interesting study, that described a link between one subunit of the exosome that shares several properties with the *Lsm1-7* complex and autoimmunity reported a connection based on the activation of RLRs in innate immune cells. Skiv2L, one part of the exosome-complex prevents

inappropriate ISG activation by hydrolyzing endogenous mRNAs from their 3' end (Eckard et al., 2014). Interestingly, humans carrying loss-of-function mutations in *SKIV2L* show a type I interferon signature in their blood (Fabre et al., 2012). In this context, it can be assumed that Lsm1 might act similar to the Skiv2L subunit as a suppressor and that its deletion might be the cause of accumulation of endogenous mRNAs that are detected by RLRs of certain immune cells, which in turn activate the immune system. Importantly, a very recent study dealing with inappropriate ISG activation found DDX6 (RCK) to be also responsible for the suppression function and strikingly this function was linked to the Lsm1 protein (Lumb et al., 2017). By crossing the Lsm1-deficient mouse with a TRIF (TIR-domain-containing adapter-inducing interferon-beta) KO mouse one might be able to answer the question whether the observed autoimmune phenotype in Lsm1-deficient mice is due to changes in the activation of TLRs. Most importantly, one essential prerequisite for the idea of Lsm1 being an important regulator of the nucleic acid metabolism in the innate immune response is the detectable deregulation and accumulation of mRNA transcripts in the cell that was, in our hands, not seen in Lsm1-deficient T cells. Determination of elevated overall mRNA levels in Lsm1-deficient cells would therefore be necessary to support this idea. Because of the T cell-intrinsic phenotype in Lsm1-deficient T cells observed *in vivo and in vitro*, I rather tend to the idea that autoimmunity in Lsm1-deficient mice is caused by a missing specific role of Lsm1 in T cells and most probably also in other cells of the hematopoietic system.

To better estimate the severity of the autoimmunity developed in Lsm1-deficient mice, I compared the phenotypes of the Lsm1-deficient mouse with the very well described *sanroque* mouse model. Similar to Lsm1, also here an RNA-binding protein is affected. Roquin-1 harboring the *san* mutation is functionally less active resulting in impaired functioning and to the development of a severe autoimmune phenotype (Vinuesa et al., 2005). I investigated abnormal activation of T cells, elevated frequencies of T_{FH} and GC B cells and differentiation towards Th1 in both mouse models and compared them to WT. Interestingly, all analyses showed the same tendency: a reproducible intermediate phenotype of Lsm1-deficient mice compared to a more severe phenotype of the *sanroque* mouse (**Figure 37**). Importantly, also in the *sanroque* mouse, the observed phenotypes were shown to have at least in part T cell-intrinsic causes (Linterman et al., 2009; Vinuesa et al., 2005). Because of these parallels, we speculated about a possible link between Lsm1 and Roquin. In line with this hypothesis, Pat1b as the main interaction partner of the Lsm1-7 complex was shown to interact directly

with several interaction partners of Roquin such as the CCR4-Not complex, RCK or Edc4 (Ozgun et al., 2010). Moreover, BioID data and immunoprecipitation experiments identified a new common interaction partner of Lsm1 and Roquin, namely 4E-T (**Figure 43; Figure 45B**). Because also CNOT4 could be identified in this approach, it appeared logical that all these proteins are linked to the same pathway (**Figure 45**). Because all mentioned proteins were shown to also translationally repress their target mRNAs, I suggest the same for Lsm1 as part of mRNP complex formation in this pathway. This idea is further supported by a very recent study in HeLa cells (Kamenska et al., 2016). When analyzing the function of 4E-T in repressing the translation of bound mRNAs, Kamenska and colleagues identified major partners of 4E-T including DDX6, Pat1b, Lsm1 and CNOT4. I therefore propose here a new model of mRNA regulation including all so far known proteins (**Figure 46**).

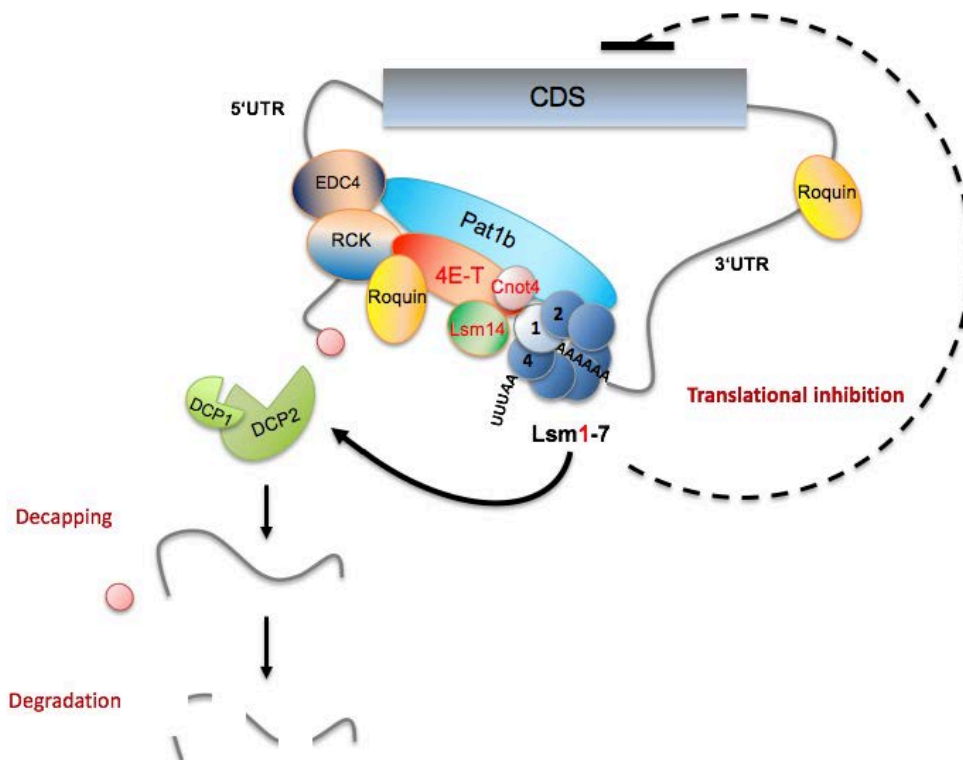


Figure 46: Suggested model of possible binding features of Lsm1
(based on obtained results in combination with previously published data)

Lsm1 as part of the Lsm1-7 complex binds oligoadenylated (or oligouridylated) mRNA transcripts and recruits DCP1 and DCP2 to the 5'end. The binding of Lsm1 to the mRNA results in many cases to the initiation of its degradation. According to the results achieved in the present work, it is most likely that Lsm1-binding also induces a state in which mRNA transcripts exit the translational process but do not get degraded immediately. This idea is enforced by the fact that 4E-T and CNOT4 are detectable in close distance to Lsm1. In addition, Pat1b as a master interactor, connecting Edc4, RCK, 4E-T and Lsm1 might strengthen the circular state of the mRNA that was already described to be induced by the presence of 4E-T. Importantly, also Roquin might also be involved in this pathway, since it interacts with Edc4, RCK and also with 4E-T as was shown in this study.

Concluding, this study described for the first time the consequences of Lsm1-deletion in the mouse. Although, other processes might be able to compensate for the function of Lsm1, I could show that the Lsm1-deficient mouse developed signs of autoimmunity, indicating that Lsm1 played an important role in preventing autoimmunity. Although, findings on molecular level provided strong evidence of compensatory mechanisms that might be able to take over the tasks of Lsm1, changes in T cell differentiation and the development of autoimmunity speak for a role of Lsm1 in T cells that could not be compensated as it was the case in MEF cells. Moreover, it cannot be excluded that Lsm1 carried out another additional unknown function, for example in the process of translational inhibition. It would be very interesting to investigate this hypothesis and to identify genes that enabled the observed spontaneous activation and/or Tfh differentiation in the absence of Lsm1 and by that complete the suggested model in Figure 46.

References

Uncategorized References

- Achleitner, M., Kleefisch, M., Hennig, A., Peschke, K., Polikarpova, A., Oertel, R., . . . Behrendt, R. (2017). Lack of Trex1 Causes Systemic Autoimmunity despite the Presence of Antiretroviral Drugs. *J Immunol*, *199*(7), 2261-2269. doi:10.4049/jimmunol.1700714
- Achsel, T., Brahms, H., Kastner, B., Bachi, A., Wilm, M., & Luhrmann, R. (1999). A doughnut-shaped heteromer of human Sm-like proteins binds to the 3'-end of U6 snRNA, thereby facilitating U4/U6 duplex formation in vitro. *EMBO J*, *18*(20), 5789-5802. doi:10.1093/emboj/18.20.5789
- Aizer, A., Brody, Y., Ler, L. W., Sonenberg, N., Singer, R. H., & Shav-Tal, Y. (2008). The dynamics of mammalian P body transport, assembly, and disassembly in vivo. *Mol Biol Cell*, *19*(10), 4154-4166. doi:10.1091/mbc.E08-05-0513
- Allmang, C., Kufel, J., Chanfreau, G., Mitchell, P., Petfalski, E., & Tollervey, D. (1999). Functions of the exosome in rRNA, snoRNA and snRNA synthesis. *EMBO J*, *18*(19), 5399-5410. doi:10.1093/emboj/18.19.5399
- Anantharaman, V., & Aravind, L. (2004). Novel conserved domains in proteins with predicted roles in eukaryotic cell-cycle regulation, decapping and RNA stability. *BMC Genomics*, *5*(1), 45. doi:10.1186/1471-2164-5-45
- Anderson, J. S., & Parker, R. P. (1998). The 3' to 5' degradation of yeast mRNAs is a general mechanism for mRNA turnover that requires the SKI2 DEVH box protein and 3' to 5' exonucleases of the exosome complex. *EMBO J*, *17*(5), 1497-1506. doi:10.1093/emboj/17.5.1497
- Andrei, M. A., Ingelfinger, D., Heintzmann, R., Achsel, T., Rivera-Pomar, R., & Luhrmann, R. (2005). A role for eIF4E and eIF4E-transporter in targeting mRNPs to mammalian processing bodies. *RNA*, *11*(5), 717-727. doi:10.1261/rna.2340405
- Arraiano, C. M., Andrade, J. M., Domingues, S., Guinote, I. B., Malecki, M., Matos, R. G., . . . Viegas, S. C. (2010). The critical role of RNA processing and degradation in the control of gene expression. *FEMS Microbiol Rev*, *34*(5), 883-923. doi:10.1111/j.1574-6976.2010.00242.x
- Ausubel, F. M. (2005). Are innate immune signaling pathways in plants and animals conserved? *Nat Immunol*, *6*(10), 973-979. doi:10.1038/ni1253
- Ayache, J., Benard, M., Ernoult-Lange, M., Minshall, N., Standart, N., Kress, M., & Weil, D. (2015). P-body assembly requires DDX6 repression complexes rather than decay or Ataxin2/2L complexes. *Mol Biol Cell*, *26*(14), 2579-2595. doi:10.1091/mbc.E15-03-0136

- Balagopal, V., & Parker, R. (2009). Polysomes, P bodies and stress granules: states and fates of eukaryotic mRNAs. *Curr Opin Cell Biol*, 21(3), 403-408. doi:10.1016/j.ceb.2009.03.005
- Barber, G. N. (2014). STING-dependent cytosolic DNA sensing pathways. *Trends Immunol*, 35(2), 88-93. doi:10.1016/j.it.2013.10.010
- Beckham, C. J., & Parker, R. (2008). P bodies, stress granules, and viral life cycles. *Cell Host Microbe*, 3(4), 206-212. doi:10.1016/j.chom.2008.03.004
- Beelman, C. A., Stevens, A., Caponigro, G., LaGrandeur, T. E., Hatfield, L., Fortner, D. M., & Parker, R. (1996). An essential component of the decapping enzyme required for normal rates of mRNA turnover. *Nature*, 382(6592), 642-646. doi:10.1038/382642a0
- Bertossi, A., Aichinger, M., Sansonetti, P., Lech, M., Neff, F., Pal, M., . . . Schmidt-Supprian, M. (2011). Loss of Roquin induces early death and immune deregulation but not autoimmunity. *J Exp Med*, 208(9), 1749-1756. doi:10.1084/jem.20110578
- Boeck, R., Lapeyre, B., Brown, C. E., & Sachs, A. B. (1998). Capped mRNA degradation intermediates accumulate in the yeast *spb8-2* mutant. *Mol Cell Biol*, 18(9), 5062-5072.
- Boeck, R., Tarun, S., Jr., Rieger, M., Deardorff, J. A., Muller-Auer, S., & Sachs, A. B. (1996). The yeast Pan2 protein is required for poly(A)-binding protein-stimulated poly(A)-nuclease activity. *J Biol Chem*, 271(1), 432-438.
- Bouveret, E., Rigaut, G., Shevchenko, A., Wilm, M., & Seraphin, B. (2000). A Sm-like protein complex that participates in mRNA degradation. *EMBO J*, 19(7), 1661-1671. doi:10.1093/emboj/19.7.1661
- Braun, J. E., Tritschler, F., Haas, G., Igreja, C., Truffault, V., Weichenrieder, O., & Izaurralde, E. (2010). The C-terminal alpha-alpha superhelix of Pat is required for mRNA decapping in metazoa. *EMBO J*, 29(14), 2368-2380. doi:10.1038/emboj.2010.124
- Brunkow, M. E., Jeffery, E. W., Hjerrild, K. A., Paepfer, B., Clark, L. B., Yasayko, S. A., . . . Ramsdell, F. (2001). Disruption of a new forkhead/winged-helix protein, scurfy, results in the fatal lymphoproliferative disorder of the scurfy mouse. *Nat Genet*, 27(1), 68-73. doi:10.1038/83784
- Bullock, W. E. (1976). Anergy and infection. *Adv Intern Med*, 21, 149-173.
- Caponigro, G., & Parker, R. (1995). Multiple functions for the poly(A)-binding protein in mRNA decapping and deadenylation in yeast. *Genes Dev*, 9(19), 2421-2432.
- Caponigro, G., & Parker, R. (1996). Mechanisms and control of mRNA turnover in *Saccharomyces cerevisiae*. *Microbiol Rev*, 60(1), 233-249.

-
- Carballo, E., Lai, W. S., & Blakeshear, P. J. (1998). Feedback inhibition of macrophage tumor necrosis factor- α production by tristetraprolin. *Science*, *281*(5379), 1001-1005.
- Chahar, H. S., Chen, S., & Manjunath, N. (2013). P-body components LSM1, GW182, DDX3, DDX6 and XRN1 are recruited to WNV replication sites and positively regulate viral replication. *Virology*, *436*(1), 1-7. doi:10.1016/j.virol.2012.09.041
- Chang, C. H., Curtis, J. D., Maggi, L. B., Jr., Faubert, B., Villarino, A. V., O'Sullivan, D., . . . Pearce, E. L. (2013). Posttranscriptional control of T cell effector function by aerobic glycolysis. *Cell*, *153*(6), 1239-1251. doi:10.1016/j.cell.2013.05.016
- Chen, C. Y., Gherzi, R., Ong, S. E., Chan, E. L., Raijmakers, R., Pruijn, G. J., . . . Karin, M. (2001). AU binding proteins recruit the exosome to degrade ARE-containing mRNAs. *Cell*, *107*(4), 451-464.
- Chen, H., Yang, T., Zhu, L., & Zhao, Y. (2015). Cellular metabolism on T-cell development and function. *Int Rev Immunol*, *34*(1), 19-33. doi:10.3109/08830185.2014.902452
- Chen, N., Walsh, M. A., Liu, Y., Parker, R., & Song, H. (2005). Crystal structures of human DcpS in ligand-free and m7GDP-bound forms suggest a dynamic mechanism for scavenger mRNA decapping. *J Mol Biol*, *347*(4), 707-718. doi:10.1016/j.jmb.2005.01.062
- Chowdhury, A., Kalurupalle, S., & Tharun, S. (2014). Pat1 contributes to the RNA binding activity of the Lsm1-7-Pat1 complex. *RNA*, *20*(9), 1465-1475. doi:10.1261/rna.045252.114
- Chowdhury, A., Kalurupalle, S., & Tharun, S. (2016). Mutagenic Analysis of the C-Terminal Extension of Lsm1. *PLoS One*, *11*(7), e0158876. doi:10.1371/journal.pone.0158876
- Chowdhury, A., Mukhopadhyay, J., & Tharun, S. (2007). The decapping activator Lsm1p-7p-Pat1p complex has the intrinsic ability to distinguish between oligoadenylated and polyadenylated RNAs. *RNA*, *13*(7), 998-1016. doi:10.1261/rna.502507
- Chu, C. Y., & Rana, T. M. (2006). Translation repression in human cells by microRNA-induced gene silencing requires RCK/p54. *PLoS Biol*, *4*(7), e210. doi:10.1371/journal.pbio.0040210
- Coller, J., & Parker, R. (2004). Eukaryotic mRNA decapping. *Annu Rev Biochem*, *73*, 861-890. doi:10.1146/annurev.biochem.73.011303.074032
- Coller, J., & Parker, R. (2005). General translational repression by activators of mRNA decapping. *Cell*, *122*(6), 875-886. doi:10.1016/j.cell.2005.07.012
- Coller, J. M., Gray, N. K., & Wickens, M. P. (1998). mRNA stabilization by poly(A) binding protein is independent of poly(A) and requires translation. *Genes Dev*, *12*(20), 3226-3235.

- Coller, J. M., Tucker, M., Sheth, U., Valencia-Sanchez, M. A., & Parker, R. (2001). The DEAD box helicase, Dhh1p, functions in mRNA decapping and interacts with both the decapping and deadenylase complexes. *RNA*, *7*(12), 1717-1727.
- Cougot, N., van Dijk, E., Babajko, S., & Seraphin, B. (2004). 'Cap-tabolism'. *Trends Biochem Sci*, *29*(8), 436-444. doi:10.1016/j.tibs.2004.06.008
- Crowl, J. T., Gray, E. E., Pestal, K., Volkman, H. E., & Stetson, D. B. (2017). Intracellular Nucleic Acid Detection in Autoimmunity. *Annu Rev Immunol*, *35*, 313-336. doi:10.1146/annurev-immunol-051116-052331
- Das, S., Sarkar, D., & Das, B. (2017). The interplay between transcription and mRNA degradation in *Saccharomyces cerevisiae*. *Microb Cell*, *4*(7), 212-228. doi:10.15698/mic2017.07.580
- Datta, S., Biswas, R., Novotny, M., Pavicic, P. G., Jr., Herjan, T., Mandal, P., & Hamilton, T. A. (2008). Tristetraprolin regulates CXCL1 (KC) mRNA stability. *J Immunol*, *180*(4), 2545-2552.
- Daugeron, M. C., Mauxion, F., & Seraphin, B. (2001). The yeast POP2 gene encodes a nuclease involved in mRNA deadenylation. *Nucleic Acids Res*, *29*(12), 2448-2455.
- Decker, C. J., & Parker, R. (1993). A turnover pathway for both stable and unstable mRNAs in yeast: evidence for a requirement for deadenylation. *Genes Dev*, *7*(8), 1632-1643.
- Decker, C. J., Teixeira, D., & Parker, R. (2007). Edc3p and a glutamine/asparagine-rich domain of Lsm4p function in processing body assembly in *Saccharomyces cerevisiae*. *J Cell Biol*, *179*(3), 437-449. doi:10.1083/jcb.200704147
- Diez, J., Ishikawa, M., Kaido, M., & Ahlquist, P. (2000). Identification and characterization of a host protein required for efficient template selection in viral RNA replication. *Proc Natl Acad Sci U S A*, *97*(8), 3913-3918. doi:10.1073/pnas.080072997
- Dong, Y., Yang, J., Ye, W., Wang, Y., Miao, Y., Ding, T., . . . Xu, Z. (2015). LSm1 binds to the Dengue virus RNA 3' UTR and is a positive regulator of Dengue virus replication. *Int J Mol Med*, *35*(6), 1683-1689. doi:10.3892/ijmm.2015.2169
- Dostie, J., Ferraiuolo, M., Pause, A., Adam, S. A., & Sonenberg, N. (2000). A novel shuttling protein, 4E-T, mediates the nuclear import of the mRNA 5' cap-binding protein, eIF4E. *EMBO J*, *19*(12), 3142-3156. doi:10.1093/emboj/19.12.3142
- Dunckley, T., & Parker, R. (2001). Yeast mRNA decapping enzyme. *Methods Enzymol*, *342*, 226-233.
- Eckard, S. C., Rice, G. I., Fabre, A., Badens, C., Gray, E. E., Hartley, J. L., . . . Stetson, D. B. (2014). The SKIV2L RNA exosome limits activation of the RIG-I-like receptors. *Nat Immunol*, *15*(9), 839-845. doi:10.1038/ni.2948

-
- Estep, P., Reid, F., Nauman, C., Liu, Y., Sun, T., Sun, J., & Xu, Y. (2013). High throughput solution-based measurement of antibody-antigen affinity and epitope binning. *MAbs*, *5*(2), 270-278. doi:10.4161/mabs.23049
- Fabian, M. R., Frank, F., Rouya, C., Siddiqui, N., Lai, W. S., Karetnikov, A., . . . Sonenberg, N. (2013). Structural basis for the recruitment of the human CCR4-NOT deadenylase complex by tristetraprolin. *Nat Struct Mol Biol*, *20*(6), 735-739. doi:10.1038/nsmb.2572
- Fabre, A., Charroux, B., Martinez-Vinson, C., Roquelaure, B., Odul, E., Sayar, E., . . . Badens, C. (2012). SKIV2L mutations cause syndromic diarrhea, or trichohepatoenteric syndrome. *Am J Hum Genet*, *90*(4), 689-692. doi:10.1016/j.ajhg.2012.02.009
- Fenger-Gron, M., Fillman, C., Norrild, B., & Lykke-Andersen, J. (2005). Multiple processing body factors and the ARE binding protein TTP activate mRNA decapping. *Mol Cell*, *20*(6), 905-915. doi:10.1016/j.molcel.2005.10.031
- Ferraiuolo, M. A., Basak, S., Dostie, J., Murray, E. L., Schoenberg, D. R., & Sonenberg, N. (2005). A role for the eIF4E-binding protein 4E-T in P-body formation and mRNA decay. *J Cell Biol*, *170*(6), 913-924. doi:10.1083/jcb.200504039
- Fillman, C., & Lykke-Andersen, J. (2005). RNA decapping inside and outside of processing bodies. *Curr Opin Cell Biol*, *17*(3), 326-331. doi:10.1016/j.ceb.2005.04.002
- Fischer, N., & Weis, K. (2002). The DEAD box protein Dhh1 stimulates the decapping enzyme Dcp1. *EMBO J*, *21*(11), 2788-2797. doi:10.1093/emboj/21.11.2788
- Folichon, M., Arluison, V., Pellegrini, O., Huntzinger, E., Regnier, P., & Hajnsdorf, E. (2003). The poly(A) binding protein Hfq protects RNA from RNase E and exoribonucleolytic degradation. *Nucleic Acids Res*, *31*(24), 7302-7310.
- Fritz, D. T., Bergman, N., Kilpatrick, W. J., Wilusz, C. J., & Wilusz, J. (2004). Messenger RNA decay in mammalian cells: the exonuclease perspective. *Cell Biochem Biophys*, *41*(2), 265-278. doi:10.1385/cbb:41:2:265
- Galao, R. P., Chari, A., Alves-Rodrigues, I., Lobao, D., Mas, A., Kambach, C., . . . Diez, J. (2010). LSM1-7 complexes bind to specific sites in viral RNA genomes and regulate their translation and replication. *RNA*, *16*(4), 817-827. doi:10.1261/rna.1712910
- Gallie, D. R. (1991). The cap and poly(A) tail function synergistically to regulate mRNA translational efficiency. *Genes Dev*, *5*(11), 2108-2116.
- Gao, M., Wilusz, C. J., Peltz, S. W., & Wilusz, J. (2001). A novel mRNA-decapping activity in HeLa cytoplasmic extracts is regulated by AU-rich elements. *EMBO J*, *20*(5), 1134-1143. doi:10.1093/emboj/20.5.1134
- Gavin, A. C., Aloy, P., Grandi, P., Krause, R., Boesche, M., Marzioch, M., . . . Superti-Furga, G. (2006). Proteome survey reveals modularity of the yeast cell machinery. *Nature*, *440*(7084), 631-636. doi:10.1038/nature04532

- Gibson, S., & Jacobson, D. M. (1996). *Below the Temple mount in Jerusalem : a sourcebook on the cisterns, subterranean chambers and conduits of the Ḥaram al-Sharīf*. Oxford: Tempus Reparatum.
- Gimenez-Barcons, M., Alves-Rodrigues, I., Jungfleisch, J., Van Wynsberghe, P. M., Ahlquist, P., & Diez, J. (2013). The cellular decapping activators LSm1, Pat1, and Dhh1 control the ratio of subgenomic to genomic Flock House virus RNAs. *J Virol*, *87*(11), 6192-6200. doi:10.1128/jvi.03327-12
- Goubau, D., Deddouche, S., & Reis e Sousa, C. (2013). Cytosolic sensing of viruses. *Immunity*, *38*(5), 855-869. doi:10.1016/j.immuni.2013.05.007
- Gough, D. J., Messina, N. L., Clarke, C. J., Johnstone, R. W., & Levy, D. E. (2012). Constitutive type I interferon modulates homeostatic balance through tonic signaling. *Immunity*, *36*(2), 166-174. doi:10.1016/j.immuni.2012.01.011
- Grawunder, U., Zimmer, D., Fugmann, S., Schwarz, K., & Lieber, M. R. (1998). DNA ligase IV is essential for V(D)J recombination and DNA double-strand break repair in human precursor lymphocytes. *Mol Cell*, *2*(4), 477-484.
- Gutierrez-Vazquez, C., Enright, A. J., Rodriguez-Galan, A., Perez-Garcia, A., Collier, P., Jones, M. R., . . . Sanchez-Madrid, F. (2017). 3' Uridylation controls mature microRNA turnover during CD4 T-cell activation. *RNA*, *23*(6), 882-891. doi:10.1261/rna.060095.116
- Haas, G., Braun, J. E., Igreja, C., Tritschler, F., Nishihara, T., & Izaurralde, E. (2010). HPat provides a link between deadenylation and decapping in metazoa. *J Cell Biol*, *189*(2), 289-302. doi:10.1083/jcb.200910141
- Hajnsdorf, E., & Regnier, P. (2000). Host factor Hfq of Escherichia coli stimulates elongation of poly(A) tails by poly(A) polymerase I. *Proc Natl Acad Sci USA*, *97*(4), 1501-1505. doi:10.1073/pnas.040549897
- Harigaya, Y., & Parker, R. (2010). No-go decay: a quality control mechanism for RNA in translation. *Wiley Interdiscip Rev RNA*, *1*(1), 132-141. doi:10.1002/wrna.17
- Hata, N., Sato, M., Takaoka, A., Asagiri, M., Tanaka, N., & Taniguchi, T. (2001). Constitutive IFN-alpha/beta signal for efficient IFN-alpha/beta gene induction by virus. *Biochem Biophys Res Commun*, *285*(2), 518-525. doi:10.1006/bbrc.2001.5159
- He, W., & Parker, R. (2001). The yeast cytoplasmic Lsm1/Pat1p complex protects mRNA 3' termini from partial degradation. *Genetics*, *158*(4), 1445-1455.
- Hentze, M. W. (1991). Determinants and regulation of cytoplasmic mRNA stability in eukaryotic cells. *Biochim Biophys Acta*, *1090*(3), 281-292.
- Hermann, H., Fabrizio, P., Raker, V. A., Foulaki, K., Hornig, H., Brahms, H., & Luhrmann, R. (1995). snRNP Sm proteins share two evolutionarily conserved sequence motifs which are involved in Sm protein-protein interactions. *EMBO J*, *14*(9), 2076-2088.

-
- Herrero, A. B., & Moreno, S. (2011). Lsm1 promotes genomic stability by controlling histone mRNA decay. *EMBO J*, *30*(10), 2008-2018. doi:10.1038/emboj.2011.117
- Hershey, J. W., Asano, K., Naranda, T., Vornlocher, H. P., Hanachi, P., & Merrick, W. C. (1996). Conservation and diversity in the structure of translation initiation factor EIF3 from humans and yeast. *Biochimie*, *78*(11-12), 903-907.
- Hoefig, K. P., Rath, N., Heinz, G. A., Wolf, C., Dameris, J., Schepers, A., . . . Heissmeyer, V. (2013). Eri1 degrades the stem-loop of oligouridylated histone mRNAs to induce replication-dependent decay. *Nat Struct Mol Biol*, *20*(1), 73-81. doi:10.1038/nsmb.2450
- Houseley, J., & Tollervey, D. (2009). The many pathways of RNA degradation. *Cell*, *136*(4), 763-776. doi:10.1016/j.cell.2009.01.019
- Ikehara, S., Kawamura, M., Takao, F., Inaba, M., Yasumizu, R., Than, S., . . . et al. (1990). Organ-specific and systemic autoimmune diseases originate from defects in hematopoietic stem cells. *Proc Natl Acad Sci U S A*, *87*(21), 8341-8344.
- Ingelfinger, D., Arndt-Jovin, D. J., Luhrmann, R., & Achsel, T. (2002). The human LSm1-7 proteins colocalize with the mRNA-degrading enzymes Dcp1/2 and Xrn1 in distinct cytoplasmic foci. *RNA*, *8*(12), 1489-1501.
- Ito, T., Hanabuchi, S., Wang, Y. H., Park, W. R., Arima, K., Bover, L., . . . Liu, Y. J. (2008). Two functional subsets of FOXP3+ regulatory T cells in human thymus and periphery. *Immunity*, *28*(6), 870-880. doi:10.1016/j.immuni.2008.03.018
- Jacobson, A. (2004). Regulation of mRNA decay: decapping goes solo. *Mol Cell*, *15*(1), 1-2. doi:10.1016/j.molcel.2004.06.031
- Janeway, C. A., Jr., & Medzhitov, R. (2002). Innate immune recognition. *Annu Rev Immunol*, *20*, 197-216. doi:10.1146/annurev.immunol.20.083001.084359
- Janowski, R., Heinz, G. A., Schlundt, A., Wommelsdorf, N., Brenner, S., Gruber, A. R., . . . Sattler, M. (2016). Roquin recognizes a non-canonical hexaloop structure in the 3'-UTR of Ox40. *Nat Commun*, *7*, 11032. doi:10.1038/ncomms11032
- Jeltsch, K. M., Hu, D., Brenner, S., Zoller, J., Heinz, G. A., Nagel, D., . . . Heissmeyer, V. (2014). Cleavage of roquin and regnase-1 by the paracaspase MALT1 releases their cooperatively repressed targets to promote T(H)17 differentiation. *Nat Immunol*, *15*(11), 1079-1089. doi:10.1038/ni.3008
- Jungfleisch, J., Chowdhury, A., Alves-Rodrigues, I., Tharun, S., & Diez, J. (2015). The Lsm1-7-Pat1 complex promotes viral RNA translation and replication by differential mechanisms. *RNA*, *21*(8), 1469-1479. doi:10.1261/rna.052209.115
- Kahvejian, A., Roy, G., & Sonenberg, N. (2001). The mRNA closed-loop model: the function of PABP and PABP-interacting proteins in mRNA translation. *Cold Spring Harb Symp Quant Biol*, *66*, 293-300.

- Kambach, C., Walke, S., Young, R., Avis, J. M., de la Fortelle, E., Raker, V. A., . . . Nagai, K. (1999). Crystal structures of two Sm protein complexes and their implications for the assembly of the spliceosomal snRNPs. *Cell*, *96*(3), 375-387.
- Kamenska, A., Simpson, C., Vindry, C., Broomhead, H., Benard, M., Ernoult-Lange, M., . . . Standart, N. (2016). The DDX6-4E-T interaction mediates translational repression and P-body assembly. *Nucleic Acids Res*, *44*(13), 6318-6334. doi:10.1093/nar/gkw565
- Kawai, T., & Akira, S. (2010). The role of pattern-recognition receptors in innate immunity: update on Toll-like receptors. *Nat Immunol*, *11*(5), 373-384. doi:10.1038/ni.1863
- Kedersha, N., & Anderson, P. (2009). Regulation of translation by stress granules and processing bodies. *Prog Mol Biol Transl Sci*, *90*, 155-185. doi:10.1016/s1877-1173(09)90004-7
- Kedersha, N., Stoecklin, G., Ayodele, M., Yacono, P., Lykke-Andersen, J., Fritzler, M. J., . . . Anderson, P. (2005). Stress granules and processing bodies are dynamically linked sites of mRNP remodeling. *J Cell Biol*, *169*(6), 871-884. doi:10.1083/jcb.200502088
- Khanna, R., & Kiledjian, M. (2004). Poly(A)-binding-protein-mediated regulation of hDcp2 decapping in vitro. *EMBO J*, *23*(9), 1968-1976. doi:10.1038/sj.emboj.7600213
- Khusial, P., Plaag, R., & Zieve, G. W. (2005). LSm proteins form heptameric rings that bind to RNA via repeating motifs. *Trends Biochem Sci*, *30*(9), 522-528. doi:10.1016/j.tibs.2005.07.006
- Killian, J. M., Tiwari, P. S., Jacobson, S., Jackson, R. D., & Lupski, J. R. (1996). Longitudinal studies of the duplication form of Charcot-Marie-Tooth polyneuropathy. *Muscle Nerve*, *19*(1), 74-78. doi:10.1002/(SICI)1097-4598(199601)19:1<74::AID-MUS10>3.0.CO;2-3
- Kowalinski, E., Lunardi, T., McCarthy, A. A., Louber, J., Brunel, J., Grigorov, B., . . . Cusack, S. (2011). Structural basis for the activation of innate immune pattern-recognition receptor RIG-I by viral RNA. *Cell*, *147*(2), 423-435. doi:10.1016/j.cell.2011.09.039
- Lai, W. S., Carballo, E., Thorn, J. M., Kennington, E. A., & Blackshear, P. J. (2000). Interactions of CCCH zinc finger proteins with mRNA. Binding of tristetraprolin-related zinc finger proteins to Au-rich elements and destabilization of mRNA. *J Biol Chem*, *275*(23), 17827-17837. doi:10.1074/jbc.M001696200
- Lai, W. S., Stumpo, D. J., & Blackshear, P. J. (1990). Rapid insulin-stimulated accumulation of an mRNA encoding a proline-rich protein. *J Biol Chem*, *265*(27), 16556-16563.
- Lau, N. C., Kolkman, A., van Schaik, F. M., Mulder, K. W., Pijnappel, W. W., Heck, A. J., & Timmers, H. T. (2009). Human Ccr4-Not complexes contain variable deadenylase subunits. *Biochem J*, *422*(3), 443-453. doi:10.1042/bj20090500

-
- Leppek, K., Schott, J., Reitter, S., Poetz, F., Hammond, M. C., & Stoecklin, G. (2013). Roquin promotes constitutive mRNA decay via a conserved class of stem-loop recognition motifs. *Cell*, *153*(4), 869-881. doi:10.1016/j.cell.2013.04.016
- Lerner, M. R., & Steitz, J. A. (1979). Antibodies to small nuclear RNAs complexed with proteins are produced by patients with systemic lupus erythematosus. *Proc Natl Acad Sci U S A*, *76*(11), 5495-5499.
- Li, L., Miles, S., Melville, Z., Prasad, A., Bradley, G., & Breeden, L. L. (2013). Key events during the transition from rapid growth to quiescence in budding yeast require posttranscriptional regulators. *Mol Biol Cell*, *24*(23), 3697-3709. doi:10.1091/mbc.E13-05-0241
- Liang, J., Song, W., Tromp, G., Kolattukudy, P. E., & Fu, M. (2008). Genome-wide survey and expression profiling of CCCH-zinc finger family reveals a functional module in macrophage activation. *PLoS One*, *3*(8), e2880. doi:10.1371/journal.pone.0002880
- Lim, J., Ha, M., Chang, H., Kwon, S. C., Simanshu, D. K., Patel, D. J., & Kim, V. N. (2014). Uridylation by TUT4 and TUT7 marks mRNA for degradation. *Cell*, *159*(6), 1365-1376. doi:10.1016/j.cell.2014.10.055
- Link, T. M., Valentin-Hansen, P., & Brennan, R. G. (2009). Structure of Escherichia coli Hfq bound to polyriboadenylate RNA. *Proc Natl Acad Sci U S A*, *106*(46), 19292-19297. doi:10.1073/pnas.0908744106
- Linterman, M. A., Rigby, R. J., Wong, R., Silva, D., Withers, D., Anderson, G., . . . Vinuesa, C. G. (2009). Roquin differentiates the specialized functions of duplicated T cell costimulatory receptor genes CD28 and ICOS. *Immunity*, *30*(2), 228-241. doi:10.1016/j.immuni.2008.12.015
- Long, R. M., & McNally, M. T. (2003). mRNA decay: x (XRN1) marks the spot. *Mol Cell*, *11*(5), 1126-1128.
- Lumb, J. H., Li, Q., Popov, L. M., Ding, S., Keith, M. T., Merrill, B. D., . . . Carette, J. E. (2017). DDX6 Represses Aberrant Activation of Interferon-Stimulated Genes. *Cell Rep*, *20*(4), 819-831. doi:10.1016/j.celrep.2017.06.085
- Lykke-Andersen, J. (2001). mRNA quality control: Marking the message for life or death. *Curr Biol*, *11*(3), R88-91.
- Maeda, K., & Akira, S. (2017). Regulation of mRNA stability by CCCH-type zinc-finger proteins in immune cells. *Int Immunol*, *29*(4), 149-155. doi:10.1093/intimm/dxx015
- Makino, D. L., Baumgartner, M., & Conti, E. (2013). Crystal structure of an RNA-bound 11-subunit eukaryotic exosome complex. *Nature*, *495*(7439), 70-75. doi:10.1038/nature11870

- Mangus, D. A., Evans, M. C., & Jacobson, A. (2003). Poly(A)-binding proteins: multifunctional scaffolds for the post-transcriptional control of gene expression. *Genome Biol*, *4*(7), 223. doi:10.1186/gb-2003-4-7-223
- Maquat, L. E. (2002). Nonsense-mediated mRNA decay. *Curr Biol*, *12*(6), R196-197.
- Marzluff, W. F. (2005). Metazoan replication-dependent histone mRNAs: a distinct set of RNA polymerase II transcripts. *Curr Opin Cell Biol*, *17*(3), 274-280. doi:10.1016/j.ceb.2005.04.010
- Mas, A., Alves-Rodrigues, I., Noueir, A., Ahlquist, P., & Diez, J. (2006). Host deadenylation-dependent mRNA decapping factors are required for a key step in brome mosaic virus RNA replication. *J Virol*, *80*(1), 246-251. doi:10.1128/jvi.80.1.246-251.2006
- Matsushita, K., Takeuchi, O., Standley, D. M., Kumagai, Y., Kawagoe, T., Miyake, T., . . . Akira, S. (2009). Zc3h12a is an RNase essential for controlling immune responses by regulating mRNA decay. *Nature*, *458*(7242), 1185-1190. doi:10.1038/nature07924
- Mayes, A. E., Verdone, L., Legrain, P., & Beggs, J. D. (1999). Characterization of Sm-like proteins in yeast and their association with U6 snRNA. *EMBO J*, *18*(15), 4321-4331. doi:10.1093/emboj/18.15.4321
- Mijatovic, T., Houzet, L., Defrance, P., Droogmans, L., Huez, G., & Kruys, V. (2000). Tumor necrosis factor- α mRNA remains unstable and hypoadenylated upon stimulation of macrophages by lipopolysaccharides. *Eur J Biochem*, *267*(19), 6004-6012.
- Mikulecky, P. J., Kaw, M. K., Brescia, C. C., Takach, J. C., Sledjeski, D. D., & Feig, A. L. (2004). Escherichia coli Hfq has distinct interaction surfaces for DsrA, rpoS and poly(A) RNAs. *Nat Struct Mol Biol*, *11*(12), 1206-1214. doi:10.1038/nsmb858
- Mino, T., Murakawa, Y., Fukao, A., Vandenbon, A., Wessels, H. H., Ori, D., . . . Takeuchi, O. (2015). Regnase-1 and Roquin Regulate a Common Element in Inflammatory mRNAs by Spatiotemporally Distinct Mechanisms. *Cell*, *161*(5), 1058-1073. doi:10.1016/j.cell.2015.04.029
- Minshall, N., & Standart, N. (2004). The active form of Xp54 RNA helicase in translational repression is an RNA-mediated oligomer. *Nucleic Acids Res*, *32*(4), 1325-1334. doi:10.1093/nar/gkh303
- Miras, M., Truniger, V., Silva, C., Verdager, N., Aranda, M. A., & Querol-Audi, J. (2017). Structure of eIF4E in Complex with an eIF4G Peptide Supports a Universal Bipartite Binding Mode for Protein Translation. *Plant Physiol*, *174*(3), 1476-1491. doi:10.1104/pp.17.00193
- Mitchell, P., Petfalski, E., Shevchenko, A., Mann, M., & Tollervey, D. (1997). The exosome: a conserved eukaryotic RNA processing complex containing multiple 3'→5' exoribonucleases. *Cell*, *91*(4), 457-466.

-
- Morgan, M., Much, C., DiGiacomo, M., Azzi, C., Ivanova, I., Vitsios, D. M., . . . O'Carroll, D. (2017). mRNA 3' uridylation and poly(A) tail length sculpt the mammalian maternal transcriptome. *Nature*, *548*(7667), 347-351. doi:10.1038/nature23318
- Moss, R., Pryme, I. F., & Vedeler, A. (1994). Free, cytoskeletal-bound and membrane-bound polysomes isolated from MPC-11 and Krebs II ascites cells differ in their complement of poly(A) binding proteins. *Mol Cell Biochem*, *131*(2), 131-139.
- Mugridge, J. S., Ziemniak, M., Jemielity, J., & Gross, J. D. (2016). Structural basis of mRNA-cap recognition by Dcp1-Dcp2. *Nat Struct Mol Biol*, *23*(11), 987-994. doi:10.1038/nsmb.3301
- Mukherjee, D., Gao, M., O'Connor, J. P., Raijmakers, R., Pruijn, G., Lutz, C. S., & Wilusz, J. (2002). The mammalian exosome mediates the efficient degradation of mRNAs that contain AU-rich elements. *EMBO J*, *21*(1-2), 165-174. doi:10.1093/emboj/21.1.165
- Mullen, T. E., & Marzluff, W. F. (2008). Degradation of histone mRNA requires oligouridylation followed by decapping and simultaneous degradation of the mRNA both 5' to 3' and 3' to 5'. *Genes Dev*, *22*(1), 50-65. doi:10.1101/gad.1622708
- Murakawa, Y., Hinz, M., Mothes, J., Schuetz, A., Uhl, M., Wyler, E., . . . Landthaler, M. (2015). RC3H1 post-transcriptionally regulates A20 mRNA and modulates the activity of the IKK/NF-kappaB pathway. *Nat Commun*, *6*, 7367. doi:10.1038/ncomms8367
- Nakayamada, S., & Tanaka, Y. (2016). T follicular helper (Tfh) cells in autoimmune diseases. *Nihon Rinsho Meneki Gakkai Kaishi*, *39*(1), 1-7. doi:10.2177/jsci.39.1
- Nesargikar, P. N., Spiller, B., & Chavez, R. (2012). The complement system: history, pathways, cascade and inhibitors. *Eur J Microbiol Immunol (Bp)*, *2*(2), 103-111. doi:10.1556/EuJMI.2.2012.2.2
- Nishimura, T., Padamsi, Z., Fakim, H., Milette, S., Dunham, W. H., Gingras, A. C., & Fabian, M. R. (2015). The eIF4E-Binding Protein 4E-T Is a Component of the mRNA Decay Machinery that Bridges the 5' and 3' Termini of Target mRNAs. *Cell Rep*, *11*(9), 1425-1436. doi:10.1016/j.celrep.2015.04.065
- Nissan, T., Rajyaguru, P., She, M., Song, H., & Parker, R. (2010). Decapping activators in *Saccharomyces cerevisiae* act by multiple mechanisms. *Mol Cell*, *39*(5), 773-783. doi:10.1016/j.molcel.2010.08.025
- Norbury, C. J. (2010). 3' Uridylation and the regulation of RNA function in the cytoplasm. *Biochem Soc Trans*, *38*(4), 1150-1153. doi:10.1042/bst0381150
- Noueiry, A. O., Diez, J., Falk, S. P., Chen, J., & Ahlquist, P. (2003). Yeast Lsm1p-7p/Pat1p deadenylation-dependent mRNA-decapping factors are required for brome mosaic virus genomic RNA translation. *Mol Cell Biol*, *23*(12), 4094-4106.
- Novotny, I., Podolska, K., Blazikova, M., Valasek, L. S., Svoboda, P., & Stanek, D. (2012). Nuclear LSm8 affects number of cytoplasmic processing bodies via controlling

- cellular distribution of Like-Sm proteins. *Mol Biol Cell*, 23(19), 3776-3785. doi:10.1091/mbc.E12-02-0085
- Ogilvie, R. L., Abelson, M., Hau, H. H., Vlasova, I., Blackshear, P. J., & Bohjanen, P. R. (2005). Tristetraprolin down-regulates IL-2 gene expression through AU-rich element-mediated mRNA decay. *J Immunol*, 174(2), 953-961.
- Ozgur, S., Basquin, J., Kamenska, A., Filipowicz, W., Standart, N., & Conti, E. (2015). Structure of a Human 4E-T/DDX6/CNOT1 Complex Reveals the Different Interplay of DDX6-Binding Proteins with the CCR4-NOT Complex. *Cell Rep*, 13(4), 703-711. doi:10.1016/j.celrep.2015.09.033
- Ozgur, S., Chekulaeva, M., & Stoecklin, G. (2010). Human Pat1b connects deadenylation with mRNA decapping and controls the assembly of processing bodies. *Mol Cell Biol*, 30(17), 4308-4323. doi:10.1128/mcb.00429-10
- Phillips, R. S., Ramos, S. B., & Blackshear, P. J. (2002). Members of the tristetraprolin family of tandem CCCH zinc finger proteins exhibit CRM1-dependent nucleocytoplasmic shuttling. *J Biol Chem*, 277(13), 11606-11613. doi:10.1074/jbc.M111457200
- Piccirillo, C., Khanna, R., & Kiledjian, M. (2003). Functional characterization of the mammalian mRNA decapping enzyme hDcp2. *RNA*, 9(9), 1138-1147.
- Pilkington, G. R., & Parker, R. (2008). Pat1 contains distinct functional domains that promote P-body assembly and activation of decapping. *Mol Cell Biol*, 28(4), 1298-1312. doi:10.1128/mcb.00936-07
- Pratama, A., Ramiscal, R. R., Silva, D. G., Das, S. K., Athanasopoulos, V., Fitch, J., . . . Vinuesa, C. G. (2013). Roquin-2 shares functions with its paralog Roquin-1 in the repression of mRNAs controlling T follicular helper cells and systemic inflammation. *Immunity*, 38(4), 669-680. doi:10.1016/j.immuni.2013.01.011
- Proudfoot, N. J., Furger, A., & Dye, M. J. (2002). Integrating mRNA processing with transcription. *Cell*, 108(4), 501-512.
- Raveh, A., Zarai, Y., Margaliot, M., & Tuller, T. (2015). Ribosome Flow Model on a Ring. *IEEE/ACM Trans Comput Biol Bioinform*, 12(6), 1429-1439. doi:10.1109/tcbb.2015.2418782
- Reijns, M. A., Alexander, R. D., Spiller, M. P., & Beggs, J. D. (2008). A role for Q/N-rich aggregation-prone regions in P-body localization. *J Cell Sci*, 121(Pt 15), 2463-2472. doi:10.1242/jcs.024976
- Reijns, M. A., Auchynnikava, T., & Beggs, J. D. (2009). Analysis of Lsm1p and Lsm8p domains in the cellular localization of Lsm complexes in budding yeast. *Febs j*, 276(13), 3602-3617. doi:10.1111/j.1742-4658.2009.07080.x
- Roberts, A. P., Doidge, R., Tarr, A. W., & Jopling, C. L. (2014). The P body protein LSM1 contributes to stimulation of hepatitis C virus translation, but not replication, by microRNA-122. *Nucleic Acids Res*, 42(2), 1257-1269. doi:10.1093/nar/gkt941

-
- Ross, J., Peltz, S. W., Kobs, G., & Brewer, G. (1986). Histone mRNA degradation in vivo: the first detectable step occurs at or near the 3' terminus. *Mol Cell Biol*, 6(12), 4362-4371.
- Roux, K. J., Kim, D. I., & Burke, B. (2013). BioID: a screen for protein-protein interactions. *Curr Protoc Protein Sci*, 74, Unit 19.23. doi:10.1002/0471140864.ps1923s74
- Sachs, A. B., & Davis, R. W. (1989). The poly(A) binding protein is required for poly(A) shortening and 60S ribosomal subunit-dependent translation initiation. *Cell*, 58(5), 857-867.
- Salgado-Garrido, J., Bragado-Nilsson, E., Kandels-Lewis, S., & Seraphin, B. (1999). Sm and Sm-like proteins assemble in two related complexes of deep evolutionary origin. *EMBO J*, 18(12), 3451-3462. doi:10.1093/emboj/18.12.3451
- Sanchez, J. G., Chiang, J. J., Sparrer, K. M. J., Alam, S. L., Chi, M., Roganowicz, M. D., . . . Pornillos, O. (2016). Mechanism of TRIM25 Catalytic Activation in the Antiviral RIG-I Pathway. *Cell Rep*, 16(5), 1315-1325. doi:10.1016/j.celrep.2016.06.070
- Santin, I., Moore, F., Grieco, F. A., Marchetti, P., Brancolini, C., & Eizirik, D. L. (2012). USP18 is a key regulator of the interferon-driven gene network modulating pancreatic beta cell inflammation and apoptosis. *Cell Death Dis*, 3, e419. doi:10.1038/cddis.2012.158
- Sauer, E. (2013). Structure and RNA-binding properties of the bacterial LSm protein Hfq. *RNA Biol*, 10(4), 610-618. doi:10.4161/rna.24201
- Scheller, N., Mina, L. B., Galao, R. P., Chari, A., Gimenez-Barcons, M., Noueiry, A., . . . Diez, J. (2009). Translation and replication of hepatitis C virus genomic RNA depends on ancient cellular proteins that control mRNA fates. *Proc Natl Acad Sci U S A*, 106(32), 13517-13522. doi:10.1073/pnas.0906413106
- Schumacher, M. A., Pearson, R. F., Moller, T., Valentin-Hansen, P., & Brennan, R. G. (2002). Structures of the pleiotropic translational regulator Hfq and an Hfq-RNA complex: a bacterial Sm-like protein. *EMBO J*, 21(13), 3546-3556. doi:10.1093/emboj/cdf322
- Schwartz, D. C., & Parker, R. (1999). Mutations in translation initiation factors lead to increased rates of deadenylation and decapping of mRNAs in *Saccharomyces cerevisiae*. *Mol Cell Biol*, 19(8), 5247-5256.
- Schwartz, D. C., & Parker, R. (2000). mRNA decapping in yeast requires dissociation of the cap binding protein, eukaryotic translation initiation factor 4E. *Mol Cell Biol*, 20(21), 7933-7942.
- Seraphin, B. (1995). Sm and Sm-like proteins belong to a large family: identification of proteins of the U6 as well as the U1, U2, U4 and U5 snRNPs. *EMBO J*, 14(9), 2089-2098.

- Servaes, J., Jacobson, T. L., & White, S. A. (1996). *Participatory communication for social change*. New Delhi ; Thousand Oaks: Sage Publications.
- Sgromo, A., Raisch, T., Bawankar, P., Bhandari, D., Chen, Y., Kuzuoglu-Ozturk, D., . . . Izaurralde, E. (2017). A CAF40-binding motif facilitates recruitment of the CCR4-NOT complex to mRNAs targeted by Drosophila Roquin. *Nat Commun*, *8*, 14307. doi:10.1038/ncomms14307
- Sharif, H., & Conti, E. (2013). Architecture of the Lsm1-7-Pat1 complex: a conserved assembly in eukaryotic mRNA turnover. *Cell Rep*, *5*(2), 283-291. doi:10.1016/j.celrep.2013.10.004
- She, M., Decker, C. J., Sundramurthy, K., Liu, Y., Chen, N., Parker, R., & Song, H. (2004). Crystal structure of Dcp1p and its functional implications in mRNA decapping. *Nat Struct Mol Biol*, *11*(3), 249-256. doi:10.1038/nsmb730
- Sheets, M. D., & Wickens, M. (1989). Two phases in the addition of a poly(A) tail. *Genes Dev*, *3*(9), 1401-1412.
- Shen, B., & Goodman, H. M. (2004). Uridine addition after microRNA-directed cleavage. *Science*, *306*(5698), 997. doi:10.1126/science.1103521
- Sheth, U., & Parker, R. (2003). Decapping and decay of messenger RNA occur in cytoplasmic processing bodies. *Science*, *300*(5620), 805-808. doi:10.1126/science.1082320
- Shortman, K., Egerton, M., Spangrude, G. J., & Scollay, R. (1990). The generation and fate of thymocytes. *Semin Immunol*, *2*(1), 3-12.
- Slevin, M. K., Meaux, S., Welch, J. D., Bigler, R., Miliani de Marval, P. L., Su, W., . . . Marzluff, W. F. (2014). Deep sequencing shows multiple oligouridylation are required for 3' to 5' degradation of histone mRNAs on polyribosomes. *Mol Cell*, *53*(6), 1020-1030. doi:10.1016/j.molcel.2014.02.027
- Song, M. G., Li, Y., & Kiledjian, M. (2010). Multiple mRNA decapping enzymes in mammalian cells. *Mol Cell*, *40*(3), 423-432. doi:10.1016/j.molcel.2010.10.010
- Stevens, A. (2001). 5'-exoribonuclease 1: Xrn1. *Methods Enzymol*, *342*, 251-259.
- Stoecklin, G., Lu, M., Rattenbacher, B., & Moroni, C. (2003). A constitutive decay element promotes tumor necrosis factor alpha mRNA degradation via an AU-rich element-independent pathway. *Mol Cell Biol*, *23*(10), 3506-3515.
- Stoecklin, G., Mayo, T., & Anderson, P. (2006). ARE-mRNA degradation requires the 5'-3' decay pathway. *EMBO Rep*, *7*(1), 72-77. doi:10.1038/sj.embor.7400572
- Stoecklin, G., Tenenbaum, S. A., Mayo, T., Chittur, S. V., George, A. D., Baroni, T. E., . . . Anderson, P. (2008). Genome-wide analysis identifies interleukin-10 mRNA as target of tristetraprolin. *J Biol Chem*, *283*(17), 11689-11699. doi:10.1074/jbc.M709657200

-
- Su, W., Slepnev, S. V., Slevin, M. K., Lyons, S. M., Ziemniak, M., Kowalska, J., . . . Rhoads, R. E. (2013). mRNAs containing the histone 3' stem-loop are degraded primarily by decapping mediated by oligouridylation of the 3' end. *RNA*, *19*(1), 1-16. doi:10.1261/rna.034470.112
- Tan, E. M. (1989). Interactions between autoimmunity and molecular and cell biology. Bridges between clinical and basic sciences. *J Clin Invest*, *84*(1), 1-6. doi:10.1172/jci114127
- Tan, E. M., Schur, P. H., Carr, R. I., & Kunkel, H. G. (1966). Deoxybonucleic acid (DNA) and antibodies to DNA in the serum of patients with systemic lupus erythematosus. *J Clin Invest*, *45*(11), 1732-1740. doi:10.1172/jci105479
- Tarun, S. Z., Jr., & Sachs, A. B. (1995). A common function for mRNA 5' and 3' ends in translation initiation in yeast. *Genes Dev*, *9*(23), 2997-3007.
- Teixeira, D., & Parker, R. (2007). Analysis of P-body assembly in *Saccharomyces cerevisiae*. *Mol Biol Cell*, *18*(6), 2274-2287. doi:10.1091/mbc.E07-03-0199
- Teixeira, D., Sheth, U., Valencia-Sanchez, M. A., Brengues, M., & Parker, R. (2005). Processing bodies require RNA for assembly and contain nontranslating mRNAs. *RNA*, *11*(4), 371-382. doi:10.1261/rna.7258505
- Tharun, S. (2009a). Lsm1-7-Pat1 complex: a link between 3' and 5'-ends in mRNA decay? *RNA Biol*, *6*(3), 228-232.
- Tharun, S. (2009b). Roles of eukaryotic Lsm proteins in the regulation of mRNA function. *Int Rev Cell Mol Biol*, *272*, 149-189. doi:10.1016/s1937-6448(08)01604-3
- Tharun, S., Muhlrud, D., Chowdhury, A., & Parker, R. (2005). Mutations in the *Saccharomyces cerevisiae* LSM1 gene that affect mRNA decapping and 3' end protection. *Genetics*, *170*(1), 33-46. doi:10.1534/genetics.104.034322
- Tharun, S., & Parker, R. (1999). Analysis of mutations in the yeast mRNA decapping enzyme. *Genetics*, *151*(4), 1273-1285.
- Tharun, S., & Parker, R. (2001). Targeting an mRNA for decapping: displacement of translation factors and association of the Lsm1p-7p complex on deadenylated yeast mRNAs. *Mol Cell*, *8*(5), 1075-1083.
- Tiedje, C., Diaz-Munoz, M. D., Trulley, P., Ahlfors, H., Laass, K., Blackshear, P. J., . . . Gaestel, M. (2016). The RNA-binding protein TTP is a global post-transcriptional regulator of feedback control in inflammation. *Nucleic Acids Res*, *44*(15), 7418-7440. doi:10.1093/nar/gkw474
- Tourriere, H., Chebli, K., & Tazi, J. (2002). mRNA degradation machines in eukaryotic cells. *Biochimie*, *84*(8), 821-837.
- Tucker, M., Valencia-Sanchez, M. A., Staples, R. R., Chen, J., Denis, C. L., & Parker, R. (2001). The transcription factor associated Ccr4 and Caf1 proteins are components of the

- major cytoplasmic mRNA deadenylase in *Saccharomyces cerevisiae*. *Cell*, *104*(3), 377-386.
- Vidal, V. P., Verdone, L., Mayes, A. E., & Beggs, J. D. (1999). Characterization of U6 snRNA-protein interactions. *RNA*, *5*(11), 1470-1481.
- Vindry, C., Marnef, A., Broomhead, H., Twyffels, L., Ozgur, S., Stoecklin, G., . . . Standart, N. (2017). Dual RNA Processing Roles of Pat1b via Cytoplasmic Lsm1-7 and Nuclear Lsm2-8 Complexes. *Cell Rep*, *20*(5), 1187-1200. doi:10.1016/j.celrep.2017.06.091
- Vinuesa, C. G., Cook, M. C., Angelucci, C., Athanasopoulos, V., Rui, L., Hill, K. M., . . . Goodnow, C. C. (2005). A RING-type ubiquitin ligase family member required to repress follicular helper T cells and autoimmunity. *Nature*, *435*(7041), 452-458. doi:10.1038/nature03555
- Vogel, K. U., Edelmann, S. L., Jeltsch, K. M., Bertossi, A., Heger, K., Heinz, G. A., . . . Heissmeyer, V. (2013). Roquin paralogs 1 and 2 redundantly repress the Icos and Ox40 costimulator mRNAs and control follicular helper T cell differentiation. *Immunity*, *38*(4), 655-668. doi:10.1016/j.immuni.2012.12.004
- Wilusz, C. J., Wang, W., & Peltz, S. W. (2001). Curbing the nonsense: the activation and regulation of mRNA surveillance. *Genes Dev*, *15*(21), 2781-2785. doi:10.1101/gad.943701
- Wu, D., Muhlrads, D., Bowler, M. W., Jiang, S., Liu, Z., Parker, R., & Song, H. (2014). Lsm2 and Lsm3 bridge the interaction of the Lsm1-7 complex with Pat1 for decapping activation. *Cell Res*, *24*(2), 233-246. doi:10.1038/cr.2013.152
- Wyers, F., Minet, M., Dufour, M. E., Vo, L. T., & Lacroute, F. (2000). Deletion of the PAT1 gene affects translation initiation and suppresses a PAB1 gene deletion in yeast. *Mol Cell Biol*, *20*(10), 3538-3549.
- Yamashita, A., Chang, T. C., Yamashita, Y., Zhu, W., Zhong, Z., Chen, C. Y., & Shyu, A. B. (2005). Concerted action of poly(A) nucleases and decapping enzyme in mammalian mRNA turnover. *Nat Struct Mol Biol*, *12*(12), 1054-1063. doi:10.1038/nsmb1016
- Yu, D., Tan, A. H., Hu, X., Athanasopoulos, V., Simpson, N., Silva, D. G., . . . Vinuesa, C. G. (2007). Roquin represses autoimmunity by limiting inducible T-cell co-stimulator messenger RNA. *Nature*, *450*(7167), 299-303. doi:10.1038/nature06253
- Zaric, B., Chami, M., Remigy, H., Engel, A., Ballmer-Hofer, K., Winkler, F. K., & Kambach, C. (2005). Reconstitution of two recombinant LSm protein complexes reveals aspects of their architecture, assembly, and function. *J Biol Chem*, *280*(16), 16066-16075. doi:10.1074/jbc.M414481200
- Zhang, A., Wassarman, K. M., Ortega, J., Steven, A. C., & Storz, G. (2002). The Sm-like Hfq protein increases OxyS RNA interaction with target mRNAs. *Mol Cell*, *9*(1), 11-22.

Zhao, J., Kessler, M., Helmling, S., O'Connor, J. P., & Moore, C. (1999). Pta1, a component of yeast CF II, is required for both cleavage and poly(A) addition of mRNA precursor. *Mol Cell Biol*, *19*(11), 7733-7740.

Zhou, L., Hang, J., Zhou, Y., Wan, R., Lu, G., Yin, P., . . . Shi, Y. (2014). Crystal structures of the Lsm complex bound to the 3' end sequence of U6 small nuclear RNA. *Nature*, *506*(7486), 116-120. doi:10.1038/nature12803

Zhu, J., & Paul, W. E. (2008). CD4 T cells: fates, functions, and faults. *Blood*, *112*(5), 1557-1569. doi:10.1182/blood-2008-05-078154

Zubay, G. (1963). Molecular model for protein synthesis. *Science*, *140*(3571), 1092-1095.

Acknowledgements

It would have not been possible to write this doctoral thesis without the help and support of many people.

First of all, I would like to thank my supervisor and mentor Prof. Dr. Vigo Heissmeyer for the committed supervision of this research project. I am deeply thankful for the unlimited support and the ingenious input into this challenging and fascinating project.

I want to thank all members of the group for their help and for creating an enjoyable working atmosphere in the lab. I want to especially thank Dr. Kai Höfig who generated the *Lsm1* MEF cell-lines that were used in this project and for his help with the qPCR measurements. I am thankful for introducing me into the lab work and for the great and continuous support and guidance.

I deeply thank Dr. Gesine Behrens who joined the *Lsm1*-project after my pregnancy and pushed the project remarkably. I am very grateful for her help in performing the BioID experiment and the last P-body analysis experiment and for critical proof-reading my thesis.

Special thanks also to Claudia Lohs for managing the mouse breedings, being a great lab organizer and for her valuable suggestions that were helpful in various phases of the project. I also would like to thank Desiree Agiriu, who did not only managed breedings of the *Lsm1^{fl/fl}* mice strain but also took great care of the mice in the Goethestraße.

Furthermore, I want to thank former members of the group, especially, Dr. Sven Brenner for helping me with the Southern blot analysis, Dr. Sebastian Warth for teaching me about T cell isolation and differentiation, Dr. Desheng Hu for teaching me blood sampling and Dr. Nina Rehage who did a great job in maintaining the FACS facility I was able to use for the many mouse analyses.

I would like to thank the members of my thesis advisory committee PD Dr. Reinhard Obst and Prof. Dr. Ludger Klein for their valuable input.

Many thanks to the group of Dr. Helmut Blum for performing the microarray hybridization and special thanks to Alexander Graf for the statistical evaluation.

Moreover, I enjoyed the collaboration with Dr. Martin Jastroch, who was interested in this project and helped in planning the Seahorse experiment. Special thanks to Daniel Lamp for his technical support.

Many thanks also to the imaging core facility for performing confocal microscopy and analyzing the many sera samples.

I also would like to thank all staff of the animal facility, especially Michael Hagemann for his excellent cooperativeness and Franziska Liebel who took great care of the mice and was always helpful and friendly.

Finally, I want to express my gratitude to my family and especially to **my mother Nafissa Ghobbich** and **my father Ibrahim Jridi** for constantly encouraging me every step of the way and for helping me keep the balance.